EMEP/MSC-W Report 2/98
Date: July 1998

emep

Co-operative programme for monitoring and evaluation of the long range transmission of air pollutants in Europe

Transboundary Photooxidant Air Pollution in Europe

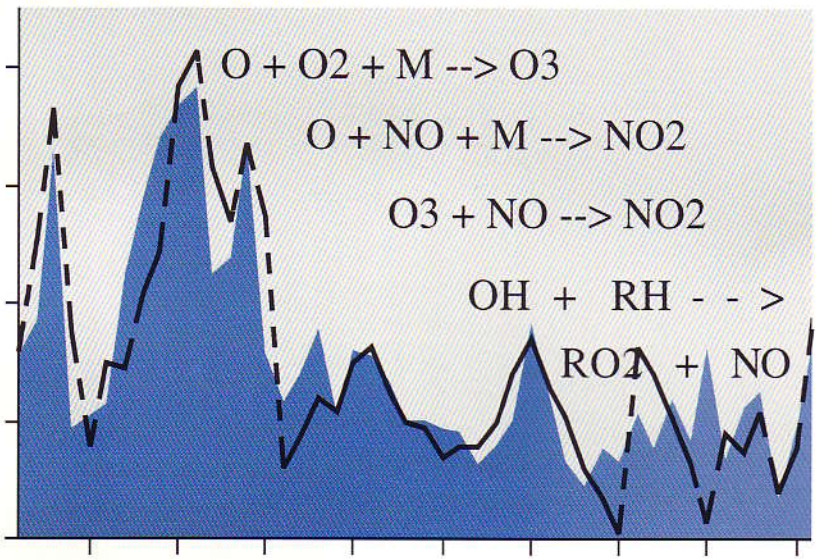

MSC-W Status Report 1998:

Calculations of tropospheric ozone and camparison with observations

msc-w

Meteorological Synthesizing Centre - West
Norwegian Meteorological Institute
P.o. Box 43-Blindern, N-0313 Oslo, Norway

EMEP/MSC-W Report 2/98
Date: July 1998

EMEP/MSC-W Report 2/98
Date: July 1998

DET NORSKE METEOROLOGISKE INSTITUTT
The Norwegian Meteorological Institute
Research Report No. 67

Transboundary Photooxidant Air Pollution in Europe:

Calculations of tropospheric ozone and comparison with observations

EMEP MSC-W
Status Report 1998

ISSN 0332-9879

Contributers

This EMEP MSC-W report has been produced as a result of collaborations between the scientists and institutions shown below.

DNMI[1]

Jan Eiof Jonsen, David Simpson, and Leonor Tarasson

GMD-FIRST[2]

Steffen Unger

IVL[3]

Johanna Altenstedt

NILU[4]

Anne-Gunn Hjellbrekke

UiO[5]

Terje Berntsen, Jostein Sundet

1. Norwegian Meteorological Institute (DNMI), Oslo, Norway
2. Research Institute for Computer Architecture and Software Technology (FIRST) of the German National Research Centre for Information Technology (GMD), Berlin
3. Swedish Environmental Research Institute (IVL), Gothenburg, Sweden
4. Norwegian Institute for Air Research (NILU), Kjeller, Norway
5. University of Oslo (UiO), Oslo, Norway

Preface and Acknowledgements

This report was prepared for presentation at the twenty-second session of the Steering Body of EMEP (Co-operative Programme for Monitoring and Evaluation of the Long Range Transmission of Air Pollutants in Europe). It provides an overview of updates to two EMEP MSC-W photo-oxidant models: the 150 km Lagrangian model and the 50km Eulerian multilayer model. This report presents an evaluation of these two models against measurements and, for the first time, against each other.

The Research Institute for Computer Architecture and Software Technology (FIRST) of the German National Research Centre for Information Technology (GMD), Berlin, is especially thanked for significantly improving the efficiency of the multi-layer Eulerian model, and for continued support with the Lagrangian model. The cooperations with the Norwegian Institute for Air Research (NILU), the Swedish Environmental Research Institute (IVL), and the University of Oslo are also gratefully acknowledged.

The calculations presented in this report depend strongly on the meteorological data obtained from the Numerical Weather Prediction Model of the Norwegian Meteorological Institute. The calculations presented here have been made possible by access to the CRAY T3E computer at the Norwegian University of Science and Technology (NTNU) in Trondheim, Norway.

Contents

Chapter 1

Overview

This status report for the photochemical oxidant models of EMEP MSC-W is divided into 3 main parts, along with 3 appendices:

Part I The Lagrangian oxidant model: status and multi-annual evaluation

Part II The Eulerian 3-D oxidant model: status and evaluation for summer 1996 results and case-studies.

Part III Comparison of Lagrangian and Eulerian models for the summer of 1996.

Appendix A The Lagrangian oxidant model: Physical and chemical formulation

Appendix B The Eulerian 3-D oxidant model: Physical and chemical formulation

Appendix C Lagrangian model: Time-series plots, 1989-1996

Parts I and II present the current status of the two EMEP photooxidant models, along with the results of some model evaluation exercises. For the Lagrangian model this evaluation has been mainly concerned with assessing how well the model performs over the many years for which simulations are now available. For the Eulerian photo-oxidant model we present for the first time the results of a simulation over a full summer period (April-September 1996). In addition, measurements from a number of field-campaigns are used to evaluate the model performance against aircraft measurements. Part III presents a side-by-side comparison of the two EMEP oxidant models, both against each other and against measurements.

1.1 Definitions, statistics used

The basic units used throughout this report are ppb (1 ppb = 1 part per billion by volume) or ppm (1 ppm = 1000 ppb). At 20°C and 1013 mb pressure, 1 ppb ozone is equivalent to 2.00 μgm^{-3}.

A number of statistics have been used to describe the distribution of ozone within each grid square:

Mean of Daily Max. Ozone - First we evaluate the maximum modelled concentration for each day, then we take the 6-monthly mean of these values, over the 6-month period 1 April - 30 September.

AOT40 - the accumulated amount of ozone over the threshold value of 40 ppb, i.e.. $AOT40 = \int max(O_3 - 40ppb, 0.0)\, dt$ where the max function ensures that only ozone values exceeding 40 ppb are included. The integral is taken over time, namely – the growing season as defined at the Bern and Kuopio critical level workshops (Fuhrer and Achermann, 1994, Kärenlampi and Skärby, 1996). For crops and natural vegetation AOT40 is taken over 3 months (May-July), which we denote $\mathbf{AOT40}_c$. For forests a six month period is used (April-September), denoted $\mathbf{AOT40}_f$. In both cases only daylight hours are included.

AOT60 - the accumulated amount of ozone over the threshold value of 60 ppb, i.e. $AOT60 = \int max(O_3 - 60ppb, 0.0)\, dt$ - in this case, the integral is taken over 6 months, and only daytime ozone included.

As the Lagrangian model does not work with hourly averages, but rather gives values of calculated ozone at 0, 6, 12 and 18 GMT each day, some approximations are necessary to compare with true 1-hour and AOT-type guidelines. We generally assume that each output value of the model corresponds to an hourly value. The daytime-average required for AOT values is simply obtained from the 12 and 18 GMT values, assuming each value is representative of a 6-hour average. This procedure introduces only moderate errors for AOT40 (see Malik et al., 1996), but is obviously less accurate for AOT60.

The AOT40 levels reflect interest in long-term ozone exposure which is considered important for vegetation - critical levels of 3 000 ppb.h have been suggested for crops and natural vegetation, and 10 000 ppb.h for forests (Kärenlampi and Skärby, 1996).

The AOT60 measure reflects the revised WHO guidelines which sets 120 μgm^{-3}(60 ppb) as an 8-hour moving average. The UN-ECE workshop on 'health effects of ozone and nitrogen oxides in an integrated assessment of air pollution' (UN-ECE, 1997) agreed that a simple statistic such as AOT60 could be used as a preliminary indication of ozone levels above the recommended WHO guideline for integrated assessment modelling purposes. The justification for this is that AOT60 is a statistic which incorporates both the amount of ozone above 60 ppb and the frequency of exceedance, both of which are known to be important. However, it is clear that this statistic cannot be directly coupled to health impact assessments. (In any case, the EMEP models are not designed for calculating ozone exposure inside urban areas, which would be required for any meaningful health-risk assessment.)

1.2 Country codes

Many tables and plots in this report make use of two (or three)-letter country codes. These codes are:

AL	Albania	LT	Lithuania
AT	Austria	LU	Luxembourg
BY	Belarus	NL	Netherlands
BE	Belgium	NO	Norway
BG	Bulgaria	PL	Poland
BA	Bosnia and Herzegovina	PO	Portugal
HR	Croatia	MD	Republic of Moldova
CS	Czech Republic	RO	Romania
DK	Denmark	RU	Russian Federation
EE	Estonia	SK	Slovakia
FI	Finland	SI	Slovenia
FR	France	ES	Spain
DE	Germany	SE	Sweden
GR	Greece	CH	Switzerland
HU	Hungary	FYM	The FYR Macedonia
IS	Iceland	TR	Turkey
IE	Ireland	UA	Ukraine
IT	Italy	GB	United Kingdom
LV	Latvia	YU	Yugoslavia

1.3 References

Fuhrer, J. and Achermann, B., editors, *UN-ECE Workshop on critical levels for ozone, 1-4 November 1993, Bern.* Swiss Federal Research Station for Agricultural Chemistry, 1994.

Kärenlampi, L. and Skärby, L., editors, *Critical Levels for Ozone in Europe: Testing and Finalising the Concepts.* University of Kuopio, Department of Ecology and Environmental Science, 1996, 15-17 April 1996, Kuopio, Finland.

Malik, S., Simpson, D., Hjellbrekke, A.-G., and ApSimon, H., 1996, Photochemical model calculations over Europe for summer 1990. Model results and comparison with observations, Norwegian Meteorological Institute, Oslo, Norway, EMEP MSC-W Report 2/96.

UN-ECE, 1997, Health Effects of Ozone and Nitrogen Oxides in an Integrated Assessment of Air Pollution, Proceedings of an International workshop, 10-12 June 1996, Eastbourne, United Kingdom.

Part I

The Lagrangian oxidant model: status and multi-annual evaluation

D. Simpson, J. Altenstedt, and A.G. Hjellbrekke

Chapter 1

Introduction and current status

Between 1989-1996 data from over 120 ozone measurement stations have been submitted to the Chemical Co-ordinating Centre of EMEP (EMEP/CCC, located at NILU). These measurements have been reported and analysed by Hjellbrekke (1995, 1996, 1997, 1998), where further details can be found concerning site location and data quality.

This report presents the results of an extensive evaluation exercise, whereby model results for these summer periods have been compared with essentially all the available measurements. Among other benefits, this long-time series of simulation enables us to compare modelled concentrations with observations for a large number of measurement stations under a wide variety of meteorological conditions.

As well as model evaluation, activity over the last year has mainly concentrated on applications and on longer-term improvements which will be reported at a later date. The applications have included a large number of scenario runs in support of the EU Acidification and Ozone strategy, mainly as support and verification of the results provided by the simplified IIASA RAINS-ozone model (Amann et al., 1998, Heyes et al., 1996).

The model itself has been described in detail in Simpson, 1992, 1993, 1995, and Simpson et al., 1993, 1997. The physical and chemical formulation of the model has remained unchanged since Simpson et al. (1997), but a brief summary is given in Appendix A.

Source-receptor matrices?

In view of the unchanged model formulation, country-to-country source receptor relationships have not been re-calculated for this report - the latest relationships calculated with this model thus remain those presented in Simpson et al. (1997).

Other publications

A number of other studies have been published in 1997/1998 (since EMEP Report 3/97) concerning the oxidant model:

- Kuhn, M., Builtjes, P.J.H., Poppe, D., Simpson, D., Stockwell, W.R., Andersson-Sköld, Y., Baart, A., Das, M., Fiedler, F., Hov, Ø., Kirchner, F., Makar, P.A., Milford, J.B., Roemer, M.G.M., Ruhnke, R., Strand, A., Vogel, B., and Vogel, H., 1998, Intercomparison of the gas-phase chemistry in several chemistry and transport models, *Atmos. Environ.*, **32**, No. 4, 693-709.

- Hass, H., Builtjes, P.J.H., Simpson, D., and Stern, R., 1997, Comparison of model results obtained with several European regional air quality models, *Atmos. Environ.*, **31**, No. 19, 3259-3279.

- Hov, Ø., Sorteberg, A., Schmidbauer, N., Solberg, S., Stordal, F. ., Simpson, D., L., A., A., Han., O., Pedr., Lätilä, H., and Heidam, N. Z., 1997, European VOC emission estimates evaluated by measurements and model calculations, *J. Atmos. Chem.*, **28**, 173-193.

- Simpson, D. , 1997a, Modelled ozone concentrations in relation to health issues, In Health Effects of Ozone and Nitrogen Oxides in an Integrated Assessment of Air Pollution. Institute for Environment and Health, University of Leicester, UK, Proceedings of an International workshop, 10-12 June 1996, Eastbourne, United Kingdom.

In addition, partly in an attempt to improve the reporting of biogenic emissions and the relevant land-use data to EMEP, a new chapter on emissions from nature and forestry for the joint EMEP/CORINAIR Atmospheric Emission Inventory Guidebook has been produced:

- Simpson, D., and Winiwarter, W. (eds), 1998, Emissions from Natural Sources, Contribution of the Nature Expert Panel to the EMEP/CORINAIR Atmospheric Emissions Inventory Guidebook (SNAP Code 11), published by Federal Ministry for Environment, Youth and Family, Umweltbundesamt, Vienna.

This work will in due course appear on the official pages of the European Environment Agency web-site http://www.eea.dk/aegb. A mirror of the EEA site, which also contains suggested updates (and which already includes the Nature Panel pages) can be found at :

- http//www.aeat.co.uk/netcen/airqual/TFEI/unece.htm.

A number of previous studies have already documented the EMEP MSC-W ozone model's performance against measurements. The most extensive of these was Malik et al. (1996), which presented statistics and time-series plots for all stations which provided data to EMEP for 1990 (ca 50 sites). Further model comparisons against measurements can be found in Builtjes et al. (1991), Hov et al. (1997), Simpson (1992), Simpson (1993), and Solberg et al. (1995).

As well as comparison with measurements, the EMEP model has also been tested against other air pollution models. See Andersson-Sköld and Simpson (1997), Builtjes et al. (1991), Derwent (1990), Derwent (1993), Hass et al. (1997), Poppe et al. (1996), and Kuhn et al. (1998).

Chapter 2

Multi-annual comparison with ozone measurements

In the course of this study comparisons with the model have been made for 460 site-years of data. Here we present summaries of these comparisons. In Appendix C time-series plots from essentially all stations are presented, in an effort to give a fair and un-selective overview of the performance of the EMEP model. A number of plots and statistics are presented:

- Time-series plots comparing the modelled versus observed daily maximum ozone concentrations.
- Tables of correlation coefficients, and AOT40 statistics, are given for all site-years.
- Histograms of AOT40 (forests) and AOT60 (health) have been calculated for the five years separately and these will be illustrated for some sites.
- Scatter plots of modelled versus observed 5-year average AOT40 and AOT60 are presented in Figure 2.5 and 2.6.
- Frequency distributions plots of the modelled and observed 12 GMT ozone values

Note that the years used in these analyses are from 1989 to 1996, excluding 1991. Unfortunately problems with the meteorological data precluded model runs for 1991.

2.1 Definitions: Multi-annual averages and plotting

As the number of stations reporting to EMEP has increased markedly from 1989 to 1996, we have adopted a procedure for making multi-annual averages (of ozone or AOT) which attempts to make use of data from as many stations as possible, and from as many years as possible for each station. The procedure is:

1. For any one year we accept data for averaging if data-capture is better than 90% for the required period.
2. For calculating mean ozone concentrations from the model results over any one year, only those days for which measurements exist are taken into the calculation. This means the mean modelled values are comparable with the observed data for each station.
3. All years of data passing test (1) are then averaged for as many years as possible.

Table 2.1 gives the full lists of stations available to this comparison exercise. For those stations passing the data-capture test (1) the correlation coefficients between modelled and observed daily maximum ozone values are given.

The presentation of maps of modelled ozone also differs in this report from that used previously. Here we have constructed the maps using only modelled results at the actual stations (as opposed to across the whole EMEP grid), using identical procedures to those used for measurements. Thus, we first make use of the same multi-annual averaging procedure as given above, then construct both modelled and observed maps using the same interpolation routine.

2.2 Results: Time-series comparison

Time-series plots comparing the modelled versus observed daily maximum ozone concentrations are given for all available stations and years (having data-capture of at least 60%) in Appendix C. (Except some sites for 1996, which are plotted in Part III, Figs 2.1-2.4). Table 2.1 lists the available sites and gives the correlation coefficients for each year where data-capture exceeds 90% over the April-September period.

Note that the plots in Appendix C are sorted alphabetically by their two-letter country code. We briefly highlight the main features of these plots below by geographical region.

Northern Europe: Denmark, Finland, Latvia, Lithuania, Norway, Sweden

In general the model performs very well for the northern European sites in almost all years, especially for the Danish sites. Measurements at the Latvian and Lithuanian sites which are relatively new to the EMEP network are also reproduced quite well by the model, with the exception of Rucava in 1996 where observed values look unrealistically low (possibly a ppb-μgm^{-3} conversion problem?). The site with worst correlations and performance generally is the Norwegian site Zeppelinfjellet, but this site lying 78°N on the arctic island of Svalbard is well outside the intended region of application of the Lagrangian model.

The main exception to the generally good performance at the Scandinavian stations is the significant model under-prediction at some sites near the start of June 1992. This underprediction occurs for a period of two weeks at most Nordic sites, but it is also notable that for sites such as Eskdalemuir in Scotland and Westerland in N Germany the model and observations match very well for this period, Thus, the under-prediction is limited to high latitudes (>60°N) - pointing to the possibility that exceptionally high background tropospheric ozone (which cannot be handled by the EMEP model) is responsible.

Western Europe: Belgium, France, Germany, Netherlands, UK

Sites in Germany, United Kingdom, and elsewhere in NW Europe seem to show broadly similar performance over all years. The model captures both the month-to-month, and day-to-day variations, rather well. Importantly, the performance seems to be rather uniform over large geographical areas, suggesting that the model copes well with changes in climate and emission patterns.

Data from Belgium have not been reported to EMEP/CCC since 1989, so only a few data are available for that country. However, the results obtained for 1989 are reasonably good, comparable to those of sites in the Netherlands. The stations in France are new additions to the EMEP network, and model performance for these is comparable to that for other NW European sites.

Eastern Europe: Czech Rep., Poland, Russia, Slovakia

The Czech stations show somewhat mixed results. The model performs well for Svratouch but less so for Kosetice. The results in Slovakia are also mixed, but the many measurement-gaps make this comparison difficult.

The results for the Polish and Russian sites are rather poor. Little is known about these sites, and the Polish sites in particular have poor data-capture, so further investigation is needed to understand these discrepancies.

Central and south-eastern Europe: Austria, N. Italy, Slovenia, Switzerland

In Austria and Switzerland the model generally performs well at most sites, and for most years (although it is hard to explain the very poor results for Illmitz in 1989 though). Performance at the relatively recent sites in Slovakia and Slovenia is also comparable (although the odd behaviour of the measurements at the Slovenian site Zavodjne in the second half of 1994 give a poor correlation for that year).

The model significantly underpredicts observed ozone at Ispra in Italy - possibly as Ispra is often influenced by the Milan plume. Simpson and Jonson (Part III, this report) show that for this site the Eulerian model with 50 km grid size performs significantly better.

Mediterranean Europe: Greece, C. Italy, Portugal, Spain, Turkey

The Spanish, Greek and central Italian stations are quite new to the EMEP network, so this is the first presentation of the EMEP model's performance against these sites. (Note that the plot for the Greek station, Aliartos, is given in Part III, Figure 2.3).

Rather surprisingly, the model generally predicts higher ozone values than the measurements for the stations in Greece Spain and Portugal. Correlations are also rather poor at many sites. Both problems are very marked for the Spanish stations Noia and Tortosa, and the Portuguese site Monte Velho.

Possible reasons for this could include a poor description of the man-made or especially biogenic emissions, or problems with the model's 1-D structure in these regions. However, discussions with some Spanish scientists have suggested that much of the reason for the low ozone values reported at these sites lies with problems with measurement site placement and/or calibration. Certainly the large step-change in the measurements at Noia and Tortosa in June 1994 looks odd. Monte Velho is sites rather near an industrial area, and Montelibretti is very close to Rome, so local NO_x sources probably influences these comparisons.

Little is known about the Aliartos station, but the poor model performance at this site needs further investigation. At the Turkish station there is hardly enough data to allow any evaluation, except that the observations are consistently about 10 ppb higher than the model results.

San Pablo is a station believed to be well placed for EMEP purposes, and this is the one where the EMEP model performs best.

Table 2.1: Correlations between predicted and observed daily maximum ozone values

CC	Site	1989	1990	1992	1993	1994	1995	1996
AT	Illmitz	0.27	0.59	0.55	0.53	0.50	0.55	0.53
AT	Achenkirch	-	-	-	0.59	0.70	0.60	0.57
AT	Koloman	-	ld	0.64	0.63	0.72	0.65	0.54
AT	Vorhegg	-	-	-	-	-	0.46	0.51
AT	Pillersdorf	-	-	-	-	-	0.64	-
AT	St leonhard	-	-	-	-	-	-	-
AT	Sulzberg	-	-	-	-	-	0.64	-
AT	Stolzalpe	-	-	-	-	-	0.48	-
BE	Offagne	ld	-	-	-	-	-	-
BE	Berendrecht	ld	-	-	-	-	-	-
BE	Eupen	ld	-	-	-	-	-	-
BE	Moerkerke	ld	-	-	-	-	-	-
CH	Payerne	ld	ld	0.57	0.60	0.63	0.58	0.50
CH	Taenikon	0.41	0.66	0.61	0.67	0.69	0.68	0.56
CH	Chaumont	-	-	0.60	0.63	0.61	0.54	0.56
CH	Rigi	-	-	0.55	0.54	0.65	0.54	0.52
CH	Sion	0.60	0.63	0.49	0.51	0.56	0.62	0.52
CS	Svratouch	-	ld	0.47	0.55	ld	ld	0.52
CS	Kosetice	-	-	ld	0.57	0.66	0.57	0.50
DE	Arkona	0.65	-	-	-	-	-	-
DE	Westerland	0.68	ld	0.71	0.67	0.67	ld	0.62
DE	Waldhof	0.60	0.68	0.56	0.65	0.73	0.58	ld
DE	Schauinsland	ld	0.61	0.61	0.72	0.70	0.66	0.58
DE	Deuselbach	0.60	ld	0.60	0.72	0.73	0.71	0.64
DE	Brotjacklriegel	0.39	ld	0.49	0.51	0.57	0.71	0.60
DE	Neuglobsow	0.61	-	0.54	0.62	0.65	0.62	ld
DE	Schmuecke	-	-	ld	ld	0.69	-	-
DE	Zingst	-	-	0.61	0.69	0.58	0.60	0.57

continued on next page

CC	Site	1989	1990	1992	1993	1994	1995	1996
DE	Hohenwestedt	ld	0.38	0.55	ld	ld	0.52	0.54
DE	Bassum	0.51	0.66	0.67	0.59	0.77	ld	0.59
DE	Rodenberg	ld	-	-	-	-	-	-
DE	Meinerzhagen	ld	ld	0.68	0.68	ld	0.69	0.61
DE	Ansbach	ld	0.56	0.60	0.63	ld	0.46	0.69
DE	Rottenburg	ld	-	-	-	-	-	-
DE	Ueckermuende	-	-	ld	0.69	0.67	-	-
DE	Wiesenburg	-	-	ld	ld	ld	0.59	0.61
DE	Lueckendorf	-	-	0.51	0.57	0.52	-	-
DK	Ulborg	ld	ld	ld	0.65	0.71	0.56	ld
DK	Frederiksborg	-	ld	0.75	0.66	0.66	0.53	0.58
ES	San pablo	-	-	-	ld	0.37	-	0.47
ES	Cartuja	-	-	-	ld	0.38	0.25	-
ES	Tortosa	-	-	-	0.39	0.10	0.25	0.37
ES	Noia	-	-	-	0.26	ld	ld	ld
ES	Viznar	-	-	-	-	-	ld	ld
ES	Logrono	-	-	-	-	-	-	ld
FI	Ahtari	0.53	0.55	ld	0.66	0.64	0.55	0.43
FI	Uto	ld	ld	0.60	0.53	0.46	0.55	0.35
FI	Virolahti	0.61	0.57	0.55	0.71	0.60	ld	0.52
FI	Oulanka	-	0.66	0.32	0.60	0.53	0.47	0.43
FR	Donon	-	-	-	-	-	ld	ld
FR	Revin	-	-	-	-	-	ld	0.41
FR	Bonnevaux	-	-	-	-	-	0.59	ld
GB	Eskdalemuir	0.67	0.67	0.61	0.40	0.26	0.53	0.38
GB	Lough Navar	0.75	0.50	ld	0.46	0.47	-	0.38
GB	Yarner Wood	-	-	-	-	-	-	0.31
GB	High Muffles	-	-	-	-	-	-	0.20
GB	Strath Vaich	-	-	-	-	-	-	ld
GB	Aston Hill	ld	0.40	0.52	ld	0.46	-	ld
GB	Bottesford	0.51	0.46	0.42	ld	0.52	0.43	0.31
GB	Bush	0.74	0.56	0.56	0.40	0.16	ld	0.34
GB	Glazebury	ld	ld	0.40	0.28	0.42	0.30	0.25
GB	Great Dun fell	0.69	0.64	0.57	0.48	0.51	-	0.41
GB	Harwell	ld	0.39	0.42	0.32	ld	ld	0.33
GB	Ladybower	0.56	0.40	ld	ld	0.53	ld	ld
GB	Lullington Heath	-	-	-	-	-	-	0.52
GB	Sibton	ld	0.60	0.61	0.46	0.66	0.46	0.61
IE	Mace Head	ld	0.67	0.56	0.40	0.33	-	0.36
IT	Montelibretti	-	-	-	-	-	ld	0.25
IT	Ispra	0.43	0.54	0.45	0.37	0.55	0.55	0.48
LT	Preila	-	-	-	ld	0.37	ld	ld
LV	Rucava	-	-	-	-	0.54	0.67	ld
NL	Witteveen	0.51	ld	0.69	0.62	0.76	-	-
NL	Bilthoven	0.45	0.59	ld	-	-	-	-
NL	Kollumerwaard	-	0.64	0.66	0.61	ld	0.55	-
NL	Vredepeel	-	-	ld	0.59	0.74	0.57	-
NO	Birkenes	0.61	0.65	0.45	0.58	0.64	0.54	0.57
NO	tustervatn	-	ld	0.34	0.55	0.54	0.40	0.40
NO	Jergul	ld	0.53	ld	0.51	ld	0.30	0.28
NO	Kaarvatn	ld	ld	0.43	0.60	0.44	0.32	0.43

continued on next page

CC	Site	1989	1990	1992	1993	1994	1995	1996
NO	Osen	-	0.59	0.54	0.55	ld	0.50	0.44
NO	Zeppelinfjellet	ld	0.05	0.14	0.14	-0.06	0.01	0.02
NO	prestebakke	0.59	0.68	ld	0.54	0.52	0.58	0.65
NO	Nordmoen	0.50	0.54	ld	0.49	0.59	0.44	0.29
NO	Jeloya	ld	0.68	ld	ld	0.68	0.42	0.53
NO	Hoylandet	0.53	-	-	-	-	-	-
NO	Svanvik	ld	0.44	ld	0.38	0.43	0.50	ld
NO	Voss	-	ld	0.43	0.56	0.62	0.48	0.49
NO	Valle	-	ld	ld	-	-	-	-
NO	Sogne	-	-	ld	0.61	0.59	-	-
PL	Jarczew	-	-	-	-	-	ld	ld
PL	Sniezka	-	-	-	-	-	ld	ld
PL	Leba	-	-	-	-	-	ld	ld
PL	Diabla gora	-	-	-	-	-	-	ld
PT	Monte Velho	ld	ld	0.20	0.43	ld	-	-
RU	Janiskoski	-	-	-	-	-	0.36	ld
RU	Shepeljovo	-	-	-	-	-	0.37	-
SE	Rorvik	ld	0.53	0.66	0.57	0.59	0.61	0.57
SE	Velen	0.60	-	-	-	-	-	-
SE	Vavihill	ld	0.68	0.68	0.67	0.65	0.54	0.57
SE	Aspvreten	0.67	ld	0.64	ld	ld	0.64	0.53
SE	Esrange	-	-	0.46	ld	0.38	0.31	0.33
SE	Ammarnas	ld	-	-	-	-	-	-
SE	Norra Kvill	-	-	-	-	-	-	0.46
SE	Sannen	ld	-	-	-	-	-	-
SE	Storulvsjon	ld	-	-	-	-	-	-
SE	Vindeln	0.57	0.51	0.48	0.60	0.62	0.45	0.46
SI	Zavodnje	-	-	ld	0.58	ld	0.57	0.60
SI	Krvavec	-	-	0.47	0.61	ld	0.69	-
SI	Kovk	-	-	ld	ld	ld	ld	0.54
SK	Chopok	-	-	-	-	ld	ld	ld
SK	Stara-lesna	-	-	0.51	ld	ld	0.53	-
SK	Starina	-	-	-	-	0.16	0.29	0.63
TR	Cubuk II	-	-	-	-	ld	-	-

Notes:
CC is country-code
"-" indicates no data submitted to CCC
"ld" indicates <90% data-capture

2.3 6-Monthly Means

In previous reports dealing with the Lagrangian ozone model we have plotted 6-monthly means of daily maximum ozone. This has the advantage of selecting for each day the peak ozone, which usually will occur at either 12 or 18 GMT in the model output. The disadvantage of this procedure is that we will sometimes be comparing a maximum ozone value obtained at, say, 18 GMT with a measured peak from, say, 8 GMT. In order to avoid this problem we will here compare maps of modelled versus observed noontime (12 GMT) ozone values. However, before considering these maps, we compare the two methodologies. Figure 2.1 shows scatter plots of the modelled versus observed ozone derived from multi-annual comparison, for both modelled

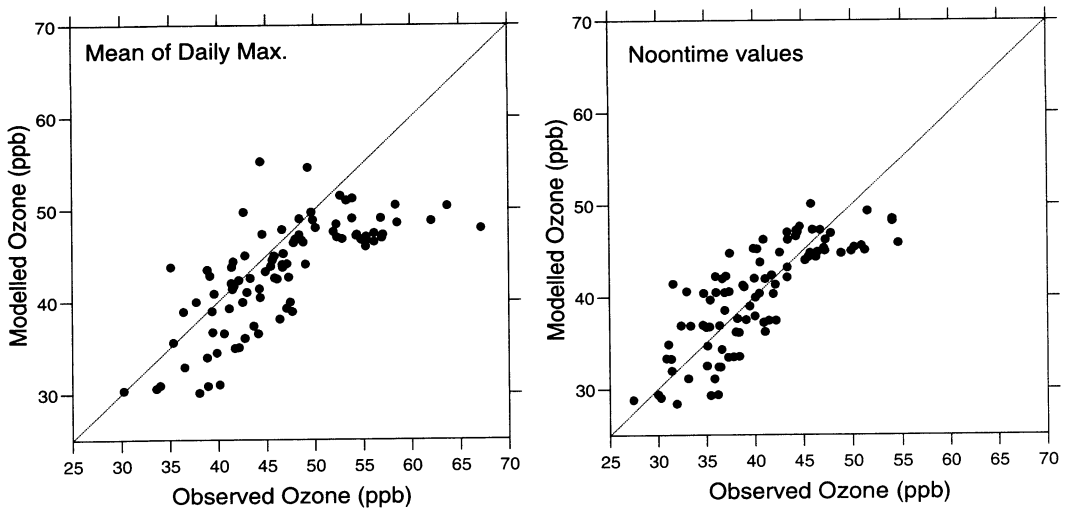

Figure 2.1: Modelled versus Observed 6-monthly Ozone Means. For Modelled Mean of Daily Max. Ozone (left) and Modelled Noontime (12 GMT) Ozone (right). Data from 1989-1996 datasets, see text.

mean of daily max. and noontime ozone. The two plots are similar and indeed both show that the modelled values have a good correlation with observed ozone. The comparison of noontime ozone is clearly better though, with a good 1:1 correspondance between modelled and observed values over the whole range, from 30-55 ppb. The plot with mean of daily max. ozone values is more scattered, with outliers at high observed ozone (the site with highest ozone here is Ispra).

Maps of modelled and observed noontime ozone values are given in Figure 2.2, with the difference between these plots illustrated in Figure 2.3. The measurement sites used to derive these maps are also indicated. The two maps show very similar gradients across Europe. Model under-predictions of about 2-8 ppb are seen in Scandinavia, central Spain, The Czech Republic, N. Italy and southern Greece. Model over-predictions of between 2-8 ppb are seen over parts of Germany, mid-Italy, N. Ireland and parts of Spain. The largest over-prediction occurs in NW Spain. Modelled and observed values match very well over most of the UK, southern Scandinavia, NE and southern Germany, Switzerland and Austria.

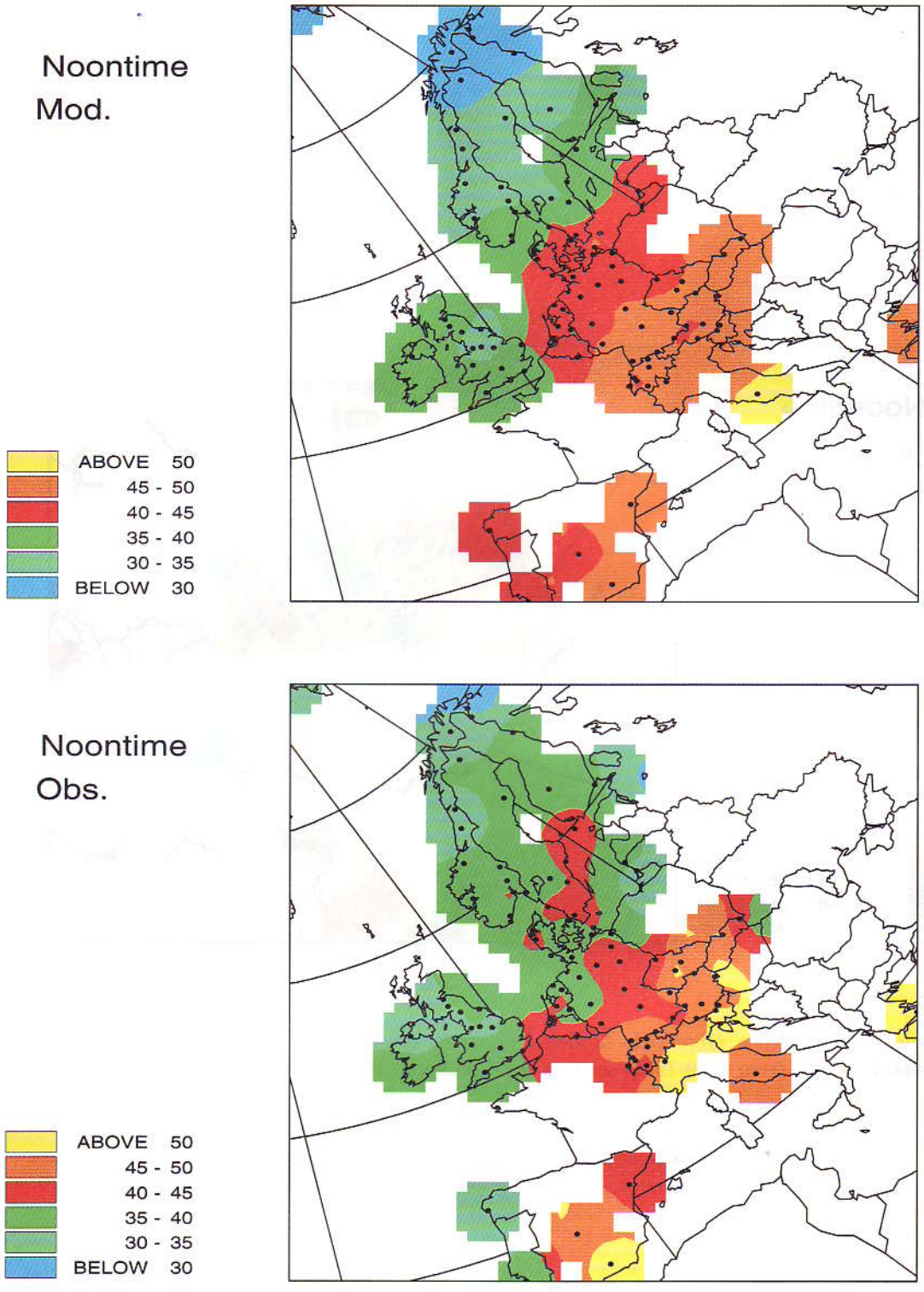

Figure 2.2: Modelled (top) and observed (bottom) noontime ozone values, averaged over April-September, using available results from 1989-1996: see text for discussion. units: ppb

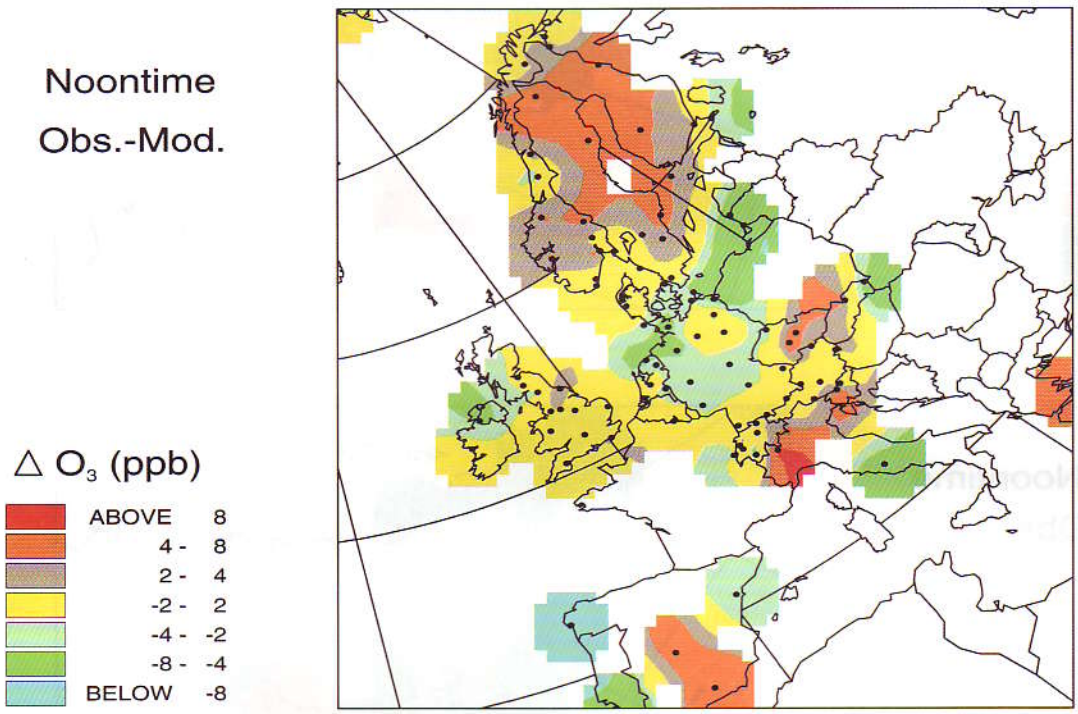

Figure 2.3: Difference, Observed - Modelled noontime ozone values, averaged over April-September, using available results from 1989-1996: see text for discussion. units: ppb

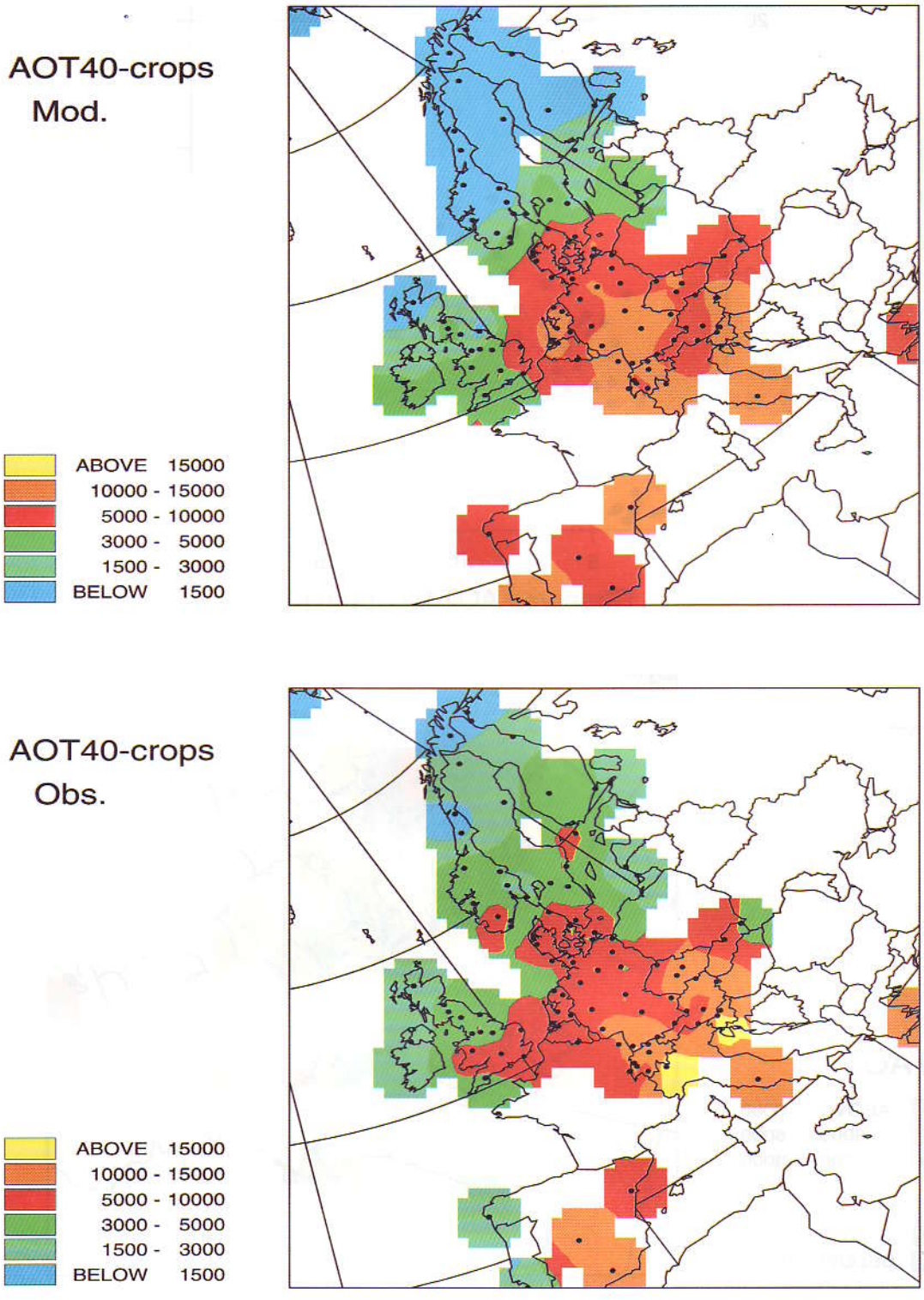

Figure 2.4: Modelled (top) and observed (bottom) AOT40-crops, average value using available results from 1989-1996: see text for discussion. units: ppb h

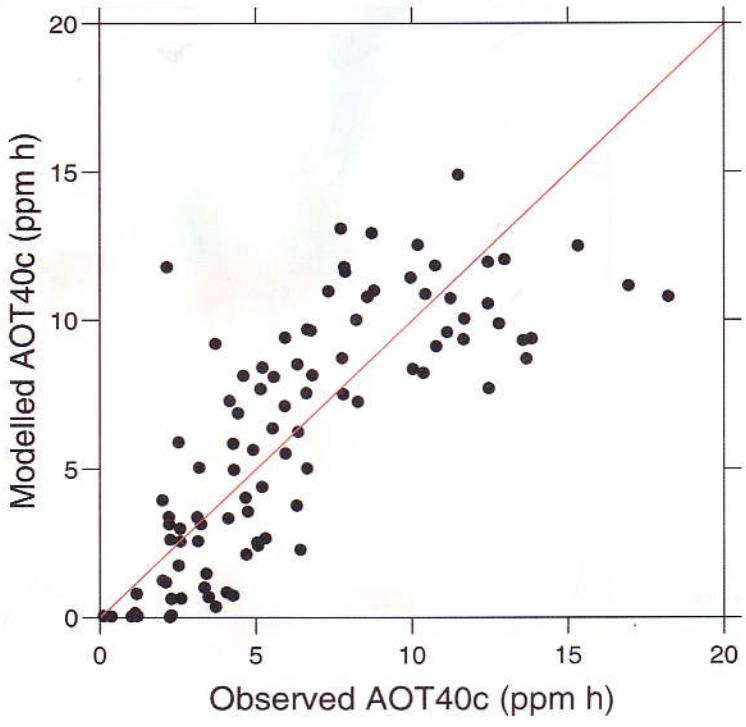

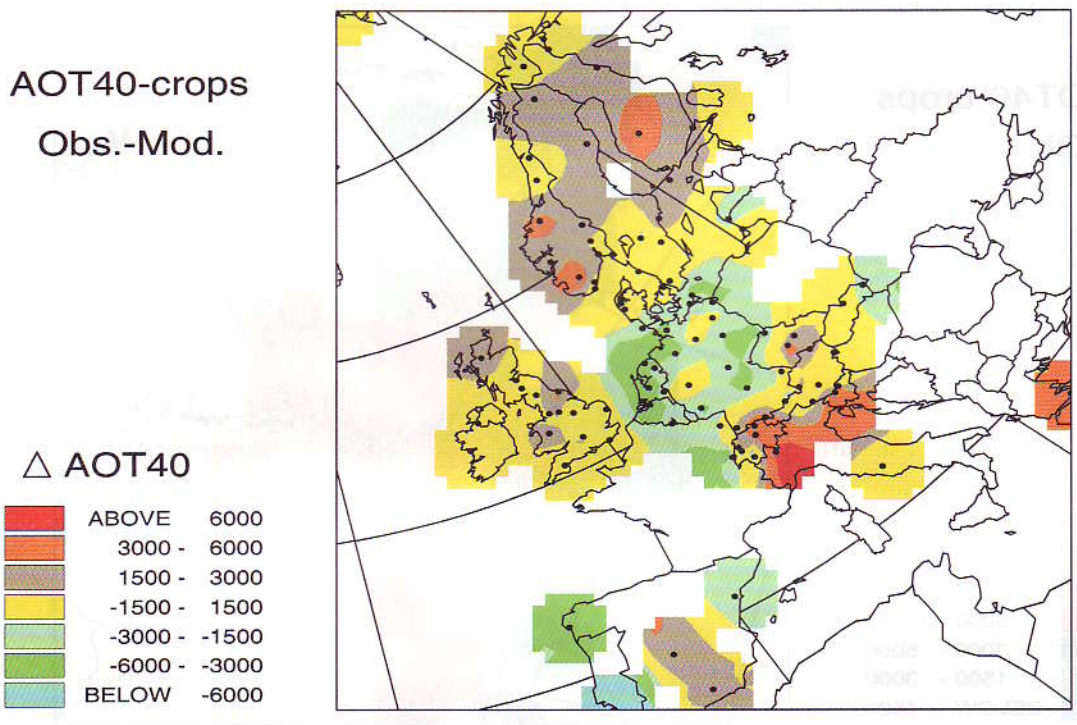

Figure 2.5: Top: Modelled versus Observed AOT40-crops, Bottom: Difference, Observed - Modelled AOT40-crops. AOT40 values derived from 2.4.

2.4 Comparisons: AOT40 and AOT60

2.4.1 First: a warning

AOT40 and AOT60 have acquired importance because of their role as indicators of ozone damage. Unfortunately both statistics have the severe disadvantage that they are very sensitive to small systematic errors in either the model or the measurements. Such errors are unavoidable and have many sources. Observations of ozone should usually have a good accuracy and precision with modern instruments, but calibration procedures are not uniform across the EMEP network and uncertainties of at least ±5% seem very likely. In addition, measurements are affected by site placement and local NO_x sources, so reported ozone values cannot represent the perfect regional average for an EMEP grid square. For the ozone model, there are obviously uncertainties introduced by the structure, chemical scheme, etc.. There are also acknowledged uncertainties in all of the input data, for example NO_x and VOC emissions inputs (especially biogenic VOC), or assumed background tropospheric ozone values.

Thus, one may assume that a model which is able to reproduce measurements within even ±10% is doing very well indeed. Unfortunately even this very good level of agreement may give rather bad comparisons with statistics such as AOT60.

In order to illustrate this, we have calculated AOT40 and AOT60 values for a number of measurement sites, assuming:

a) The "real" ozone concentrations are represented by the measurements

b) The "real" ozone concentrations are 10% lower than the measurements

c) The "real" ozone concentrations are 10% higher than the measurements

The calculated AOT values are given in Table 2.2. This Table clearly shows that all AOT calculations are very sensitive to even moderate bias, especially AOT60. Of course, sites with very low AOT (e.g. Uto) have the greatest uncertainty, but even sites with high AOT values (Waldhof, Ispra) show factor of two differences in both AOT values. As 10% biases are very likely in either measurements or modelling, then this table suggests that it is unreasonable to expect better much agreement for the model versus observed comparison than that suggested by the illustrative Table 2.2.

A corollary of this large uncertainty is that AOT-comparisons are very poor tools for evaluating models. However, such comparisons are shown in this report because of the strong policy interest in the model predictions of AOT values.

2.4.2 Results

Figure 2.5(top) illustrates the agreement between modelled and observed multi-year average $AOT40_c$. The agreement is very satisfactory, especially given the inevitable problems discussed above. Despite some scatter there is an almost 1:1 correspondence between modelled and observed values. The outlier at high observed AOT on these plots is the Italian site Ispra. The outlier at low (ca. 2.5 ppm h) observed AOT and high modelled AOT40 (ca. 8 ppm h) is the Portuguese site Monte Velho, another site where local influences may be rather strong.

Year-by-year AOT40 comparisons are presented for some sites in Fig. 2.7. These plots also indicate surprisingly good agreement, almost always within a factor of two except for those sites with very low AOT40 values, or for the two problem sites Ispra and Monte Velho.

Figure 2.6 illustrates the corresponding agreement between modelled and observed 5-year average AOT60. The year-by-year AOT60 are given for a number of sites in Fig 2.8. Again, the outlier at high observed AOT on these plots is Ispra. Overall the results are not as good as those obtained for AOT40, but this is expected for such a sensitive statistic. As noted above these plots can not be used to evaluate the EMEP model, but especially for policy use it is encouraging that the EMEP results are again generally within a factor of two for these sites.

Table 2.2: Illustration of the effects of biases on calculated AOT40 and AOT60 values

CC	Site	AOT40[1]			Uncertainty[2]
		(a)	(b)	(c)	(%)
AT	Koloman	23152	15256	32025	72
CH	Payerne	15880	10228	22617	78
DE	Waldhof	22752	15644	30877	67
FI	Uto	3124	1464	5560	131
IT	Ispra	32785	24344	41778	53
NO	Birkenes	6549	3509	10559	108
CC	Site	AOT60[1]			Uncertainty[2]
		(a)	(b)	(c)	
AT	Koloman	4135	1649	7951	152
CH	Payerne	2324	702	4964	183
DE	Waldhof	6627	3783	10357	99
FI	Uto	27	250	0	914
IT	Ispra	12867	8042	18576	82
NO	Birkenes	534	165	1301	213

Notes:
1. AOT values calculated using (a) observations directly, (b) observations minus 10%, (c) observations plus 10%. All AOT values are 6-monthly, calculated between 9-21 hours.
2. Uncertainty calculated as $100 \times |AOT(c) - AOT(b)|/AOT(a)$

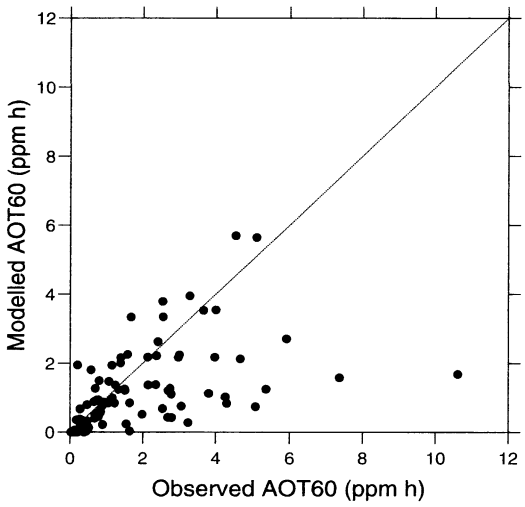

Figure 2.6: Modelled versus observed AOT60 - multi-annual average

2.5 Frequency distributions

Cumulative frequency distributions (CFD) plots of the modelled and observed 12 GMT ozone values have been calculated for 24 sites which have a data–capture of better than 90% for the 5-year period 1989-1994 (ex 91). The intention is to illustrate the ability of the EMEP model to reproduce the statistical behaviour of ozone over long periods. These plots are shown in figures 2.9-2.10.

These plots highlight some interesting differences in performance though. For example, the modelled CFDs for most Swedish sites (Vavihill, Aspvreten, Rorvik) are very similar to the observed, but for the most northerly site, Vindeln, the model shows significant underprediction. The most northerly Norwegian sites (Jergul, and to a lesser extent Svanvik) show similar underpredictions. On the other hand a large number of sites in southern Scandinavia, the United Kingdom, and Germany show very close agreement at nearly all percentile levels. As usual Ispra in Italy stands out, with much higher observed values than modelled for most percentiles.

On the whole, these frequency distributions demonstrate that the Lagrangian model achieves a very acceptable performance for most countries and sites, and for all concentration levels, when predicting ozone over a 5-year period.

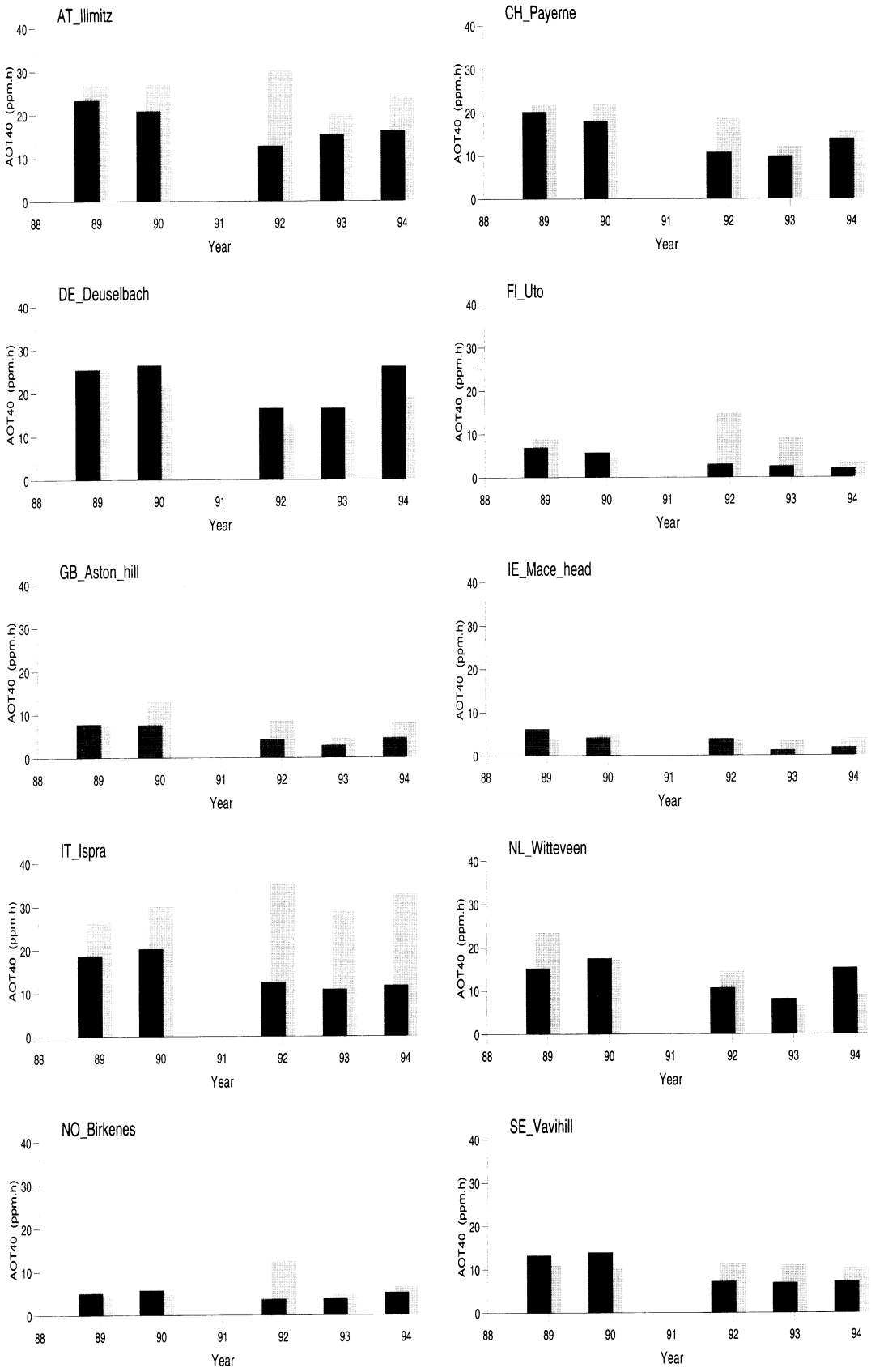

Figure 2.7: Modelled (dark shading) versus observed (light shading) AOT40 (ppm.h)

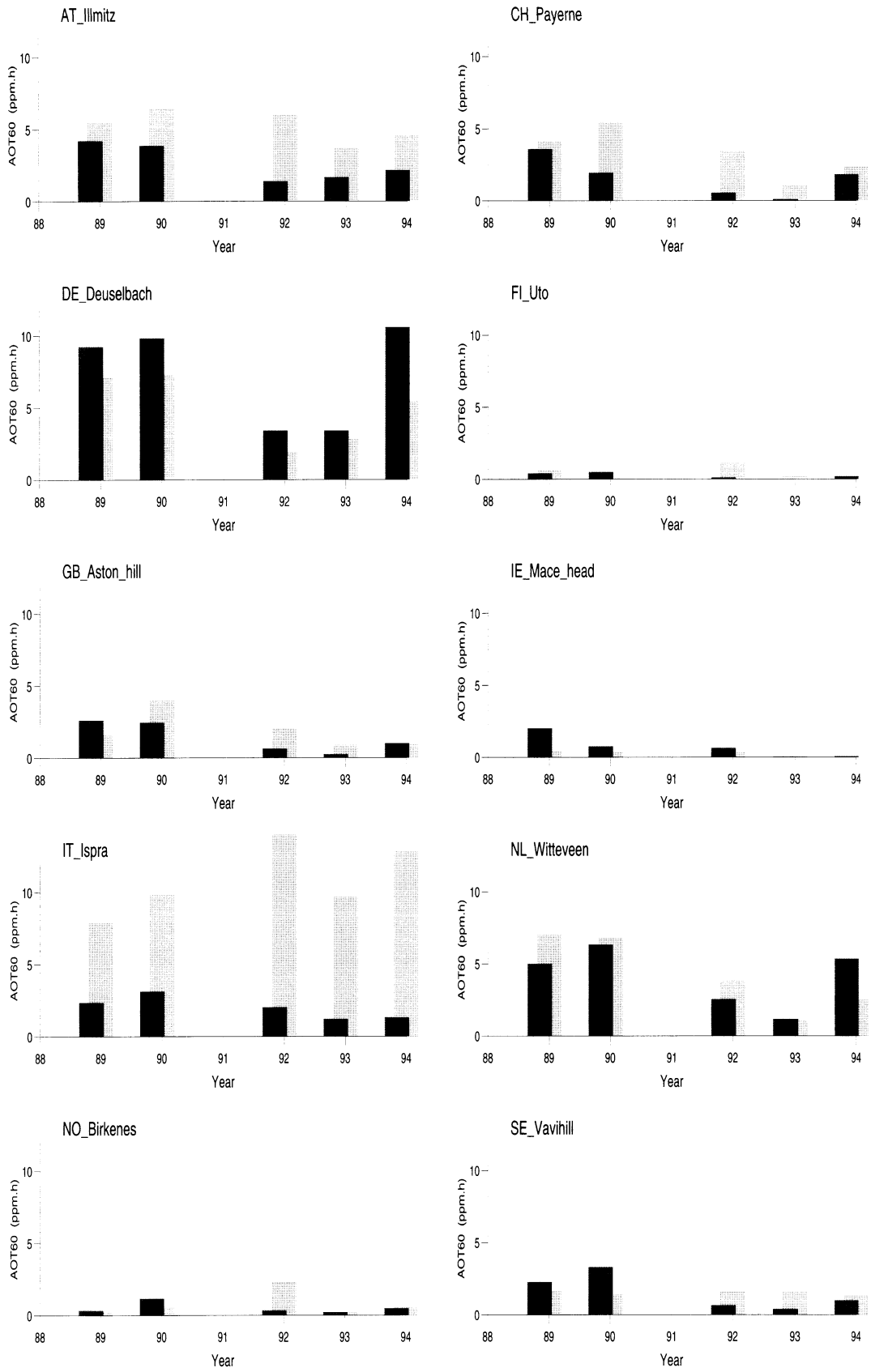

Figure 2.8: Modelled (dark shading) versus observed (light shading) AOT60 (ppm.h)

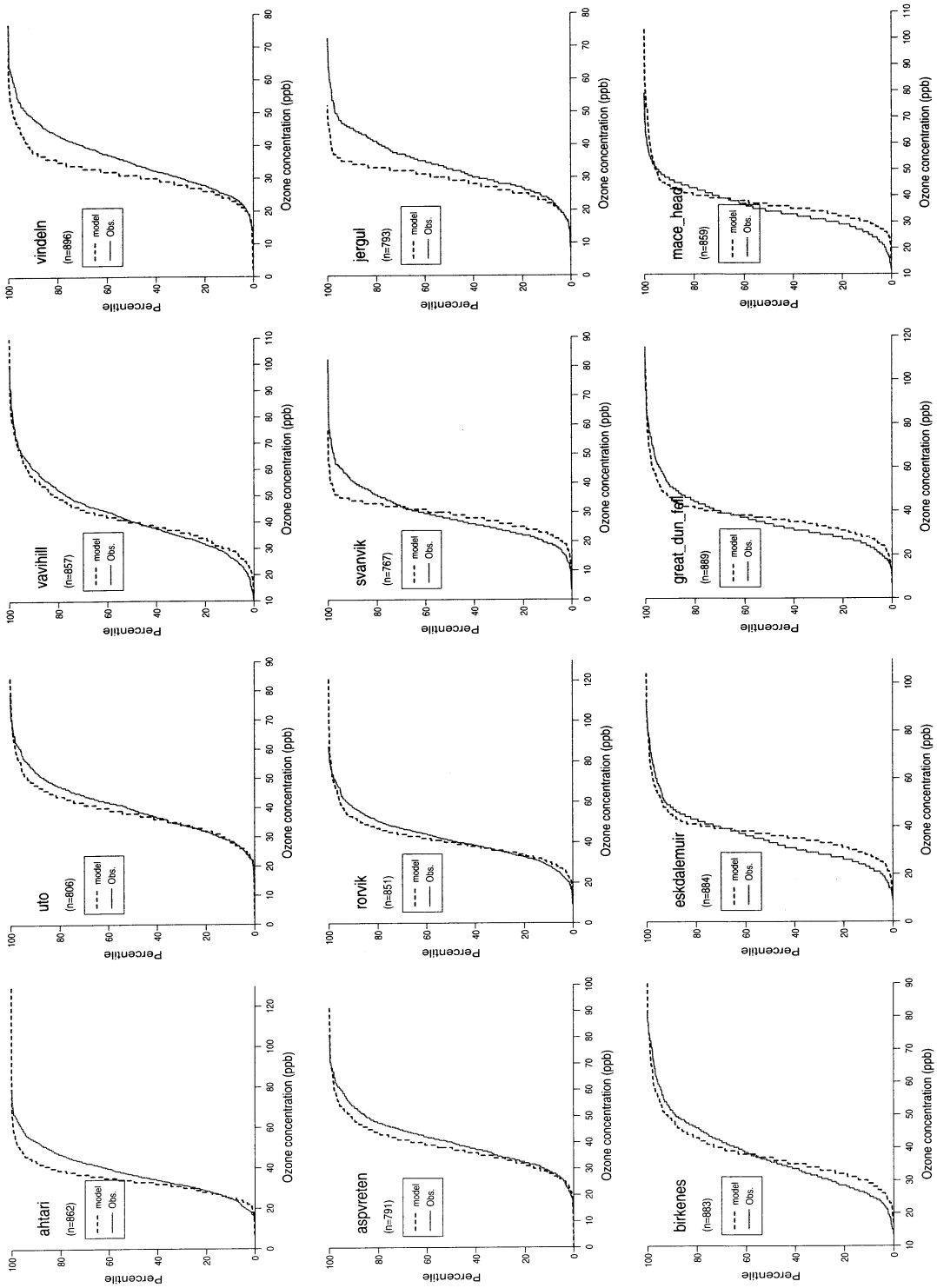

Figure 2.9: Frequency distributions of 12 GMT ozone concentrations. No. of data values given in parentheses. Sites from Finland (Ahtari, Uto), Sweden (Vavihill, Vindeln, Aspvreten, Rorvik), Norway (Svanvik, Jergul, Birkenes), and the UK (Eskdalemuir, Great Dun Fell, Mace Head).

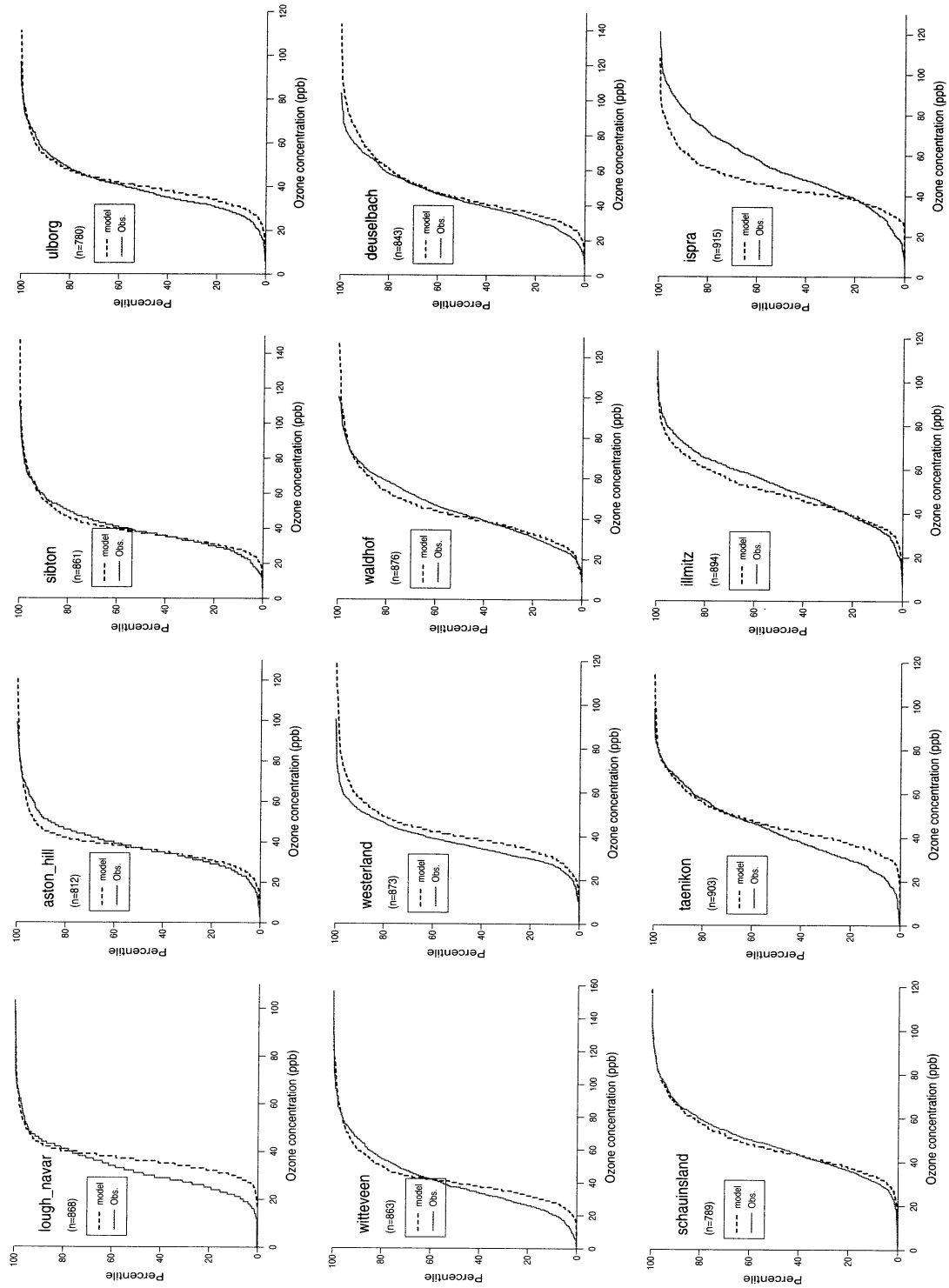

Figure 2.10: Frequency distributions of 12 GMT ozone concentrations, cont.. No. of data values given in parentheses. Sites from UK (Lough Navar, Aston Hill, Sibton), Denmark (Ulborg), Netherlands (Witteveen), Germany (Westerland, Waldhof, Deuselbach, Schauinsland), Switzerland (Taenikon), Austria (Illmitz), and Italy (Ispra).

Chapter 3

Discussion and Conclusions

This report has presented the results of a multi-year comparison of the results from the EMEP MSC-W Lagrangian oxidant model with measurements. One of the main motivations for this comparison was that the model and its results are already in use in helping to guide environmental decisions within the framework of the EU acidification and ozone strategy and within UN-ECE activities. Whilst policy makers cannot wait for the perfect ozone model (they would have to wait forever) it is important to show that the tools which are in use do reproduce the main features of ozone formation in Europe to a reasonable extent.

There have also been a large number of requests from scientists running the measurement sites, or with interest in seeing how the model performs in particular areas. In order to satisfy all these requests we have presented data from all stations and all years in this report.

A very large number of sites are now available for evaluating the performance of the EMEP ozone models. The geographical domain of the measurement network has been substantially extended, both eastwards and southwards since the last extensive model evaluation exercise of Malik et al. (1996).

In general, model performance over the years is similar to that obtained in this previous comparison, at least for the older sites for which data was available in that year. Over most of northern, western and central Europe the model performs rather well for all years (excluding a two-week episode at high latitudes). At many of the new sites, in the Czech Republic, Latvia, Lithuania, Slovenia, and Slovakia the model also seems to perform almost as well. The model performance in southern Europe and in Poland and Russia is markedly worse, but unfortunately there are still not many sites covering this area, and there are some questions about the representativeness of the existing sites. More measurements from these areas are still required before any good analysis can be given of how well any large-scale air pollution model performs in the Mediterranean.

It should be noted that there are other difficulties in evaluating the model in some of these regions, especially in the Mediterranean. The quality of the emissions inventory has been in most cases not assessed to the same extent as those in NW Europe. The biogenic emissions in particular are still very poorly known (Simpson, 1995, Seufert et al., 1997). Terpene emissions may be significant, but because of a lack of knowledge of their atmospheric chemistry we have not attempted to include these yet into the EMEP model. All of these questions need addressing before much progress can be made in reliably evaluating any model in these regions.

Ozone alone does not form the best basis for evaluating photochemical oxidant models. It is a pollutant whose concentrations vary within quite a small range, usually within a factor of two or three. This is in marked contrast to the concentrations of other primary and even secondary species where concentrations often range over an order of magnitude. However, the fact that the ozone model seems to perform consistently well over so many years and in many different geographical regions is encouraging. The main problems arising from this study seem to be in southern Europe, so more attention should be paid to model evaluation in this region in future. (Still, very few measurements have been submitted, which prevents any thorough

analysis of either the extent to which the model does have problems, or to suggest any likely causes for this).

Comparisons for a few other species, including PAN and total nitrate, were presented in Simpson (1992), with quite acceptable agreement, although worse results were found by Hov et al. (1997) . Generally very few measurements exist of species which are suitable for evaluating model performance very strictly. However, a very useful set of hydrocarbon and carbonyl measurements has been collected within EMEP and used for model evaluation, as reported by Solberg et al. (1995). This work has demonstrated that the EMEP model does a very good job of predicting HCHO, sum of aldehydes and even total VOC at most sites. As the aldehydes are an end-product of ozone chemistry, and thus an indicator of the chemical processing of the air mass, the ability of the model to match both the total VOC and the products is very encouraging.

In Part III of this report the modelled 6-monthly mean results for SO_2, NO_2, total nitrate (HNO_3+particulate NO_3), and sulphate are compared with observed results for 1996. These seasonal results add little in helping to interpret the performance of the model, however. More detailed analysis, using a range of high-quality measurements from the same site are probably necessary to make further progress in evaluating the model, and in particular if we are to disentangle the effects of model structure from model chemistry, anthropogenic emissions from biogenic emissions, etc.

3.1 A final word

Comparisons between modelled and observed ozone values have been presented at a large number of meetings over the last 8 years. An almost unavoidable conversation has recurred at nearly of these meetings:

> **Questioner** You have shown plots for many sites. However, why haven't you shown plots from my country ? We have 1067 ozone stations ...
>
> **EMEP modeller** I have heard rumours about those stations. Have you sent them to EMEP/CCC ?
>
> **Q.** No, but you should have them ...
>
> **E.M.** Please send your data to CCC. If you do, I will run simulations for those data and we can both see the result. We are keen to evaluate the model in your country.
>
> **Q.** I'll do that!

All good and well. Two years later, usually another person, from possibly another country, but often the same, stands up, and begins:

> **Questioner** You have shown plots for many sites. However, why haven't you shown plots from my country ? We have 1067 ozone stations .....
>
> .....

3.2 References

Amann, M., Bertok, I., Cofala, J., Gyarfas, F., Heyes, C., Klimont, Z., Makowski, M., Schöpp, W., and Syri, S., 1998, Cost-effective control of acidification and ground level ozone. part b: Ozone scenarios, Fifth Interim Report to the European Commission, DG-XI, International Institute for Applied Systems Analysis (IIASA), Part 2 of the Report to CONCAWE, July 1994.

Andersson-Sköld, Y. and Simpson, D., 1997, Comparison of the chemical schemes of the EMEP MSC-W and the IVL photochemical trajectory models, Norwegian Meteorological Institute, EMEP MSC-W Note 1/97.

Builtjes, P.J.H., Simpson, D., Zlatev, Z., Christensen, J., and Frohn, T.P. ., 1991, Comparison of three models for long term photochemical oxidants in Europe, Report 3/91.

Derwent, R.G., 1990, Evaluation of a number of chemical mechanisms for their application in models describing the formation of photochemical ozone in Europe, *Atmos. Environ.*, 24A, No. 10, 2615–2624.

Derwent, R.G., 1993, Evaluation of the chemical mechanism employed in the EMEP photochemical oxidant model, *Atmos. Environ.*, 27A, No. 2, 277–280.

Hass, H., Builtjes, P.J.H., Simpson, D., and Stern, R., 1997, Comparison of model results obtained with several European regional air quality models, *Atmos. Environ.*, 31, No. 19, 3259–3279.

Heyes, C., Schöpp, W., and Amann, M., 1996, A simplified model to predict long-term ozone concentrations in Europe: The core of an integrated assessment model, In *Workshop on the control of photochemical oxidants over Europe, 24-27 October 1995, St. Gallen, Switzerland*, pages 47–62. Federal Office of Environment, Forests and Landscape, Bern.

Hjellbrekke, A.-G., 1995, Ozone measurements 1990-1992, Norwegian Institute for Air Research (NILU), Kjeller, Norway, EMEP/CCC-Report 4/95.

Hjellbrekke, A.-G., 1996, Ozone measurements 1993-1994, Norwegian Institute for Air Research (NILU), Kjeller, Norway, EMEP/CCC-Report 1/96.

Hjellbrekke, A.-G., 1997, Ozone measurements 1995, Norwegian Institute for Air Research (NILU), Kjeller, Norway, EMEP/CCC-Report 3/97.

Hjellbrekke, A.-G., 1998, Ozone measurements 1996, Norwegian Institute for Air Research (NILU), Kjeller, Norway, EMEP/CCC-Report 3/98.

Hov, Ø., Sorteberg, A., Schmidbauer, N., Solberg, S., Stordal, F., Simpson, D., L., A., A., Han., O., Pedr., Lätilä, H., and Heidam, N. Z., 1997, European VOC emission estimates evaluated by measurements and model calculations, *J. Atmos. Chem.*, 28, 173–193.

Kuhn, M., Builtjes, P.J.H., Poppe, D., Simpson, D., Stockwell, W.R., Andersson-Sköld, Y., Baart, A., Das, M., Fiedler, F., Hov, Ø., Kirchner, F., Makar, P.A., Milford, J.B., Roemer, M.G.M., Ruhnke, R., Strand, A., Vogel, B., and Vogel, H., 1998, Intercomparison of the gas-phase chemistry in several chemistry and transport models, *Atmos. Environ.*, 32, No. 4, 693–709.

Malik, S., Simpson, D., Hjellbrekke, A.-G., and ApSimon, H., 1996, Photochemical model calculations over Europe for summer 1990. Model results and comparison with observations, Norwegian Meteorological Institute, Oslo, Norway, EMEP MSC-W Report 2/96.

Poppe, D., Andersson-Sköld, Y., Baart, A., Builtjes, P.J.H., Das, M., Hov, Ø., Kirchner, F., Kuhn, M., Makar, P.A., Milford, J.B., Roemer, M.G.M., Ruhnke, R., Simpson, D., Stockwell, W.R., Strand, A., Vogel, B. ., and Vogel, H., 1996, Intercomparison of the gas-phase chemistry of several numerical chemistry and transport models, EUROTRAC special report, Garmisch-Partenkirchen.

Seufert, G., Bartzis, J., Bomboi, T., Ciccioli, P., Cieslik, S., Dlugi, R. ., Foster, P., Hewitt, C. N., Kesselmeier, J., Lenz, D. Kotzias R., Manes, F., Perez-Pastor, R., Steinbrecher, R., Torres, L., Valentini, R., and Versino, B., 1997, The bema-project: and overview of the castelporziano experiments., *Atmos. Environ.*, 31, No. SI, 5–18.

Simpson, D., Andersson-Sköld, Y., and Jenkin, M. E., 1993, Updating the chemical scheme for the EMEP MSC-W oxidant model : current status, Norwegian Meteorological Institute, EMEP MSC-W Note 2/93.

Simpson, D., Olendrzyński, K., Semb, A., Støren, E., and Unger, S., 1997, Photochemical ox-

idant modelling in Europe: multi-annual modelling and source-receptor relationships, Norwegian Meteorological Institute, EMEP MSC-W Report 3/97.

Simpson, D., 1992, Long period modelling of photochemical oxidants in Europe. Calculations for July 1985, *Atmos. Environ.*, 26A, No. 9, 1609–1634.

Simpson, D., 1993, Photochemical model calculations over Europe for two extended summer periods: 1985 and 1989. Model results and comparisons with observations, *Atmos. Environ.*, 27A, No. 6, 921–943.

Simpson, D., 1995, Biogenic emissions in Europe 2: Implications for ozone control strategies, *J. Geophys. Res.*, 100, No. D11, 22891–22906.

Solberg, S., Dye, C., Schmidbauer, N., and Simpson, D., 1995, Evaluation of the VOC measurement programme within EMEP, Kjeller, Norway, Norwegian Institute for Air Research (NILU) Report 5/95.

Part II

The Eulerian 3-D oxidant model: status and evaluation for summer 1996 results and case-studies.

J. E. Jonson, L. Tarrason, J. Sundet, T. Berntsen and S. Unger

Chapter 1

Introduction

In 1997 results from the EMEP Eulerian photo-chemistry model, also called the MACHO model (Multi-layer Atmospheric CHemistry Model, Oslo) were presented for the first time (Jonson et al. 1997) for a one month calculation. Comparisons with measurements were made, predominantly for ozone. It was shown that the model was able to reproduce major ozone events over Europe for May 1992.

Since last year several model updates have been made. A major difference is that the model chemistry has been extended so that sulphur and ammonia components are also included. Thus, all chemical components calculated in the EMEP Eulerian acid deposition model (Bartnicki et al., 1998) are also included in the EMEP Eulerian photo-chemistry model. The aqueous phase chemistry and wet deposition parameterization from the EMEP Eulerian acid deposition model is also included. A major activity in the past year has been to upgrade the program code to reduce CPU time for the calculations. The model changes are described in more detail later in the text.

In this report model calculations and measurements in the EMEP network are compared for the 6 summer months April-September 1996 The EMEP Eulerian acid deposition model is also run for 1996.

In collaboration with the University of Oslo (UiO), model results are also compared to surface and free tropospheric measurements from several European research projects.

- In the first part of June 1996 extensive measurements were carried out under the EU project PAUR - see section 3.1.3.
- An extensive set of measurement were made in the upper troposphere as part of the German Schadstoffe in der Luft campaign in July 1996. This campaign is related to the EU project POLINAT - see section 3.2.1.
- The model has also been run for the June -July 1995 period, corresponding to the POLINAT 1 measurement campaign (section 3.2.2). Model results are compared to measurements in the upper troposphere for this period.

Chapter 2

Model updates

Several model updates have been made since the first presentation of the model. Model updates have been made serving two purposes:

- Optmisation of the model performance with regard to speed up of model simulations.
- Extensions and improvements of the parameterizations in the mode.

2.1 Model optimisation

The performance of the model was analyzed introducing time measurements for the main parts by means of irtc()-calls. Test runs have been made for a real time period of 6 hours, reading in two sets of meteorological data. Runs were performed on 8, 16, 24 and 32 processors on a CRAY T3E parallel computer, assuming a fixed decomposition into 4 parts in the y-direction and a decomposition into 2, 4, 6, 8 parts respectively in the x-direction. The higher number of processors in the x direction was chosen, since the total number of points in this direction (151) better fits a division into 8 parts than the number of points in the y-direction (133). From the measured time characteristics of the pre-optimised model the following conclusions could be drawn:

1. There was a super linear speed-up for the calculation part of the model (without initialization time) for up to 32 processors with respect to the 8 processors run.
2. This super linear speed-up came mostly from the horizontal advection part (speed-up of 4.3 for 32 processors with respect to 8 processors), preparation of the rates and coefficients for the chemistry solver (speed-up of 5.19 for 32 processors with respect to 8) and from the chemistry solver (speed-up of 5.18 for 32 processors with respect to 8).
3. These three parts of the program required a large part of the CPU-time of the model (about 52% for a 8 processor run and 41% for a 32 processor run). The other part that required a large fraction of the CPU-time is vertical advection/diffusion (27% for 8 processors and 26% for 32 processors) and has a linear scaling factor.

Consequently, to shorten the computation time of the model one must look closer to the advection modules and the chemistry solver.

The advection is done by a fourth order Bott scheme in the horizontal and a second order Bott scheme in the vertical (Bott, 1989a, 1989b). A considerable part of the calculations in these schemes is independent of the actual species to be transported. This part of the computations was done separately for each species in the original version of the model. These subroutines were reformulated, so that as much as possible of the calculations can now be made only once, independently of the number of species. The computed, direction dependent fluxes, are subsequently applied to all species in one pass. Here arises another problem: In the original formulation the concentration array had the structure of indices (i,j,k,n), where i index in the west to east direction, j the index in the south to north direction, k the vertical index and n the index for the model species. Consequently, the species dependent coordinate 'n' was the slowest varying index. To avoid introducing large additional 3D arrays for the fluxes, etc. and to hold the structure of the advection routines as it is (with local 1D or 2D

arrays - one geometric dimension + species dimension) the order of indexes in the concentration array was changed to (n,i,j,k). Since the species dependent index n is now the fastest varying index, the loop over n can be the inner most loop, the inflow/outflow tests in the advection routine can be moved outside of this loop and the code can be highly optimized by the compiler. The resulting horizontal advection code is about 7 times faster then the old one. The vertical advection/diffusion code, which allowed in addition other optimization steps, is now more than 18 times faster in the 8 processors case and more than 17 times faster in the 32 processors case. Of course, the super linear speed-up has now virtually disappeared, only a small super linear speed-up in the y-direction (second geometric coordinate) of the advection remains as the program has to access data in the memory, which are separated by smaller strides for higher numbers of processors.

The same reordering of indexes in the concentration array improves performance in the chemistry solver and in the preparation phase, too, since now concentration values for one point of the domain are stored in the memory one after the other and are much faster to access.

The super linear speed-up of the chemistry solver in the original model version arose mainly because the solver accessed concentration values directly from the concentration array, solving the chemical system separately for each point in space. This lead to large jumps through the memory, which are much smaller for higher number of processors where the array dimensions are smaller. Since now concentration values are stored one after the other in the memory, access to memory is much faster, reducing the computation time by a factor 2 for 8 processors and 1.5 on 32 processors.

In the preparation of coefficients for the solver, much time is spent in computing power functions. Since the corresponding powers and bases are clearly away from zero, the power function x^y can be replaced by $exp(y * log(x))$ which is much faster. This results in a 4 to 5 times faster execution of the chemistry in the new model version.

Computation time with the new model version is more than 4 times shorter with 8 processors and more than 3 times shorter with 32 processors. The super linear speed-ups disappear, indicating that the model version makes better use of the cache also for smaller numbers of processors. The speed-up characteristics of the program, when increasing the number of processors, are now smaller but still remain quite high: For the part executed at each time step, speed-up for 32 processors with respect to 8 processors is 3.7, the advection shows slight super linear speed-up of 4.02.

From a practical point of view the main conclusion is that a computation, which previously required the use of 32 processors, can now be made on 8 processors in even somewhat shorter time. A one month run can be made in 6 hours on 8 processors.

The strongest effect of the reordering of indexes is reached in the advection/diffusion part. This can be illustrated by comparing the advection/diffusion times for the EMEP Eulerian acid deposition model and the EMEP Eulerian photo-chemistry model. In the acid deposition model 9 species undergo advection, in the photo-chemistry model 44. In the original model the relation between the times spent in advection for the photo-chemistry model and acid deposition model is about 5.2, reflecting the fact, that the corresponding concentration arrays for the photo-chemistry model are 5 times larger than in the acid deposition model, leading to further decrease in performance above the theoretical value 5. In the new approach this quotient is reduced to about 3.2. This is also illustrated in Figure 2.1

2.2 Model extensions and improvements

In appendix B a comprehensive model description, including changes made since the last report, is presented. Below a short description of these changes, and the motivation for making them, is given.

The number of chemical components in the model has been extended to also include SO_2, SO_4^{2-}, NH_3, ammonium nitrate and ammonium sulphate. Thus all the chemical components calculated in the EMEP Eulerian acid deposition model are now also included in the EMEP Eulerian photo-chemistry model. The model is now using the parameterization of aqueous phase chemistry and wet deposition already implemented in the EMEP Eulerian acid deposition model. Thus, the new model version now includes oxidation of SO_2 by OH in the gas phase

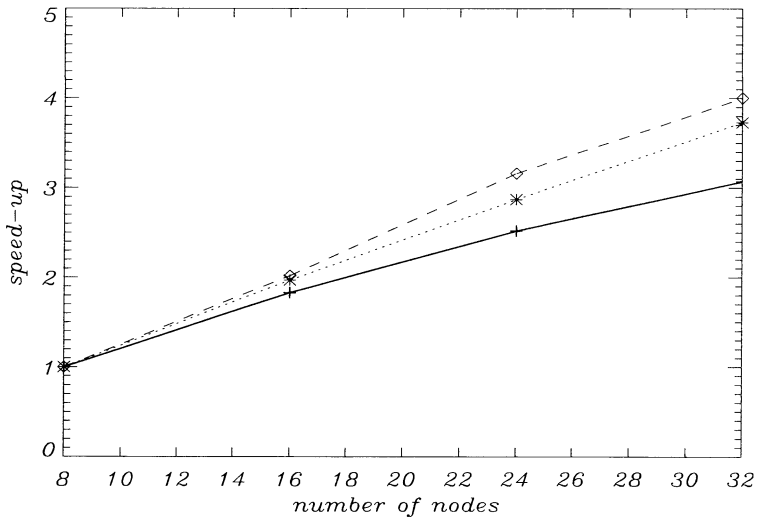

Figure 2.1: The full line is for a total 6 hours model run. The dotted line is for a 6 hour total model run without initialization and the dashed line is for a 6 hours model run with advection only.

and by H_2O_2 and O_3 in the aqueous phase. With the EMEP Eulerian photo-chemistry model we are now able to study concentrations and depositions of sulphur and nitrogen components with a much more comprehensive chemistry scheme than what is used in the EMEP Eulerian acid deposition model. Furthermore, the parameterization of components that are prescribed in the acid deposition model (OH, O_3, H_2O_2) can be validated by using the photo-chemistry model.

The calculation of photolysis rates have been updated according to the recommendations of DeMore et al. (1997). The photolysis rate for O_3 giving O'D is now substantially higher (about 30%) than calculated with previous recommendations.

In the four uppermost model layers initial and lateral boundary concentrations of ozone are now scaled to the potential vorticity. Potential vorticity is a good tracer for stratospheric air. Whereas typical ozone concentrations in the upper troposphere are around 100 ppb_v, concentrations even in the lower stratosphere are often several hundred ppb_v.

Chapter 3

Model results

This chapter is divided into two parts. In the first part model results and model validations against surface measurements are presented. whereas in the second part model results and model comparisons of model results with measurements for the free troposphere are presented,

3.1 Surface concentrations

Here model calculated concentrations are compared to measurements in the EMEP network. Calculated and measured concentrations of NO_2, SO_2, total nitrate (HNO_3 + ammonium nitrate) and ammonium + ammonium nitrate, as well as wet deposition of sulphur, oxidized nitrogen and reduced nitrogen are compared as scatter plots. For ozone NO_2 and total nitrate we also show time-series for a few sites we believe to be representative of their respective regions. For ozone a more comprehensive comparison with measurements, including also the calculations by the EMEP Lagrangian ozone model, is included in part III.

When interpreting the results one should bear in mind that the lifetime of these components is short in the atmosphere (of the order of a few days or less) and large natural variations in concentrations are expected even within a 50 km grid.

3.1.1 Scatter plots.

In Figure 3.1 mean calculated and measured concentrations for the 6 months April to September 1996 are compared as scatter plots. A perfect fit between calculated and measured concentrations would require that the sites should lie along the middle diagonal dotted line. The two dotted lines on the side represent a factor of two difference between calculations and measurements. We require at least 150 days of measurements in the 6 month period for a site to be included.

For NO_2 (Figure 3.1, top left) the calculated mean value for all sites is in good agreement with the measurements. There is however a large scatter. This not surprising as the lifetime of NO_2 in summer can be as low as a few hours only.

Calculated concentrations of total nitrate (Figure 3.1 top right) are over-predicted compared to the measurements. The reason for this is unclear. Calculations with the EMEP Eulerian acid deposition model (Bartnicki et al., 1998) show the same thing. In a recent paper by Slanina et al. (1998) problems related to measurements of particulate nitrate is discussed. They conclude that the measured nitrate concentrations are probably too low, as nitrate particles are likely to evaporate from the filters. However the measurements made in the EMEP network use denuders, and should not have this bias.

Whereas calculated SO_2 concentrations compare well with the measurements (Figure 3.1, bottom left), sulphate (SO_4 + ammonium sulphate) (Figure 3.1, bottom right) is under-predicted by the model, in particular in the bottom left corner of the Figure, where concentrations are low. This underestimation is much less pronounced in the calculations with the EMEP Eulerian acid deposition model (Bartnicki et al., 1998). This is most likely caused by an insufficient oxidation of SO_2 in the aqueous phase. The parameterization of this process will have to be studied in more detail. In polluted areas with high NO_x concentrations the HO_2 radical will react with NO instead of producing H_2O_2. However, other oxidant may contribute

in the oxidation of SO_2 in the aqueous phase as O_2 catalysed by metal ions. There may also be local production of H_2O_2 in the cloud droplets (Jonson and Isaksen, 1993)

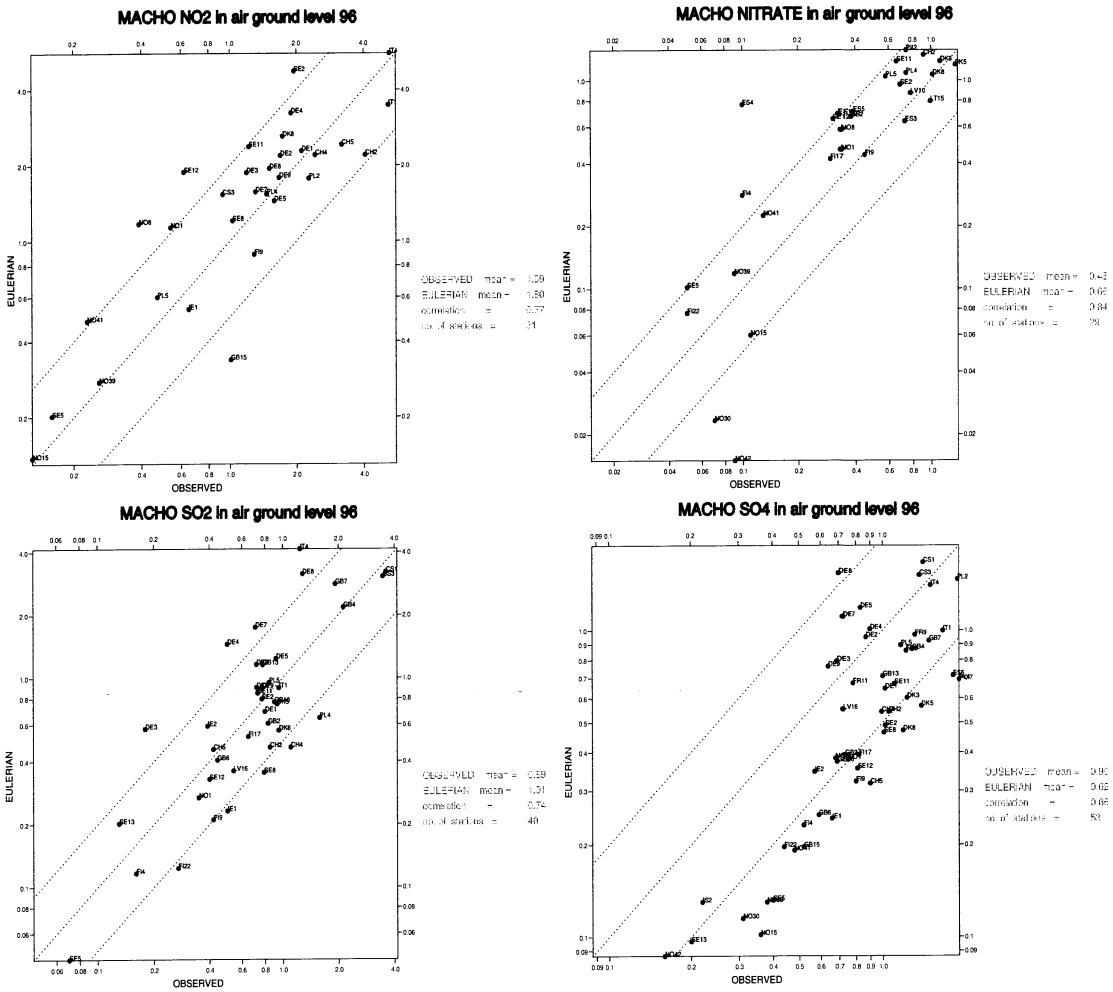

Figure 3.1: Scatter plots for calculated versus measured concentrations μg m^{-3}) for NO_2 and total nitrate as N and SO_2 and sulphate (SO_4) as S.

Calculated concentrations of ammonia + ammonium (Figure 3.2, left) compares favorably with the measurements. Wet deposition of reduced nitrogen (Figure 3.2, right) is under-predicted. This may be related to an under-prediction of sulphate, and subsequently of ammonium sulphate at cloud level, as discussed above.

Also the wet deposition of sulphur (Figure 3.3, left) is under-predicted by the model, again probably caused by an insufficient in-cloud oxidation of SO_2.

For oxidized nitrogen (Figure 3.3, right) the mean calculated deposition is close to the measured.

3.1.2 Time series.

In this part time series with calculated and measured concentrations For O_3, NO_2 and total nitrate are shown for a few selected sites. For O_3, concentrations are shown as daily maximum values. For NO_2 and HNO_3 diurnally averaged concentrations are shown.

In Figure 3.4 calculated and measured ozone at 4 sites, representing northern Europe (Birkenes), central Europe (Schauinsland), southern Europe (Zavodnje) and southwest Europe (Donon), are shown. In part III a more comprehensive comparison of calculated and measured ozone is included. For all four sites the model is to a large extent able to reproduce the day by day ozone variations seen in the measurements. There is a tendency for the model to under-predict concentrations in northern parts of Europe (as Birkenes), and to over-predict concentrations in southern Europe (as Zavodnje).

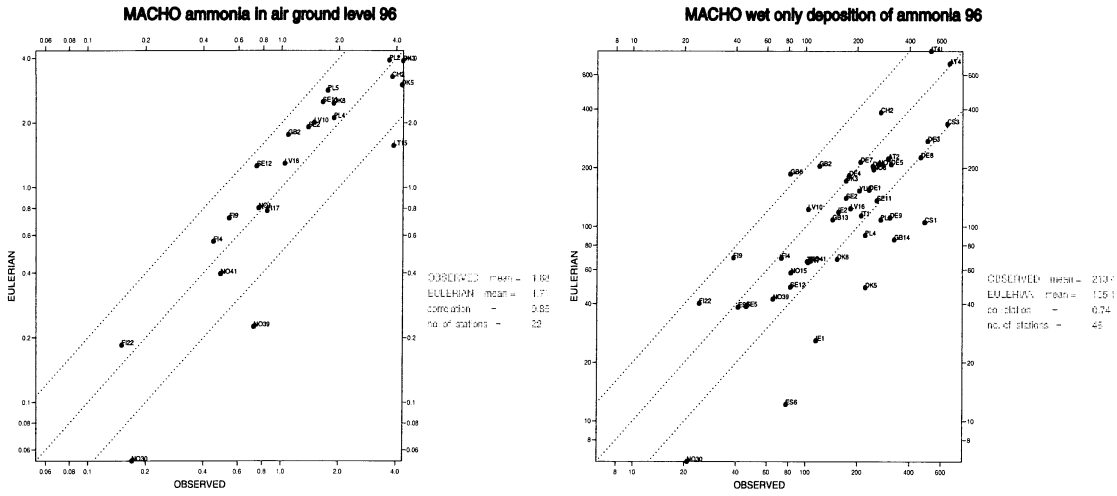

Figure 3.2: Scatter plots for calculated versus measured concentrations of ammonia + ammonium μg N m^{-3}) and as mg N m^{-3} for wet deposition of reduced nitrogen (ammonia).

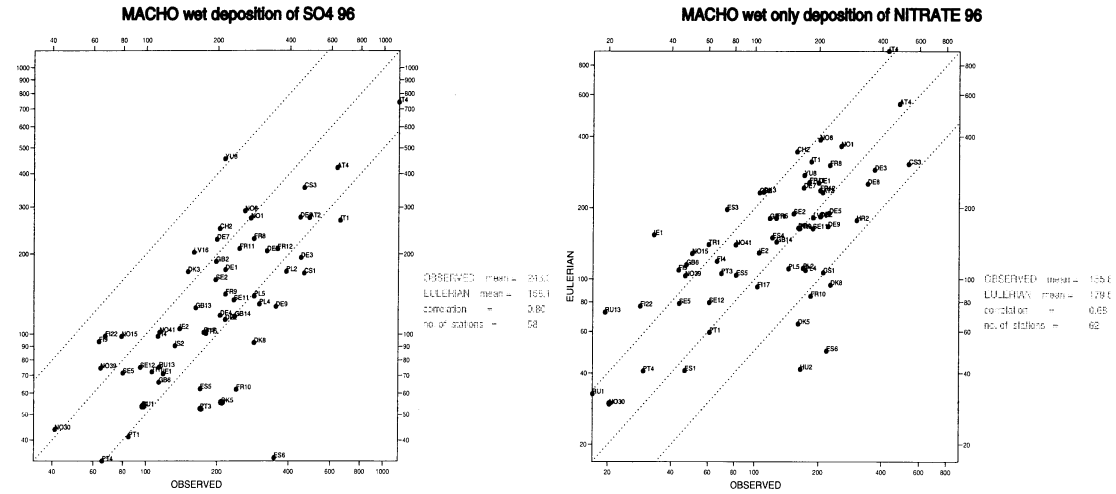

Figure 3.3: Scatter plots for calculated versus measured wet deposition of sulphur as S and oxidized nitrogen (nitrate) as N, both in mg m^{-3}.

In the summer months the lifetime of total nitrate, and in particular NO_2, is short, and much of the variability in the concentrations will be on a smaller scale than the model resolution (50 km). We believe this to be the main reason why the day by day agreement between calculated and measured concentrations For NO_2 (Figure 3.5) and total nitrate (Figure 3.6) is much less impressive than for ozone. Even so, the model does reproduce much of the variations in time seen in the measurements.

3.1.3 The PAUR project

The main objective of the EU project PAUR is to qualify and quantify how increased penetration of UV-B solar radiation through the atmosphere, resulting from stratospheric ozone depletion, affects photochemical production and chemical transformation of ozone and other photochemically active species in the lower atmospheric layers. The project involves a comprehensive set of investigations, which include observed and estimated variations and changes in ozone column densities, observed and calculated solar fluxes and ozone photo-dissociation rates, as well as measurements of ozone, NO_x and other key chemical compounds. Models will also be used to study the transport out of polluted regions and its contribution to ozone background levels on larger regional scales.

As part of the PAUR project an intensive measurement campaign was set up in June 1996. Measurements were made at Tatoi, close to Athens and on the small island of Agios Fstatios,

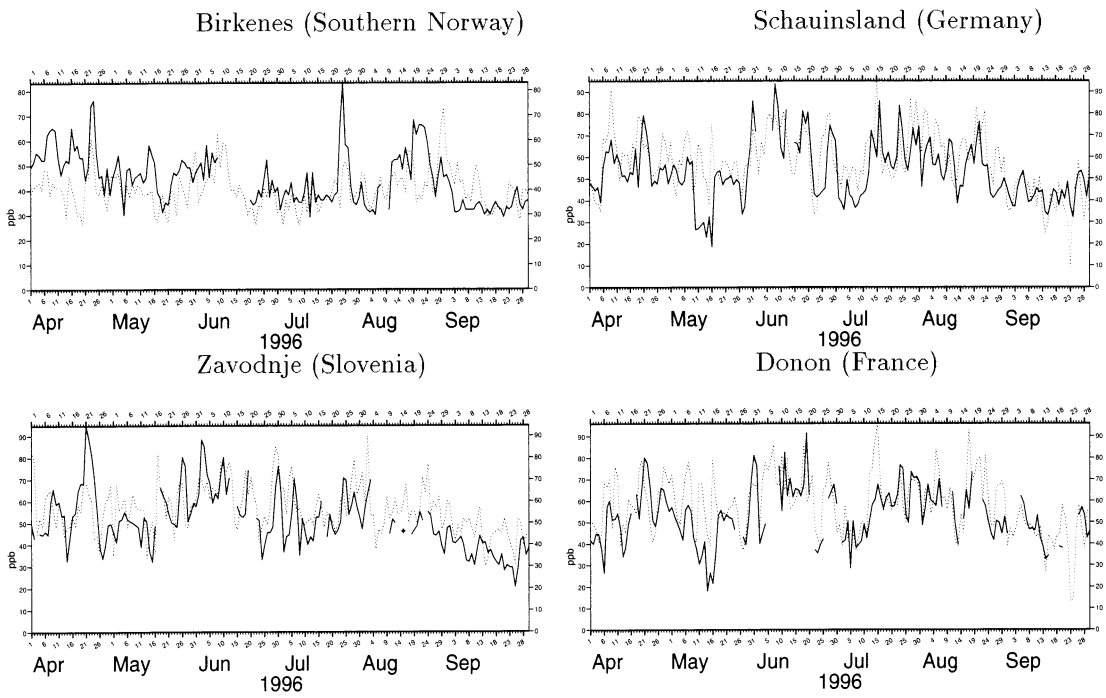

Figure 3.4: Measured (full line) versus calculated (dotted line) daily maximum concentrations of ozone inn ppb_v.

in the northern Aegean ocean.

Meteorological situation. The meteorological situation during the first 10 days of the two week campaign (1.-14. June) was dominated by a high pressure system over northern Europe with a ridge extending towards the Balkan. This gave a circulation pattern with air transported from Scandinavia over eastern Europe, the Black sea and finally over Turkey before entering the Aegean sea. Later the high pressure system moved towards the British Isles, and a more direct flow pattern from eastern Europe towards the Aegean sea was established. Figure 3.7 shows the mean sea level pressure (MSLP) and winds in the lower free troposphere at 12 UTC for 6., 10., and 14. of June 1996 as calculated by the numerical weather prediction model. During this long transport over the European continent the air in the planetary boundary layer was subject to significant input of pollutants from surface sources. Calculated ozone concentrations at 12 UTC for the same three days is shown in Figure 3.14
Figure 3.8 and 3.9 show the time-series of 1-hour averaged concentrations (measured and calculated) for Agios Efstratios and Tatoi between 1. June and 14. June 1996 The (yet unpublished) measurements were made as part of the PAUR project (Zerefos et al., 98).

Aghios Efstratios. Over the Aegean sea the ozone budget is enriched both in ozone and ozone precursors. Over the ocean, surface deposition is slow, and local sources of nitrogen oxides are small. The combination of these effects gives much less ozone loss during night than for the European continent. Consequently, quite small diurnal variations of ozone are found in both observations and model results. (Figure 3.8, top left panel). During the first six days of the campaign, the levels of calculated and measured ozone were in very good agreement. During the following week, the observed concentrations of ozone slowly increased, reaching a maximum of between 70 and 80 ppbv in the afternoon, while the calculated concentrations remained at the 50 ppbv level without significant diurnal variations. This can be caused by local circulation effects around the small island, not resolved by the model. During daytime a stronger surface heating over the island than over the surrounding ocean is likely to cause vertical mixing, bringing down air enriched in ozone. Towards the end of the period the weather pattern changed, giving a more direct northwesterly flow from the industrialized areas of central Europe towards the Island (Figure 3.7, lower panel). In the calculations this can be seen as a sharp increase (from about 150 ppb_vv to 225 ppb_v) in the concentrations of CO, accompanied by an increase in ozone, peaking at 75 ppb_v at 4 pm local time on the 14. June. This calculated

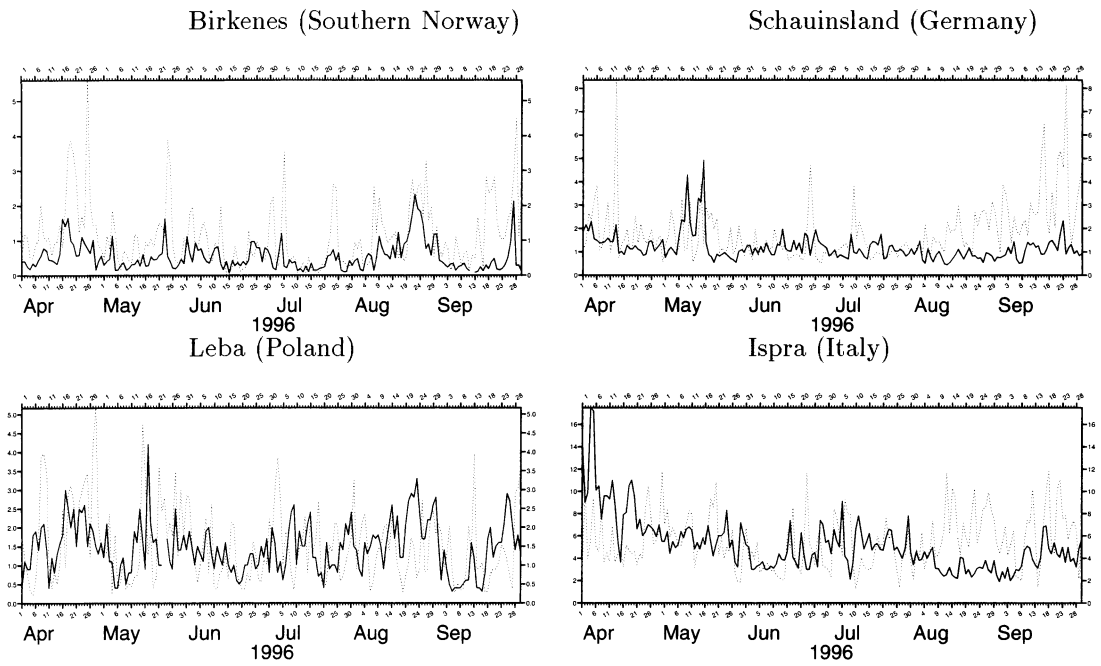

Figure 3.5: Measured (full line) versus calculated (dotted line) daily mean concentrations of NO_2 inn μg m^{-3} as N.

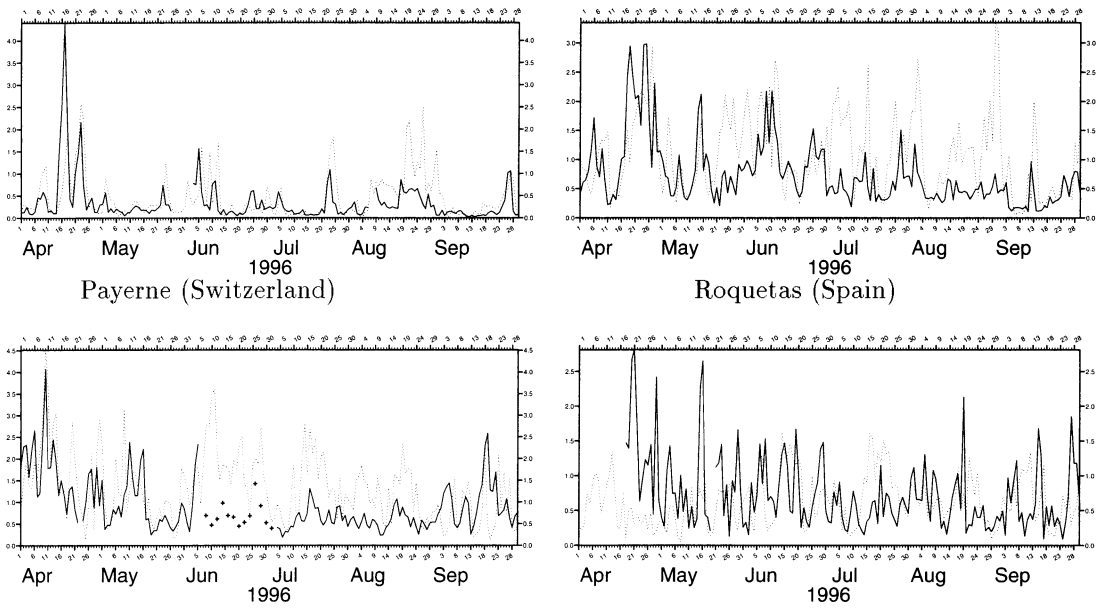

Figure 3.6: Measured (full line) versus calculated (dotted line) diurnally averaged concentrations of total nitrate (HNO_3 + ammonium nitrate) inn μg m−3.

peak in ozone is also seen in the measurements. A similar peak in ozone is calculated for the Tatoi station near Athens about 8 hours later.

For NO and NO_2 (Figure 3.8, middle two panels) and PAN (Figure 3.8, upper right panel) the agreement between calculations and measurements is less satisfactory than for ozone. For PAN model calculations and measurements have a similar diurnal cycle, but the model overestimates the daytime maximum concentrations by a factor of 3-10. This is probably a result of the coarse resolution for the forest database (150 km). With this version of the model there are emissions of isoprenes over large parts of the Aegean sea. Isoprene is rapidly oxidized to radicals that form PAN. Excess PAN formation may also contribute to the low calculated NO_2 concentrations during day. At night calculated NO_2 levels are in good agreement with the observed values.

Such a large under-prediction of NO_2 is not at all typical for the model performance. (Figure 3.1 and Figure 3.5). There may be sources of NO_x, as local shipping, not accounted for by the model. It may also be that reported NO_x emissions in general are to low in the whole region.

In later versions of the model (used in all other calculations in this report) isoprene emissions are set to zero over sea in the 50 km grid.

Tatoi, Athens The campaign period can be divided into two parts with respect to chemistry in the model. In the first 4 days and on 13. June, the model is strongly influenced by local urban sources, with NO_2 concentrations of up to 30 ppbv (Figure 3.9, middle right panel). High NO and NO_2 concentrations were also found in the measurements, however, the peak NO_2 concentrations were only about 10 ppbv. With such high NO_x concentrations in the model, ozone is lost through the reaction

$$NO + O_3 \rightarrow NO_2 + O_2$$

and for short periods almost all the ozone vanish.
During the rest of the period, both the model and the observations seems to be representing air-masses advected from the Aegean sea in the north easterly flow, without significant influence from local sources. For O_3 both measurements and model results show a lack of diurnal variation. The absolute concentrations are about 15 ppbv lower in the model than in the measured values. This corresponds to the difference found for Aghios Efstratios, indicating that ozone levels at Tatoi are mostly determined by a regional scale build-up of ozone.

3.2 The free troposphere.

In this section model results are compared to measurements from the POLINAT 1 summer 95 measurement campaign, and from the national German project "Schadstoffe in der Luft", campaign in the summer of 1996.

In the upper troposphere the residence time in the model domain is of the order of a few days only. Much less than the typical chemical lifetime of key chemical species as O_3 and HNO_3. **The level of these components in the upper troposphere and lower stratosphere are strongly** influenced by the concentrations at the lateral boundaries. The large variations in O_3 often seen in the upper troposphere are determined by dynamical effects, in particular stratospheric exchange, rather than local chemistry.

3.2.1 The POLINAT and Schadstoffe in der Luft projects.

The aim of the EU projects POLINAT 1 and 2 (Pollution from Aircraft Emissions in the North Atlantic Flight Corridor) is to study the effects of aircraft emissions in the north Atlantic flight corridor. As stated in the work program the overall objectives of the project are:

1. To determine by measurements and analysis the relative contribution from air traffic exhaust emissions to the composition of the lower stratosphere and upper troposphere at altitudes between 9 and 13 km within and near the flight corridor over the North Atlantic.

2. To assess the effects of air traffic emissions in that region in relation to clean background concentrations and pollutant concentrations from various sources and to analyze their importance for changes in ozone, oxidizing capacity, aerosols and clouds.

During POLINAT 1 there were two extensive measurement campaigns. One in November 1994 and a second campaign in June July 1995.

As a direct follow up to the POLINAT projects a national German project (Schadstoffe in der luft) was set up, and similar measurements with the same aircraft were carried out in the summer of 1996. For the second POLINAT project extensive measurements were carried out in September and October 1997. The POLINAT measurement campaign was coordinated wit the US project SONEX. As meteorological data for this period are not yet available, the results from this period will be studied at a later stage.

All measurements have been made with the DLR (Deutsche Forschungsanstalt für Luft und Raumfart) Falcon aircraft based at Shannon airfield in Ireland. A large fraction of the flights

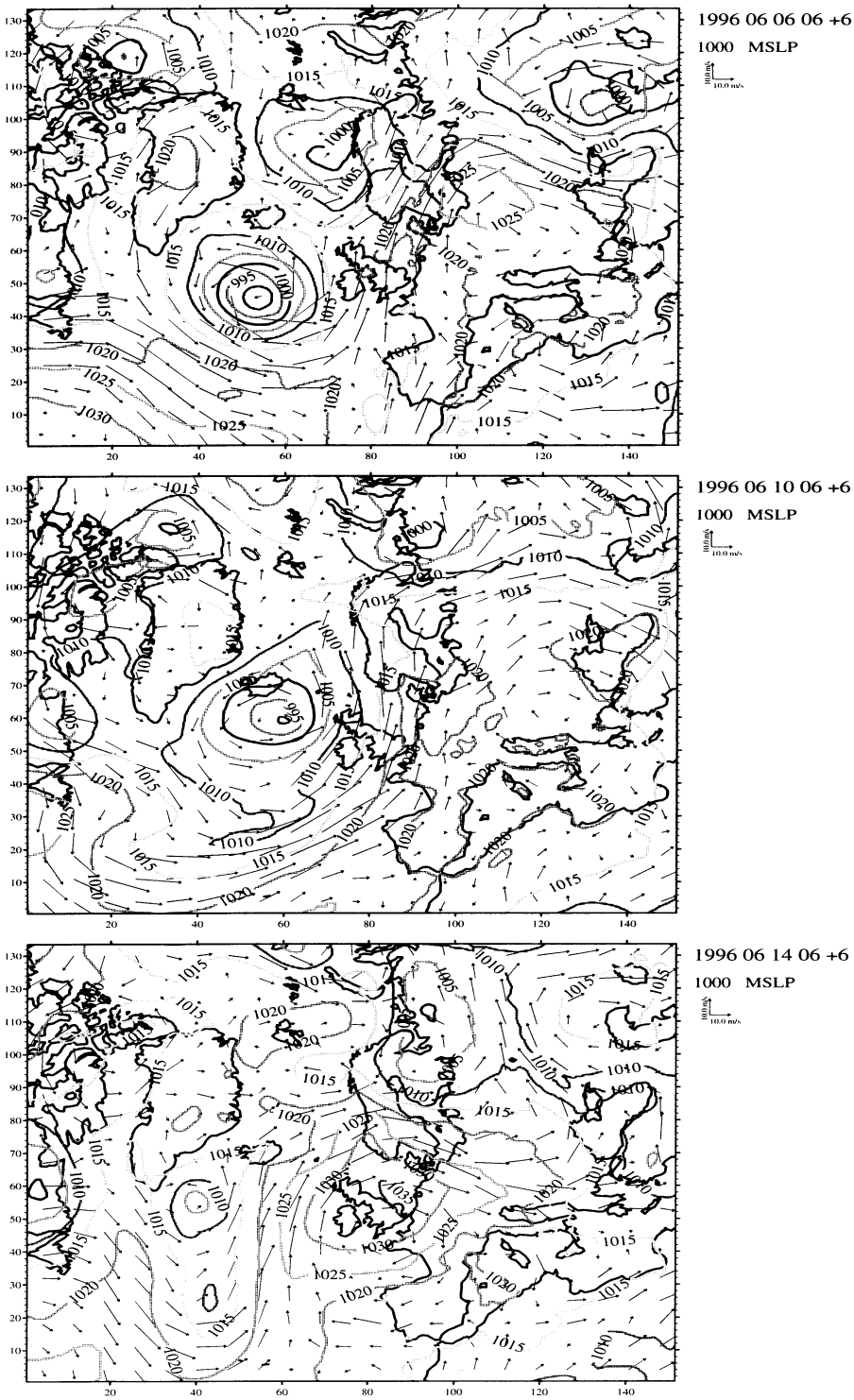

Figure 3.7: Mean sea level pressure and winds in the lower free troposphere at Jun 6, 10 and 14 at 12 UTC.

were made chasing commercial airliners. The use of these data for verification of the EMEP Eulerian photo-chemistry model is a result of the on-going collaboration between EMEP and the University of Oslo. The measurements from the POLINAT campaign are published in the final report to the European commission from the POLINAT project (Schlager et al. 1996 for NO and O_3 and Arnold et al. 1996 for HNO_3).

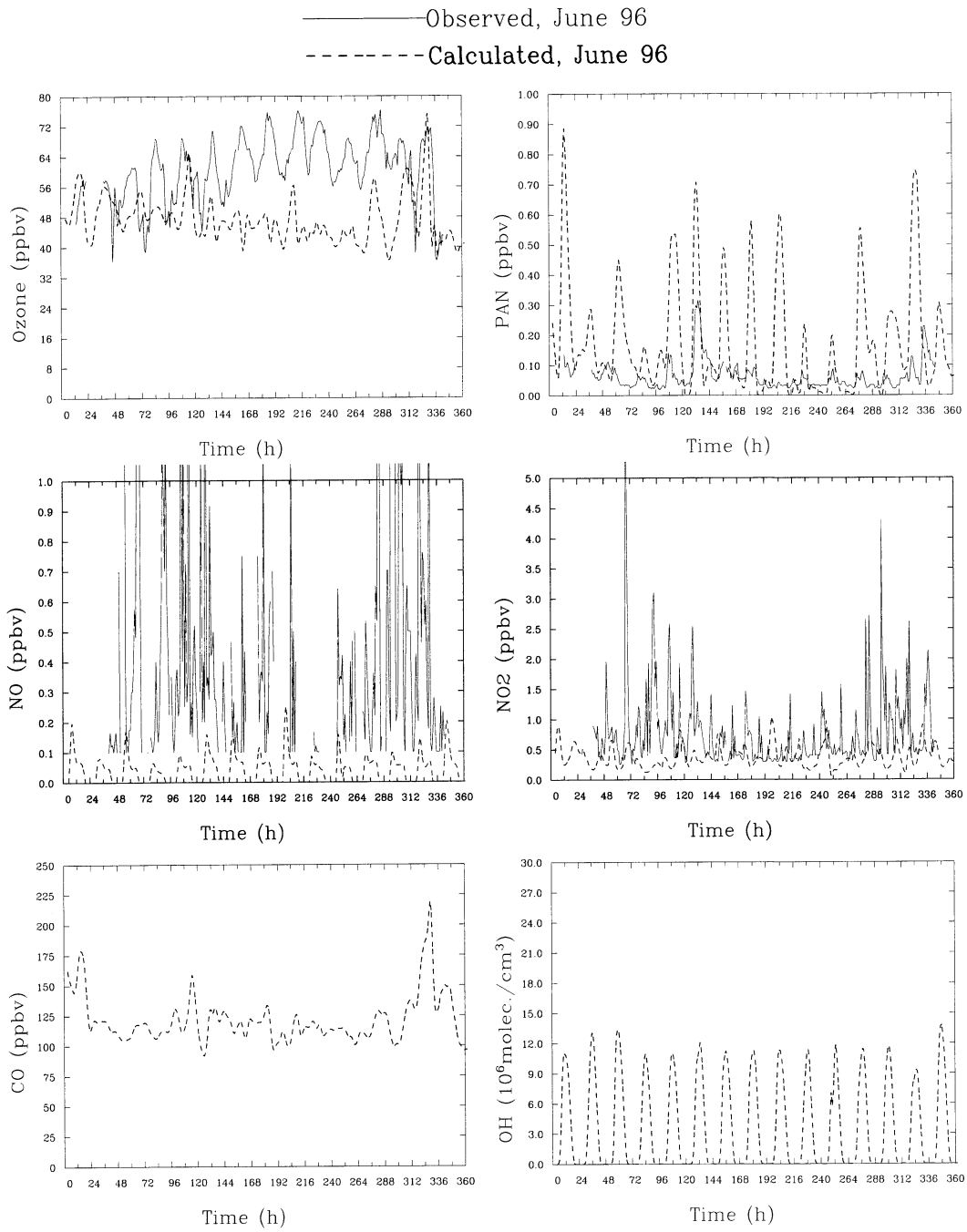

Figure 3.8: Calculated and measured hourly concentrations of key chemical components during the Paur campaign at the island of Aghios Efstratios June 1 - June 14 1996.

3.2.2 Model calculations for the POLINAT 1 summer 1995 campaign.

The last part of June 1995 proved to be a well suited period to study the effects of aircraft emissions in the eastern parts of the north Atlantic flight corridor. At flight altitude in this region the weather pattern was dominated by a high pressure system with stagnant air, allowing concentrations of NO_x, and to some extent O_3, to build up. As the NO and NO_2 concentrations in the data provided from this version of the Oslo CTM2 were known to be to low, a minimum concentration of 100 ppb_v of NO_x is assumed at the lateral boundaries.

Calculated concentrations of O_3, HNO_3 and NO are printed to file during model run time given the position of the aircraft. In Figure 3.10 calculated and measured concentrations of O_3 and HNO_3 are compared, and Figure 3.11 depicts calculated and measured concentrations of NO along the same flight tracks. Most of the measurements were made at regular flight

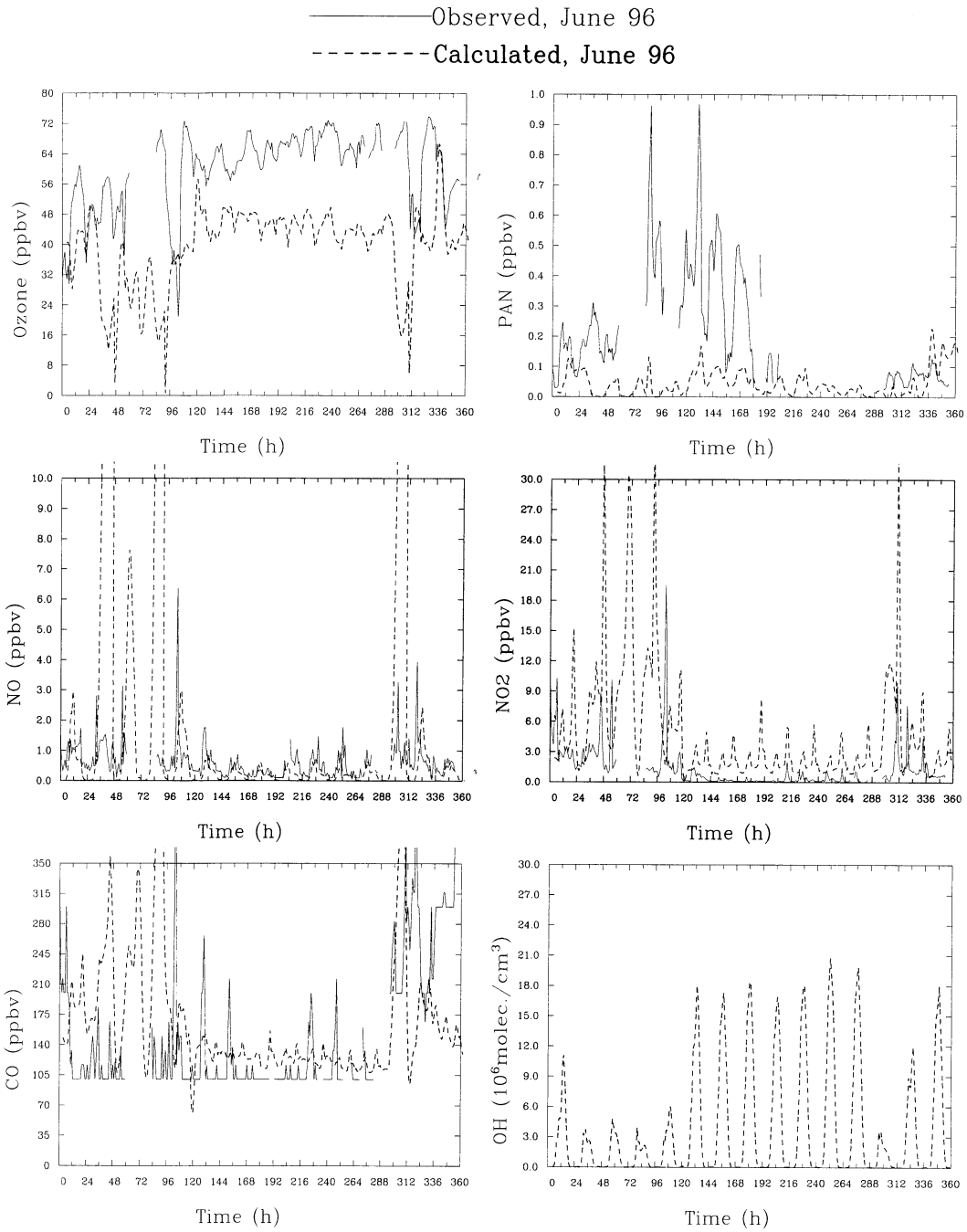

Figure 3.9: Calculated and measured hourly concentrations of key chemical components during the Paur campaign at Tatoi, near Athens, June 1 - June 14 1996.

altitude, at around 10 km altitude, in the upper part of the troposphere. The aircraft also ascended into the lower stratosphere, shown as peaks in the O_3 concentrations in Figure 3.10. The comparison between modeled and measured concentrations of O_3 shows that ozone levels in the upper tropopause and lower stratosphere are well reproduced in the model. In particular for the two flights on June 26. there is a remarkable good agreement between model calculations and measurements. This suggests that the overall O_3 concentrations provided by the Oslo CTM2 (Sundet, 1997), and adjusted by the potential vorticity, are reasonable. In addition the model is capable of reproducing the effects of the dynamics on a regional scale.

Figure 3.15 depicts the concentrations of O_3, NO_x and HNO_3 at 12 UTC June 26 at 230 hpa. A minimum in the O_3 concentrations (upper panel) is seen in the high pressure region in the north eastern parts of the Atlantic. In the same region NO_x concentrations (middle panel),

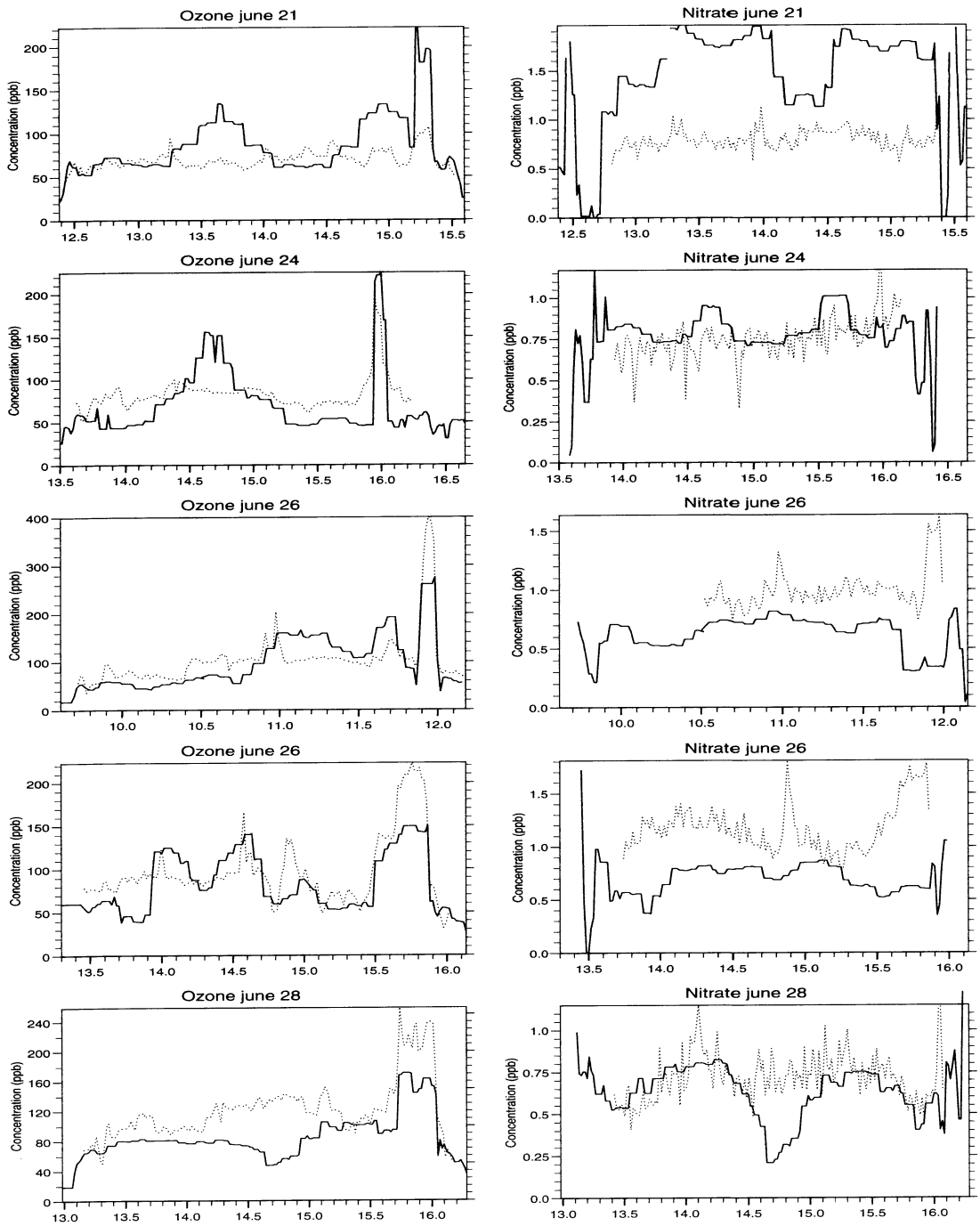

Figure 3.10: Measured (dotted line) versus calculated (full lines) concentrations inn ppb_v of ozone and total nitrate for the Falcon flights in June 1995.

and to some extent HNO_3 concentrations lower panel), are high.

Figure 3.16 depicts the difference in NO concentration between a standard model run and three model scenarios:

- standard versus No aircraft emissions (upper panel)
- standard versus No lightning emissions (middle panel)
- No wet deposition of total nitrate (HNO_3 and ammonium nitrate) versus standard model run (lower panel).

The largest difference is seen for the case with no aircraft emissions. In this case NO concentrations (and likewise NO_2) are reduced by up to 0.1 ppb, corresponding to a more than

50% reduction in NO_x concentrations in the high pressure region.

Lightning appears to have only a small effect on the concentrations. Lightning is included as a monthly averaged source. However, it is expect that there will be large temporal and spatial variations for this source.

Without wet deposition of HNO_3 there is a substantial increase in NO concentrations in parts of the upper troposphere. Without being washed out by precipitation more HNO_3 is advected to the upper troposphere, where it is photolysed, acting as a source for NO_x.

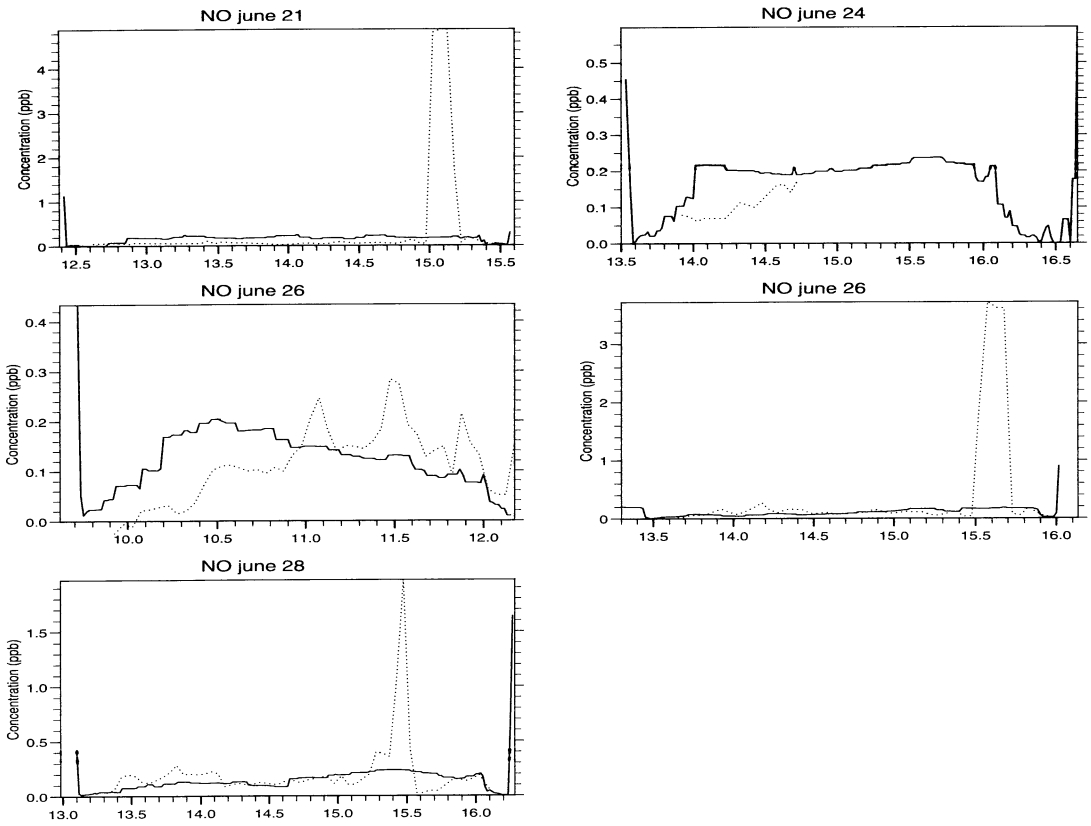

Figure 3.11: Measured (dotted line) versus calculated (full lines) concentrations inn ppb_v of NO for the Falcon flights in June 1995.

3.2.3 Model calculations for the Schadstoffe in der luft summer 1996 campaign.

As part of POLINAT, two flights from the German project Schadstoffe in der luft has been selected for model inter-comparison. The yet unpublished data have been made available for EMEP by courtesy of Dr. Hans Schlager, DLR. Both flights were made from Shannon airfield, starting in the morning, to the Canary islands. There the Falcon aircraft stopped for refueling etc, and then returned to Shannon in the evening. The flights were made on the 1. and 11. of July 1996. As the Canary islands are outside the model domain no comparison with measurements can be made for the last part of the southbound flight and the first part of the return flight. Flight altitude was mostly between 10 and 11 km.

In Figure 3.12 calculated and measured O_3 concentrations for the two flights are shown (southbound flight on the left). Parts of the flights were clearly made in stratospheric air-masses, with concentrations sometimes peaking well above 300 ppb. In Figure 3.17 O_3 at model level 4 (approx. 230 hpa) at 12 UTC for the two days is shown. For the first of July (upper panel) high O_3 concentrations are found over the British isles, corresponding to the first part of the southbound flight and the last part of the return flight. For the 11 July the Falcon is mostly flying in the upper troposphere. High O_3 concentrations are encountered as the aircraft is flying through a cold front extending southwest from the Iberian peninsula.

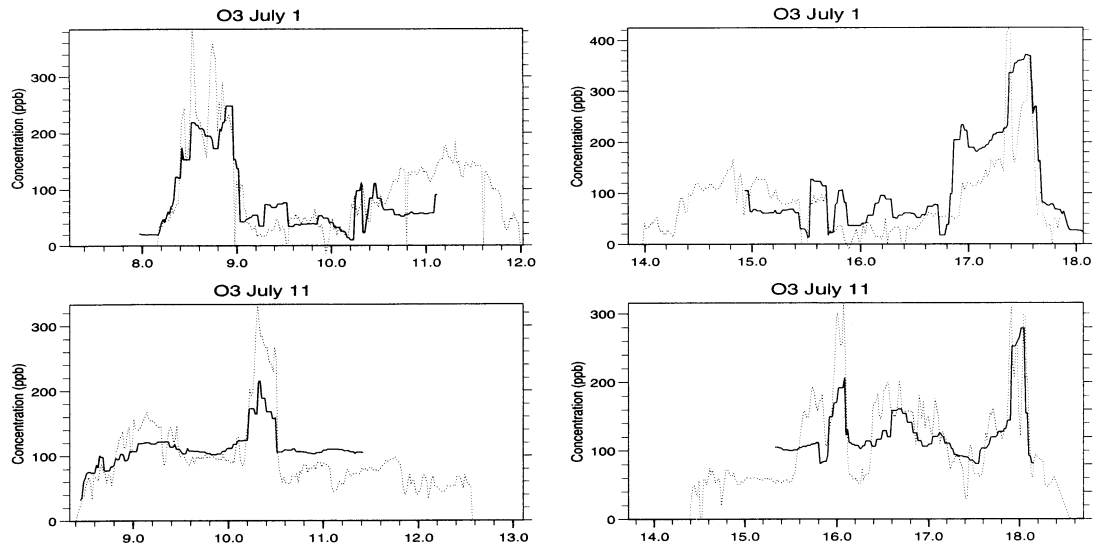

Figure 3.12: Measured (dotted line) versus calculated (full lines) concentrations inn ppb_v of O_3 for the Falcon flights on the 1'th and 11'th of July, 1996.

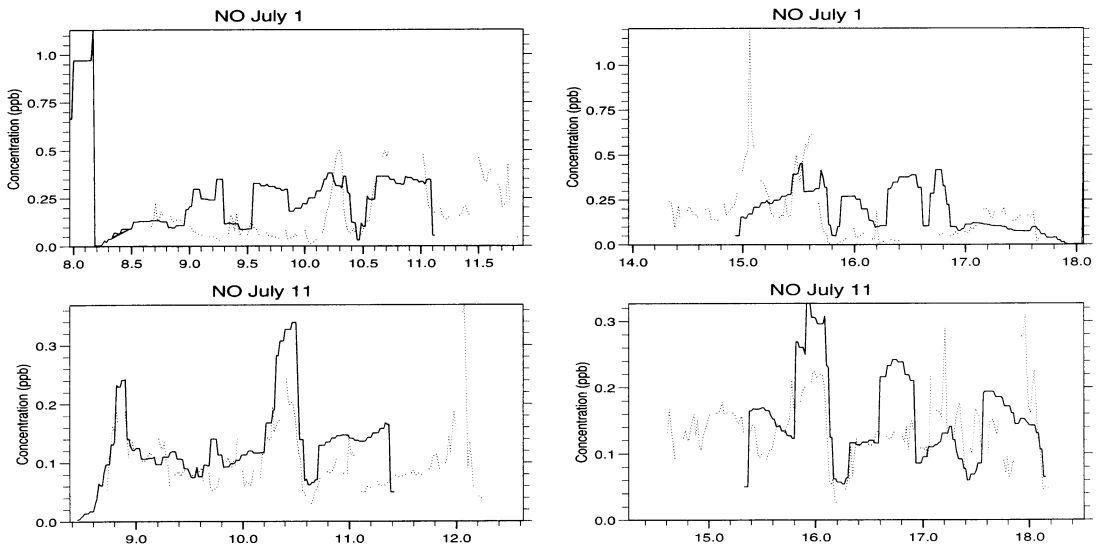

Figure 3.13: Measured (dotted line) versus calculated (full lines) concentrations inn ppb_v of O_3 for the Falcon flights on the 1'th and 11'th of July, 1996.

Considering its short chemical lifetime, overall calculated NO levels are in reasonable good agreement with the measurements (Figure 3.13). Contrary to the summer 1995, measurements are mostly made in "aged" air-masses, outside of the north Atlantic flight corridor.

In the present version of the Oslo CTM2 global model the wet removal of HNO_3 is not sufficiently accounted for, resulting in unrealistically high concentrations for this component in the upper troposphere. HNO_3 is relatively long-lived in the upper troposphere and calculated HNO_3 concentrations are, to a large extent determined by the lateral boundary concentrations. Thus it is not surprising that the calculated concentrations are substantially higher than the measurements for this component (Figure 3.18).

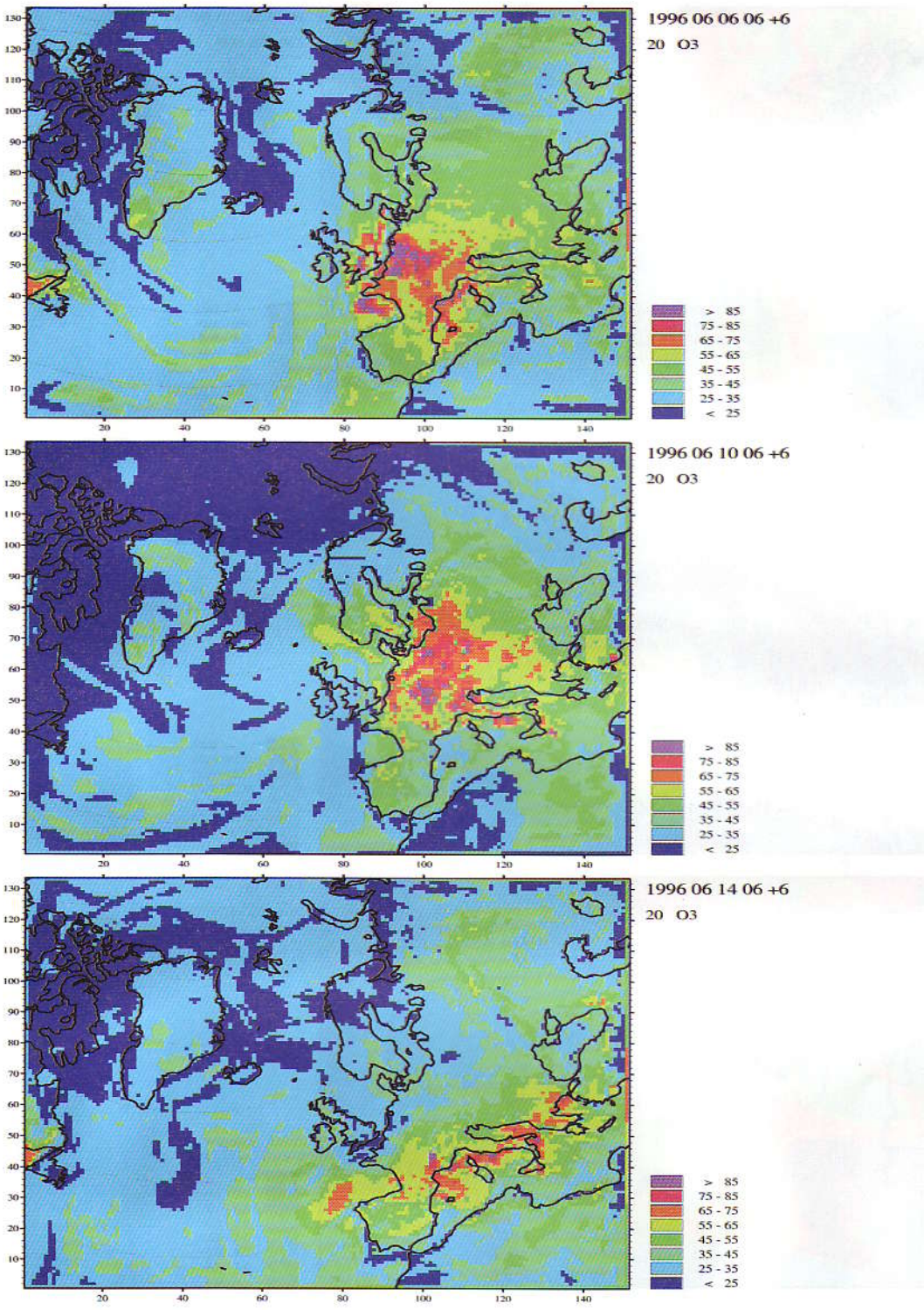

Figure 3.14: Concentrations of O_3 in ppb_v at 12 UTC depicted for the same days as for the meteorological situation in Figure 3.7.

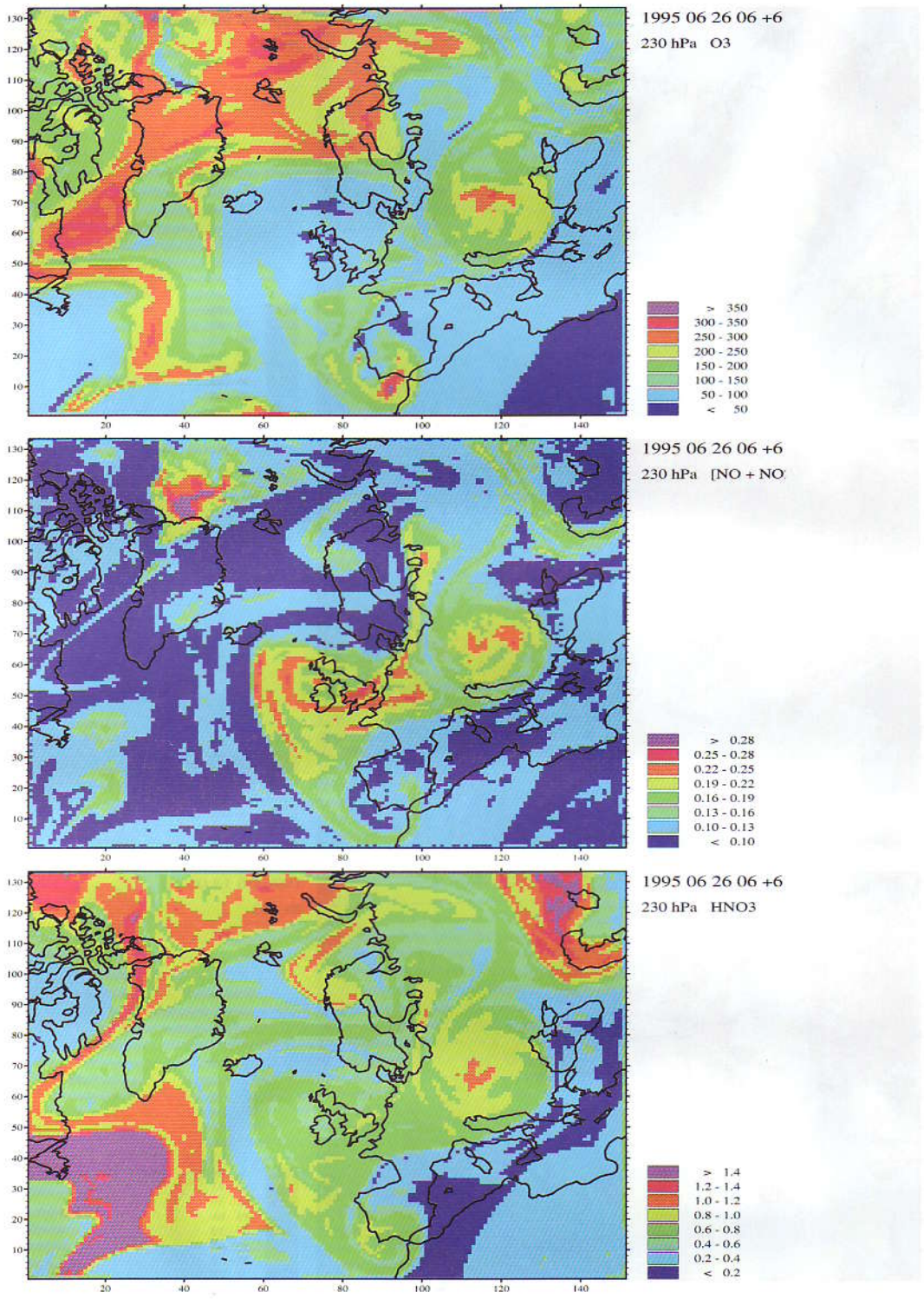

Figure 3.15: Concentrations of O_3 (upper panel), NO_x (middle panel) and total nitrate (lower panel) in ppb_v at 12 UTC June 26 at 230 hpa.

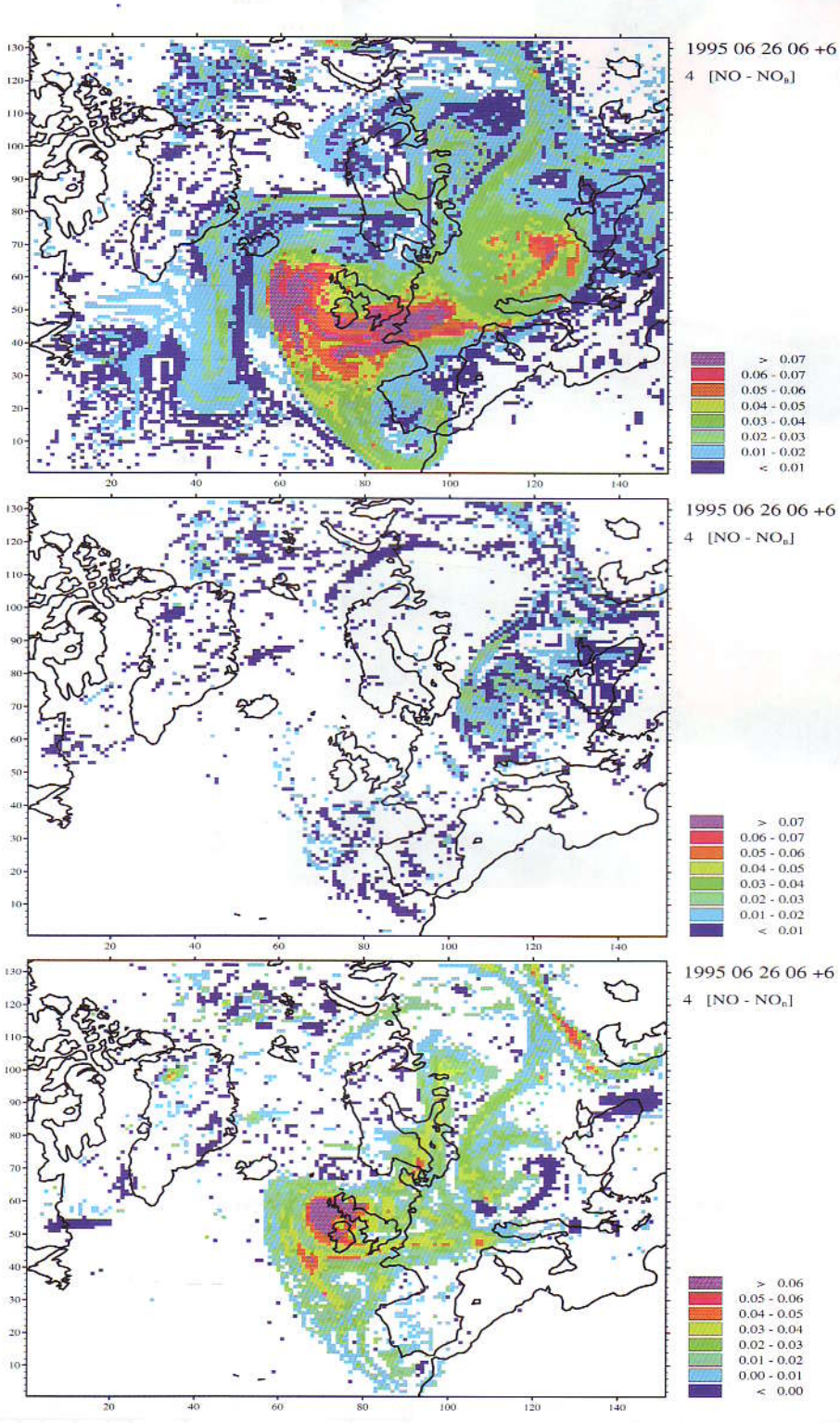

Figure 3.16: Difference in NO concentrations in ppb$_v$ between a standard model run and three model scenarios (see text) at 12 UTC June 26.

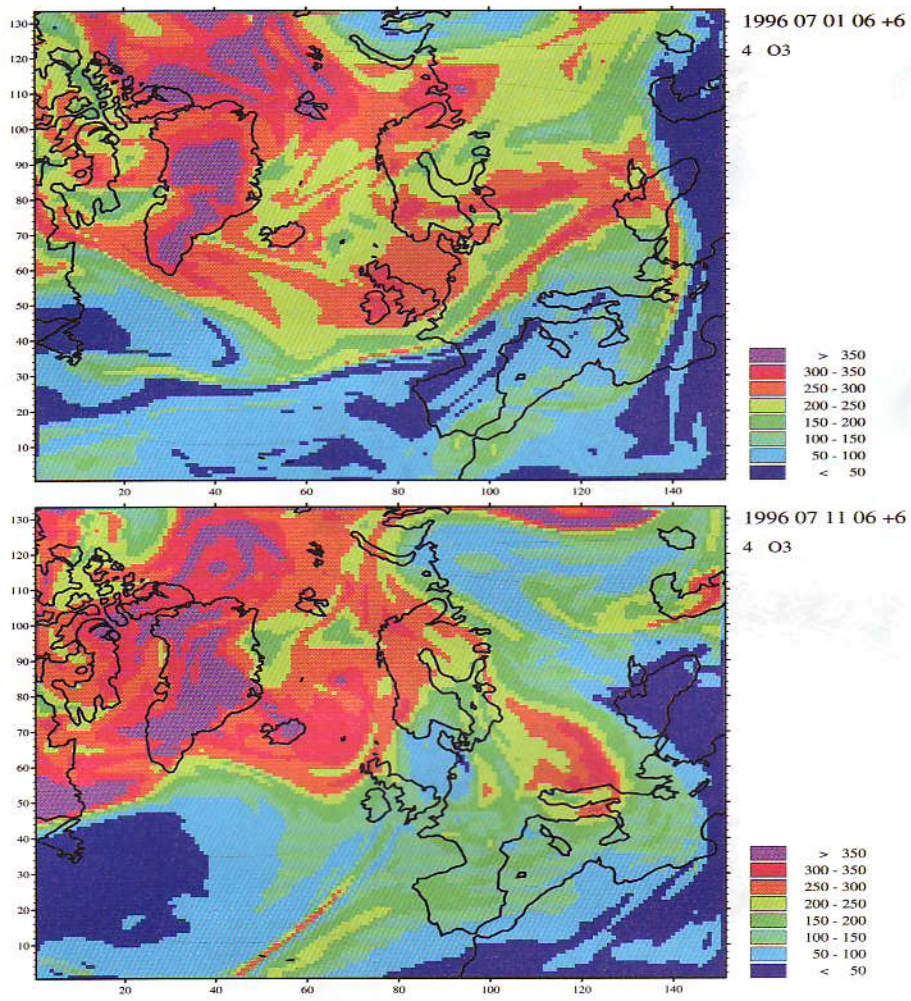

Figure 3.17: Ozone concentrations at 12 UTC in ppb_v at model level 4 (approx. 230 hpa at July 1 and July 11.

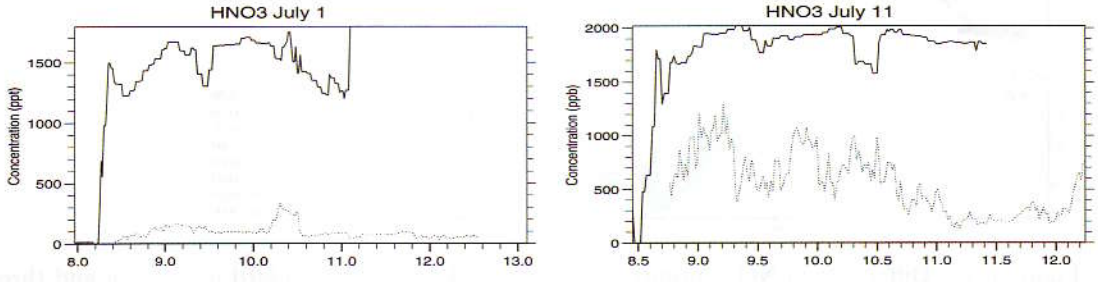

Figure 3.18: Measured (dotted line) versus calculated (full lines) concentrations inn ppb_v of HNO_3 for the Falcon flights on the 1'th and 11'th of July, 1996.

Chapter 4

Conclusions from the model results.

For most of the chemical components considered the model calculated concentrations compare favourablly with the measurements both at the surface and in the free troposphere. For short-lived components as NO, NO_2 etc. the overall agreement is good, but there is a considerable scatter for the individual measurements and sites. This must be attributed to the large natural variability of chemically short-lived components. Compared to measurements total nitrate concentrations appears to be over-predicted by the model. However, as argued above, for concentrations measured at the surface the air concentrations may be under-estimated, as nitrate particles can evaporate from the filters. For the upper troposphere the overestimation is caused by to high concentrations at the lateral boundaries. As total nitrate levels at the surface are over-predicted also in regions where concentrations are high, it is unlikely that the high concentrations in the upper troposphere will contribute significantly to the over-prediction at the surface. In the free troposphere section it was shown that the photolysis of HNO_3 can be a significant source of NO_x in the upper troposphere. Improving the the parameterization of the wet removal for HNO_3 may give to low NO_x concentrations. Most models have a tendency to overestimate the HNO_3 to NO_x ratio in the free troposphere, indicating that the estimated production of nitric acid is to rapid, or that there are some unknown processes in the atmosphere that are able to regenerate NO_x from nitric acid. (Chatfield, 1994).

For SO_2 the agreement between the model calculations and the measurements is good. For SO_2 the results are better than the calculations with the present version of the EMEP EUlerian acid deposition model. The results are comparable to the calculations with the acid deposition model with the same dry deposition scheme presently used in the photo-chemistry model (Jakobsen et al. 1996). For sulphate the results are less satisfactory. We suspect that the in-cloud oxidation of SO_2 is to slow, indicating that SO_2 is oxidized by other oxidants than O_3 and H_2O_2 or that H_2O_2 is produced in the cloud droplets.

4.1 References

Arnold F., Klemm M., Schneider J., Burger V., Droste-Franke B., Kirchner G., Preissler B., Jung A. and Dann W. (1996) Trace gas measurements by aircraft based ion molecule reaction mass spectrometry. In *Pollution from aircraft emissions in the north Atlantic flight coridor (POLINAT)*. Edited by U. Schumann. Report EUR 16978 EN, pp 20-48.

Bartnicki, J., Olendrzynski, K. and Jonson, J.E. (1998) Performance of the Eulerian Acid Deposition Model. In Transboundary acidifying air pollution in Europe. EMEP/MSC-W Status Report 1998 - Part 1. The Norwegian Meteorological Institute, Oslo, Norway.

Bott A. (1989a) A positive definite advection scheme obtained by non-linear renormalization of the advective fluxes. *Monthly Weather Review*, **117**, pp 1006-1015.

Bott A. (1989b) Reply. *Monthly Weather Review*, **117**, pp 2633-2636.

Chatfield R.H. (1994) Anomalous HNO_3/NO_x ratio of remote tropospheric air: Conversion of nitric acid to formic acid and NO_x? *Geophys. Res. Lett..*, Vol. 21, NO. 24, pp 2705-2708.

DeMore W.B., Sander D.M, Golden D.M., Hampson R.F., Kurylo M.J., Howard C.J, Ravishankara A.R., Kolb C.E. and Molina M.J. (1997) Chemical kinetics and photochemical data for use in stratospheric modeling. *NASA/jpl Publ.*, 97-4.

Jakobsen, H.A., Jonson J.E. and Berge, E. (1996). Transport and deposition calculations of sulphur and nitrogen compounds in Europe for 1992 in the 50 km grid by use of the multi-layer Eulerian model. EMEP/MSC-W, Note 2/96. The Norwegian Meteorological Institute, Oslo, Norway.

Jonson J.E. and Isaksen I.S.A. (1993) Tropospheric chemistry. The impact of cloud chemistry. *J. Atm. Chem.*, **16**, pp 99-122.

Jonson J.E. Jakobsen H.J. and Berge, E. (1997) Status of the development of the regional scale photo-chemical multi-layer model. EMEP/MSC-W, Note 2/97. The Norwegian Meteorological Institute, Oslo, Norway.

Schlager H., Schulte P., Ziereis H., Konopka P., Schumann U., Feigl C., Marquardt R. and Huntrieser H. (1996) Aircraft-borne measurements of NO_xO_3 and CO_2. In *Pollution from aircraft emissions in the north Atlantic flight coridor (POLINAT).* Edited by U. Schumann. Report EUR 16978 EN, pp 20-48.

Slanina J., ten Brink H.J. and Yuhua Bai (1998) The analysis of bulk-elements in aerosols: An underdeveloped area with grave consequences. In *Measurements and modeling in environmental pollution,* Edited by R. San Jose and C.A. Brebbia, Computational Mechanics Publications, Southhamton, UK, pp 343-358.

Zerefos C. et al. (1998) Final report of the PAUR project. Submitted to the European commission.

Part III

Comparison of Lagrangian and Eulerian models for the summer of 1996

D. Simpson and J.E. Jonson

Chapter 1

Introduction

Parts I and II of this report have discussed the Lagrangian photo-oxidant model and the 3-D Eulerian photo-oxidant model (MACHO). The model results have been compared with measurements, either for a number of years (Part I) or for various height levels for 1996 and some campaign periods (Part II). Here we present for the first time a side-by-side comparison of the two EMEP models. The aim is to give a first illustration of the results of the two models as they stand now, in relation to each other and in relation to measurements.

Appendices A and B detail the physical and chemical structure of the two models in detail. These models have been described previously in Simpson (1992), Simpson (1993), Simpson (1995), Simpson et al. (1993) and Jonson et al. (1997). Table 1.1 summarises the similarities and differences. In terms of chemistry the two models are similar, but not identical. Both chemistries are developed from the original University of Oslo chemistries (Hov et al., 1978, Eliassen et al., 1982), and so both use the same lumped-molecule approach and similar species. However, over the years the two mechanisms have diverged, especially in their reaction-pathways. Possibly the most important differences are:

- The photolysis schemes are very different. As pointed out in Jonson et al. (Part II) the Eulerian model's scheme has been recently updated to take into account the new recommendations of DeMore et al. (1997). This gives a photolysis rate for the key $O_3 + h\nu \rightarrow O^1D$ reaction which is about 30% higher than previous values.

- The isoprene chemistries are very different, and have never been tested against each other.

The basic emissions input-data are similar, but handled in more detail by the Lagrangian model. The biogenic emission inputs are very similar in the two models, although of course the temperature fields for the Eulerian model have higher spatial resolution. The boundary conditions (BCs) used by the two models are very different. The Lagrangian model uses BCs based mainly upon measured data, whereas the Eulerian uses BCs derived from the global model of the University of Oslo (Sundet, 1997, Berntsen et al., 1997).

Of course,the main differences between the models are in their physical structure, with the Eulerian model featuring 20 vertical levels and 50x50 km^2 horizontal resolution, whereas the Lagrangian model has just one layer and 150x150 km^2 horizontal resolution.

Table 1.1: The Lagrangian and Eulerian models, brief summary

	Lagrangian	Eulerian	Comment
Resolution:			
Horizontal	150 km	50 km	
Vertical	1	20	
Vertical extent	to mixing height, ca. 1-2.5 km	to 100 hPa, ca. 15 km	
Emission inputs:			
Source	EMEP, 1997	EMEP, 1998	See Olendrzyński (1997), Mylona (1998)
Resolution	50 km	50 km	
Source-sector split	yes	no	i.e. separate road-traffic, solvents, etc.
Temporal resolution	Daily	Monthly	Both from GENEMIS (e.g.Friedrich, 1993)
Biogenic Emissions	E-94 methodology	E-94 methodology	Simpson et al. (1995)
Boundary conditions	Climatalogical (Mainly measurement-based)	Monthly average for June 96 from global Tropospheric model	
Meteorological input:	DNMI; LAM50	DNMI; LAM50	Identical except for resolution
Chemistry:			
Type	lumped-molecule	lumped-molecule	
Reactions	140	88	
Species	66	50	
Photolysis	Jenkin et al. (1997), Derwent et al. (1996)	DeMore et al. (1997) Kylling (1995)	
Deposition module	Resistance-based	Resistance-based	Different implementations
CPU-requirements 6-month run (per processor)	ca. 1000 s	ca. 70 000 s	CRAY T3E, 16 processors

Chapter 2

Results

2.1 Time-series comparisons

The two model's predictions of daily maximum ozone against measurements are compared for 22 sites in Figures 2.1-2.4. For convenience, Table 2.1 also gives the correlation coefficients obtained from these time series.

In general, results from the two models are comparable, although the Eulerian model usually has a higher correlation with the measurements. There is a tendency for the Eulerian model to perform better in spring-time than the Lagrangian (e.g. the Austrian sites). The site where the Eulerian model is clearly superior is Ispra. This site is often influenced by the Milan plume, so it may be that this effect is resolved better in the Eulerian model than in the Lagrangian. Another feature seems to be that the Lagrangian model is more likely to predict ozone peaks much higher than measurements (e.g. early June, Rorvik), wheras the Eulerian is more likely to substantially under-predict measured peaks (e.g. late April, Rorvik). Otherwise, it is difficult to find any general pattern in these comparisons.

2.2 AOT40

As pointed out in Part I (section 2.4.1) AOT-statistics are rather poor tools for evaluating models. However, they have obvious policy-importance, and they do help to show the regions where the models are predicting substantial ozone production.

Figures 2.5 shows the calculated 3-monthly $AOT40_c$ values obtained from the Lagrangian and Eulerian models. In general the model results show rather similar gradients, but with obvious differences also.

Some similarities:

- Low AOT40 values (generally < 3 ppm.h) over most of the UK, Scandinavia and northern Russia.
- Similar areas of exceedance of the 3 ppm.h Critical level for crops.
- Only moderate AOT40 (5-10 ppm.h) over most of southern Europe.

Some differences:

- The Eulerian model has a region of higher AOT40 (>15ppm.h) in the western parts of France, extending into Germany, N. Italy, much of central Europe and into the Balkans. The Lagrangian model does have high AOT40 (>12 ppm.h) in N. Italy, and also elevated levels ($>$ 10 ppm.h) in France, but does not show the same broad-expanse of high AOT40 into eastern and southern Europe as the Eulerian model.
- The Lagrangian model predicts increased AOT40 along the coast of Portugal compared to Spain, but the Eulerian model predicts deacreased AOT40.
- The Lagrangian model predicts areas of exceedance of the Critical level in southern parts of the UK and Sweden, and over the whole of Denmark. The Eulerian model suggests no exceedance in these areas

Table 2.1: Modelled and Observed 6-monthly AOT40 (forests) and Correlation-coefficients, Lagrangian and Eulerian models

Code	Station	Data Capture (%)	Height (m a.s.l.)	AOT40-forests (ppb h)			Corr. Coeff[1]	
				Obs.[2]	Lagrang.	Euler.	Lagrang.	Euler.
AT03	Achenkirch	98.2	960	9263	6972	19254	0.57	0.51
AT02	Illmitz	94.6	117	13778	11142	8478	0.53	0.54
CH02	Payerne	98.4	500	16601	6366	9864	0.50	0.59
CS03	Kosetice	95.1	633	20451	8304	7806	0.50	0.62
DE03	Schauinsland	93.0	1205	15867	6996	6714	0.58	0.69
DE02	Waldhof	67.5	74	10634	6102	4506	0.69	0.81
DE01	Westerland	97.9	12	8625	4464	1782	0.62	0.34
ES01	San pablo	93.7	917	26228	6246	5418	0.47	0.52
FI09	Uto	98.5	7	8980	3766	4020	0.35	0.60
FR08	Donon	87.3	775	15022	7717	10680	0.55	0.61
GB33	Bush	98.3	180	3668	1030	1416	0.34	0.62
GB15	Strath vaich	90.7	270	5029	936	2304	0.47	0.54
IT04	Ispra	100.0	209	24042	7548	11700	0.48	0.64
IT01	Montelibretti	99.5	48	11274	13110	14166	0.25	0.36
NO45	Jeloya	99.7	3	5659	2046	1206	0.53	0.53
NO44	Nordmoen	99.9	200	4141	1236	1362	0.29	0.52
NO41	Osen	100.0	440	7795	894	1830	0.44	0.58
NO01	Birkenes	91.7	190	7317	4332	1566	0.57	0.32
NO42	Zeppelinfjellet	100.0	474	975	84	66	0.02	0.27
SE02	Rorvik	99.2	10	8773	4386	1536	0.57	0.36
SI31	Zavodnje	92.1	770	12793	9822	12690	0.60	0.68
SK06	Starina	93.1	345	11520	10800	6846	0.63	0.72

Notes:

1. Correlation coefficents are calculated between modelled and observed max. daily ozone values over April-Sept., i.e. from a maximum of 183 values.
2. Observations calculated by EMEP/CCC, correcting for data-capture.

Figure 2.6 presents the $AOT40_c$ values as derived from the EMEP measurement networks. Compared to this figure we see that both models tend to under-predict AOT40 values in southern Scandinavia and in the UK. The Lagrangian model appears to match the measurements better in Germany and central Europe. In other parts of Europe it is very difficult to draw conclusions as the number of sites is so few. Greece has one measurement station which shows more than 12 ppm.h. If this site is regionally representative for all of Greece both models seem to underpredict AOT40 in this region. However, both models do show individual grid squares near Athens with AOT40 values of around 10 ppm.h. In Spain two stations report high AOT40 (>15ppm.h), which would suggest that both models under-predict in this region. However, model *over*-prediction was found for other Spanish sites with the Lagrangian model in Part I, so it is difficult to assess the overall performance until more measurements become available. Only one site covers central Italy, and this site suggests much lower AOT40 values than the models perdict. However, this site (Montelibretti) is often influenced by emissions from the Rome urban area, so NO-titration of ozone may be responsible for the low observed AOT values.

The 6-monthly AOT40 (forests) values are given in Table 2.1, along with the observed values for 22 sites. Both models show a similar performance against the available measurements. Measured $AOT40_f$ is generally under-predicted by both models to a similar extent.

Figure 2.7 illustrates the predicted AOT60 values from the two models. Here gradients in much of Europe are remarkably similar in the two models. The main difference appears in the France/Germany region, with the Eulerian model predicting much more AOT60 than the Lagrangian model. Hoewever, it is worth noting here that AOT60 is a statistic which magnifies differences in modelled concentrations (see Part I, section 2.4.1), so even small differences in modelled ozone concentrations may cause large differences in AOT60.

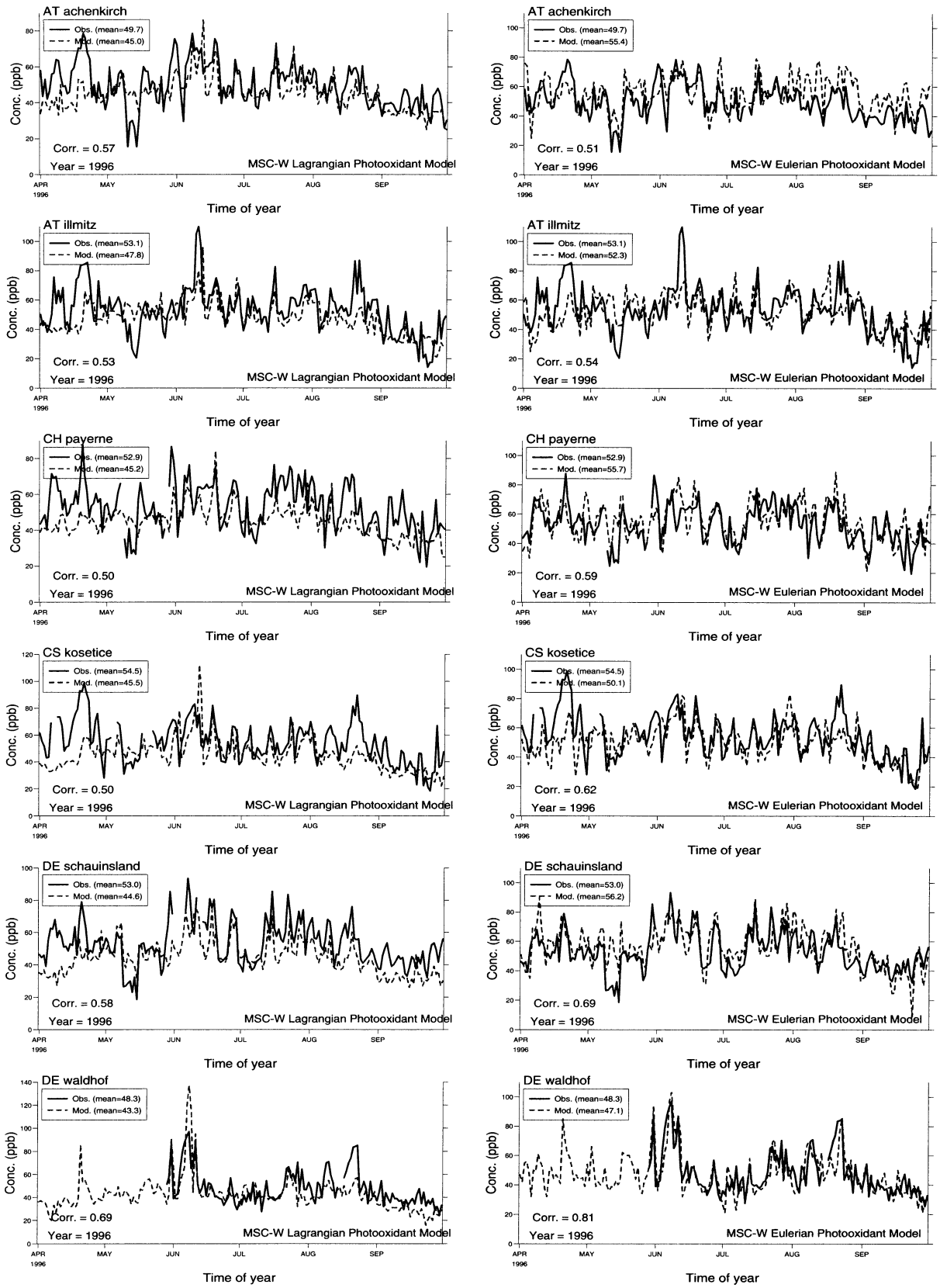

Figure 2.1: Comparison, Modelled versus observed daily max. ozone (ppb), Lagrangian model (left) and Eulerian model (right)

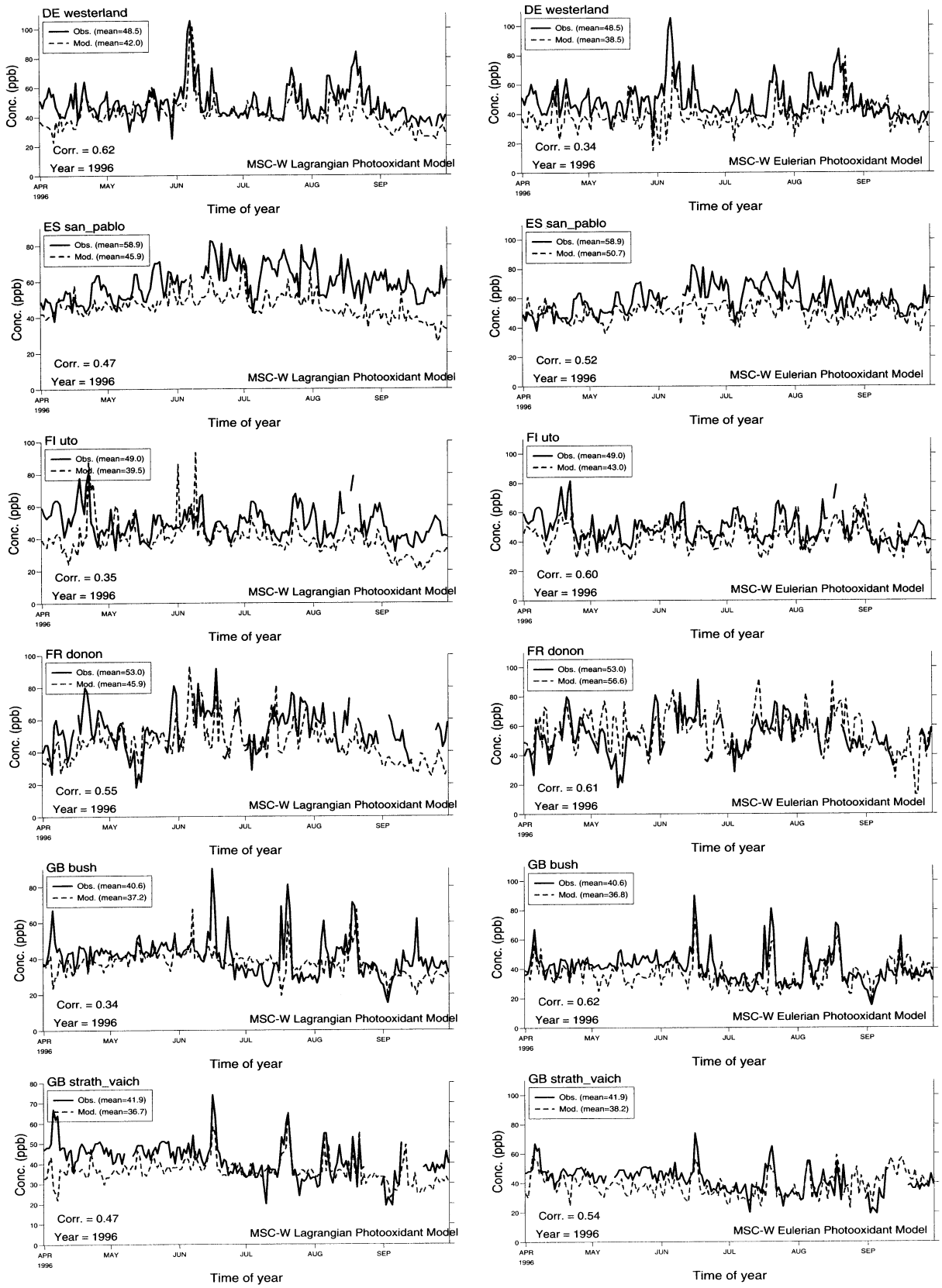

Figure 2.2: Comparison, Modelled versus observed daily max. ozone (ppb), Lagrangian model (left) and Eulerian model (right)

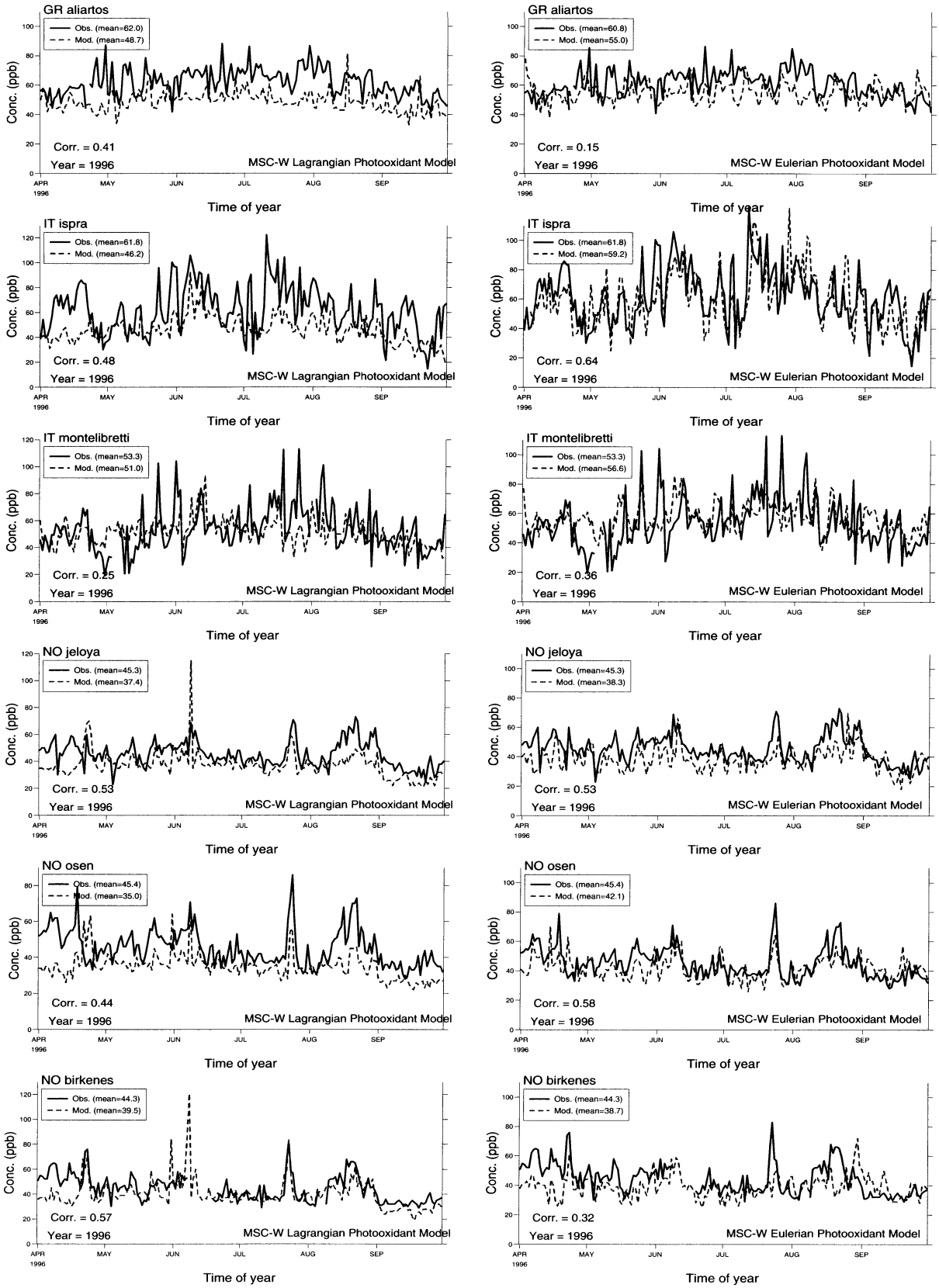

Figure 2.3: Comparison, Modelled versus observed daily max. ozone (ppb), Lagrangian model (left) and Eulerian model (right)

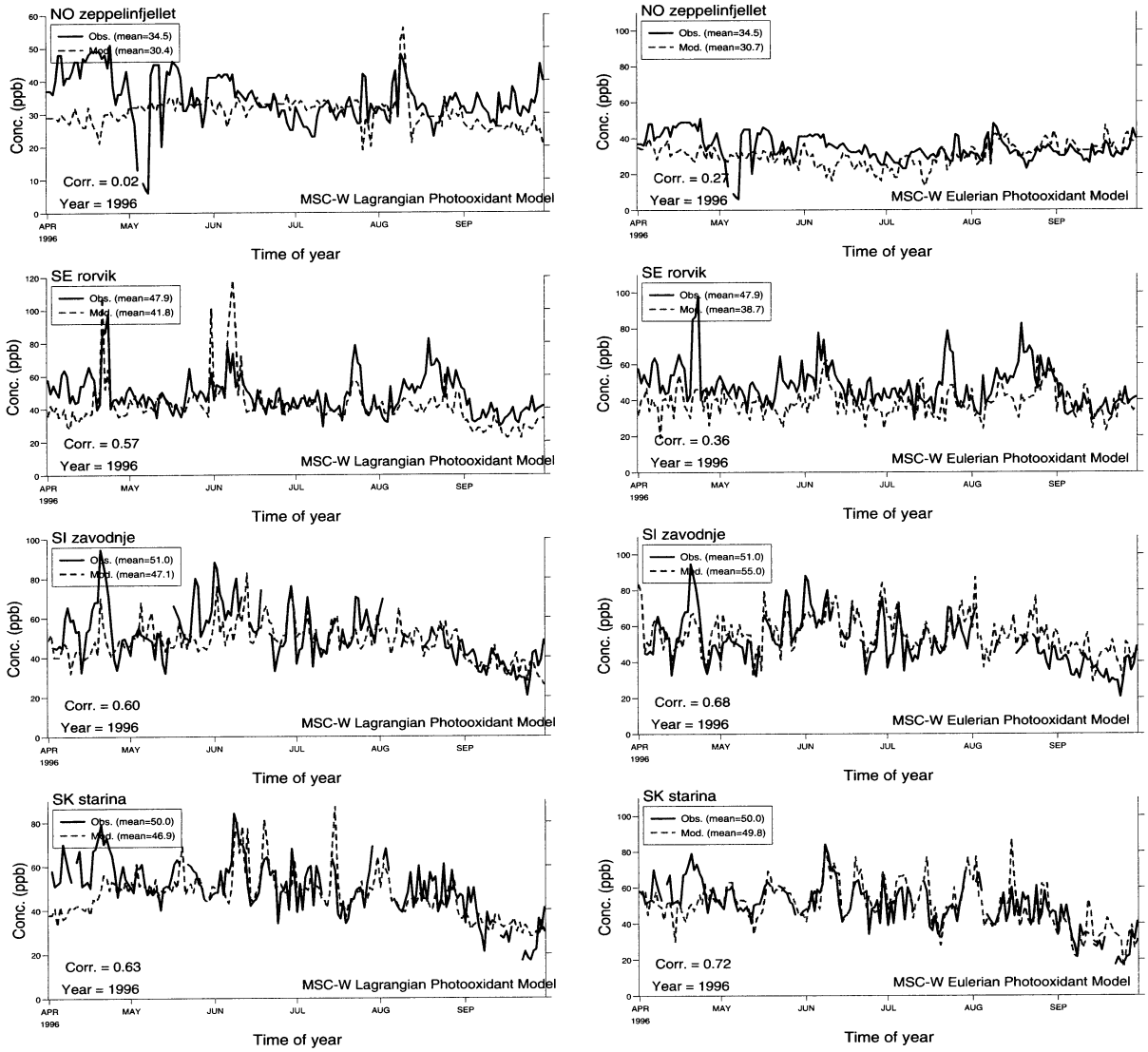

Figure 2.4: Comparison, Modelled versus observed daily max. ozone (ppb), Lagrangian model (left) and Eulerian model (right)

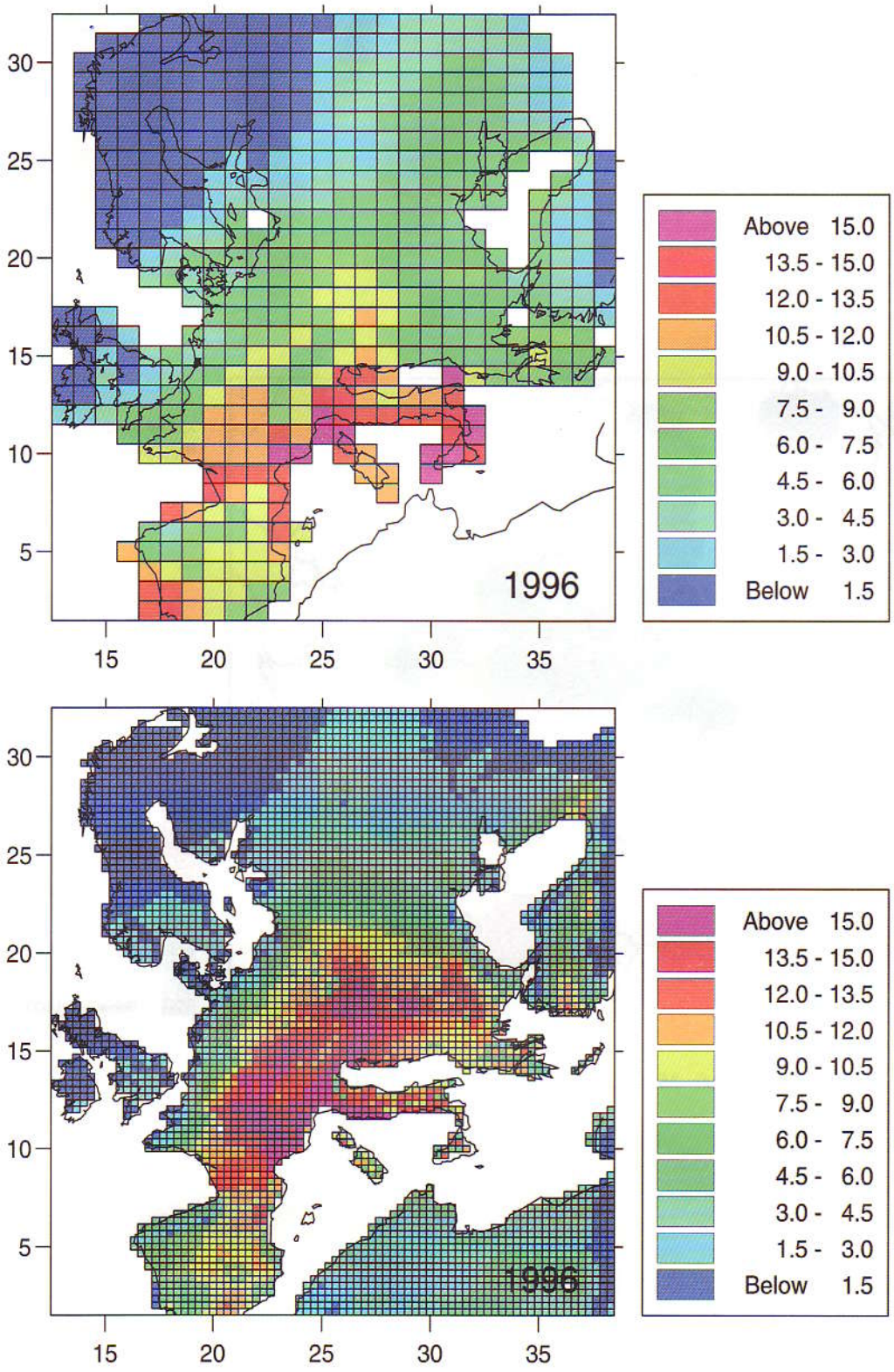

Figure 2.5: Comparison of $AOT40_c$ values predicted from the Lagrangian model (top) and Eulerian model (bottom), May-July 1996. Units: ppm h

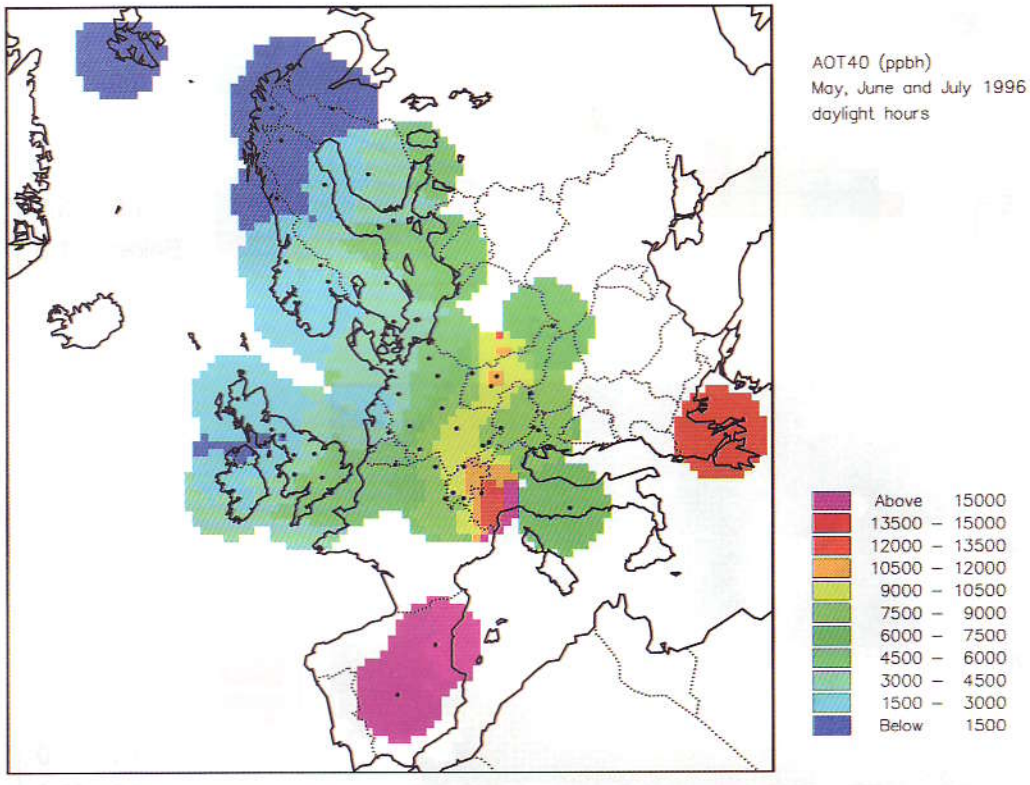

Figure 2.6: Measured AOT40 values, May-July 1996. Units: ppb h

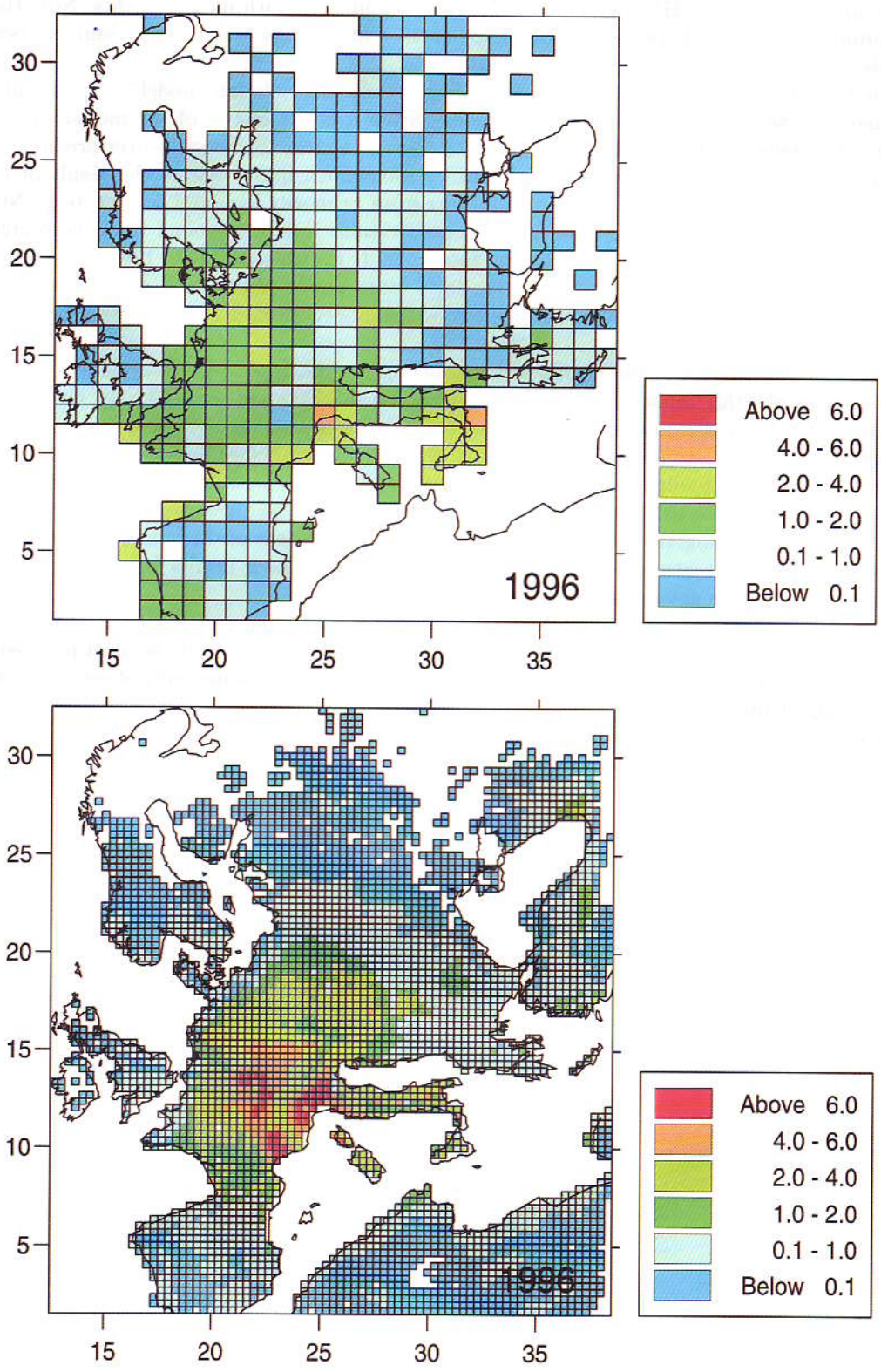

Figure 2.7: Comparison of AOT60 values predicted from the Lagrangian model (top) and Eulerian model (bottom), April-September 1996. Units: ppm h

2.3 Scatter Plots

In figure 2.8-2.9 the summertime-mean (April-September) concentrations of SO_2, NO_2, sulphate, and total nitrate (HNO_3+partulate NO_3^-) are compared with measurements. Note that the number of modelled-stations available for these scatter plots was not the same in both models, so the statistics are not directly comparable.

For the primary species (SO_2 and NO_2, Fig. 2.8) the Eulerian model performs quite reasonably, with most calculated concentrations within a factor of two of the measurements, and good correlation. For the Lagrangian model there is a clear tendancy to over-predict SO_2 and under-predict NO_2. These tendancies can be explained quite well as the result of the single-layer formulation of this model: pollutants from primarily low-level sources (e.g. NO_x from road traffic) will in reality have higher concentrations near the ground than those given by the boundary-layer average predicted by the model (e.g. Simpson et al., 1990). Pollutants from primarily high-level sources (e.g. SO_2 from large power plants) will often have lower concentrations near the ground than those given by the model. Both of these effects are greatest at night.

For sulphate (Fig. 2.9) the results of both models are much poorer. As discussed in Part II (Jonson et al., this report) this may be caused for the Eulerian model by an insufficient oxidation of SO_2 in the aqueous phase. The Lagrangian model has the same linear sulphur chemistry as the acid deposition model (Hov et al., 1988, Tsyro, 1998), but so far no attention has been paid to the modelling of this species within the ozone modelling work. (There is no feedback from sulphate to the ozone chemistry, so this species has been regarded purely as a sink). Thus the Lagrangian model has only a very crude treatment of the boundary conditions for sulphate, and no treatment of natural (DMS) inputs, so the poor results for the Lagrangian model in this case are not too surprising.

For nitrate, on the other hand, the results are again reasonable for both models. This is encouraging as the amount of nitrate formed is a good indicator of the overall chemical-processing of the models. However, there are large difficulties both in the measurements of even the sum of the components used here (HNO_3,partulate NO_3^-), and in modelling the concentration of a species like HNO_3 near the ground surface - concentation gradients can be very large and determined very locally. Thus all comparisons against these species will involve considerable uncertainities.

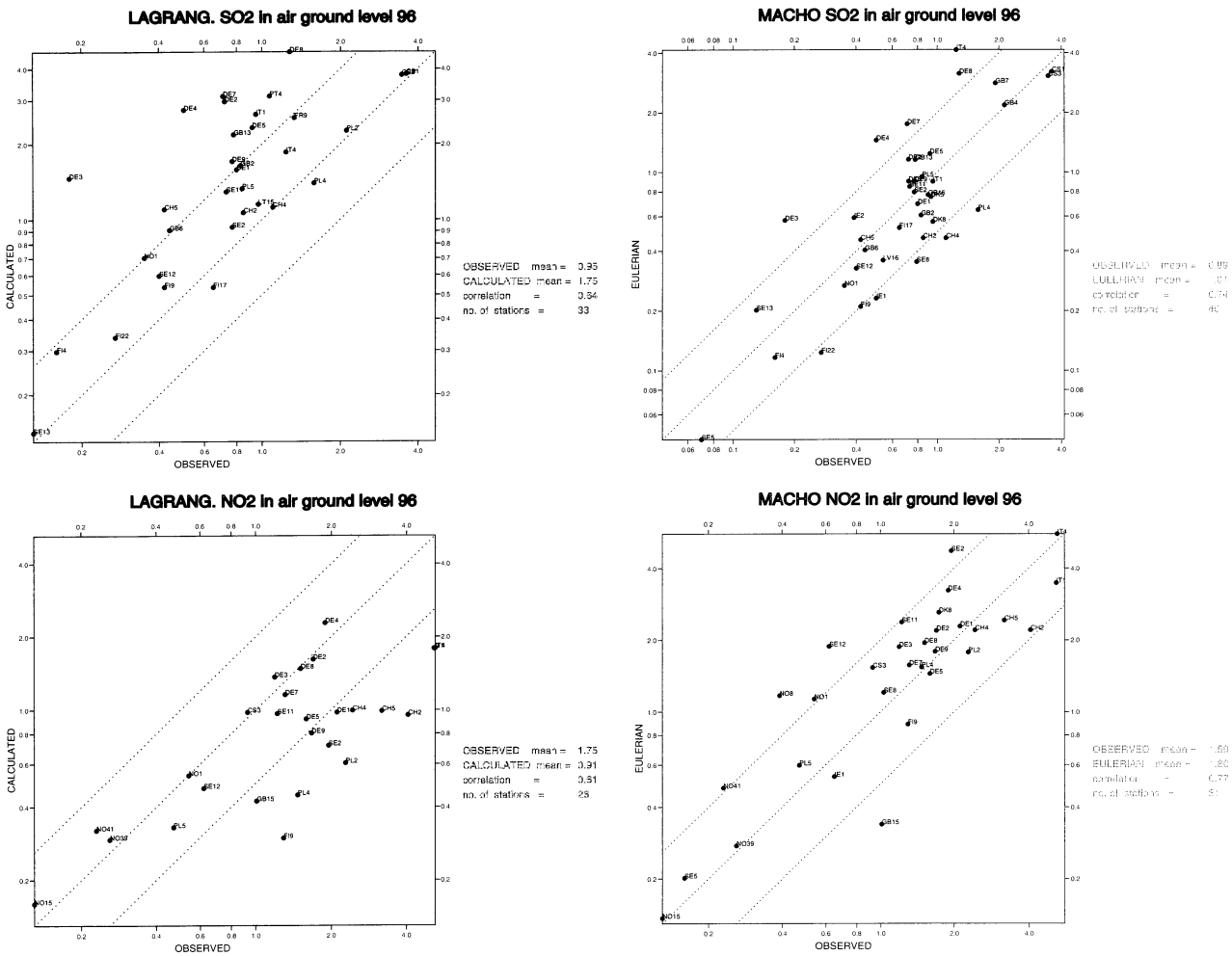

Figure 2.8: Scatter plots for calculated versus measured concentrations of SO_2 (μg m^{-3} S) and NO_2 (μg m^{-3} N), for the Lagrangian model (left) and Eulerian model (right). Stations identified by 2-letter country codes

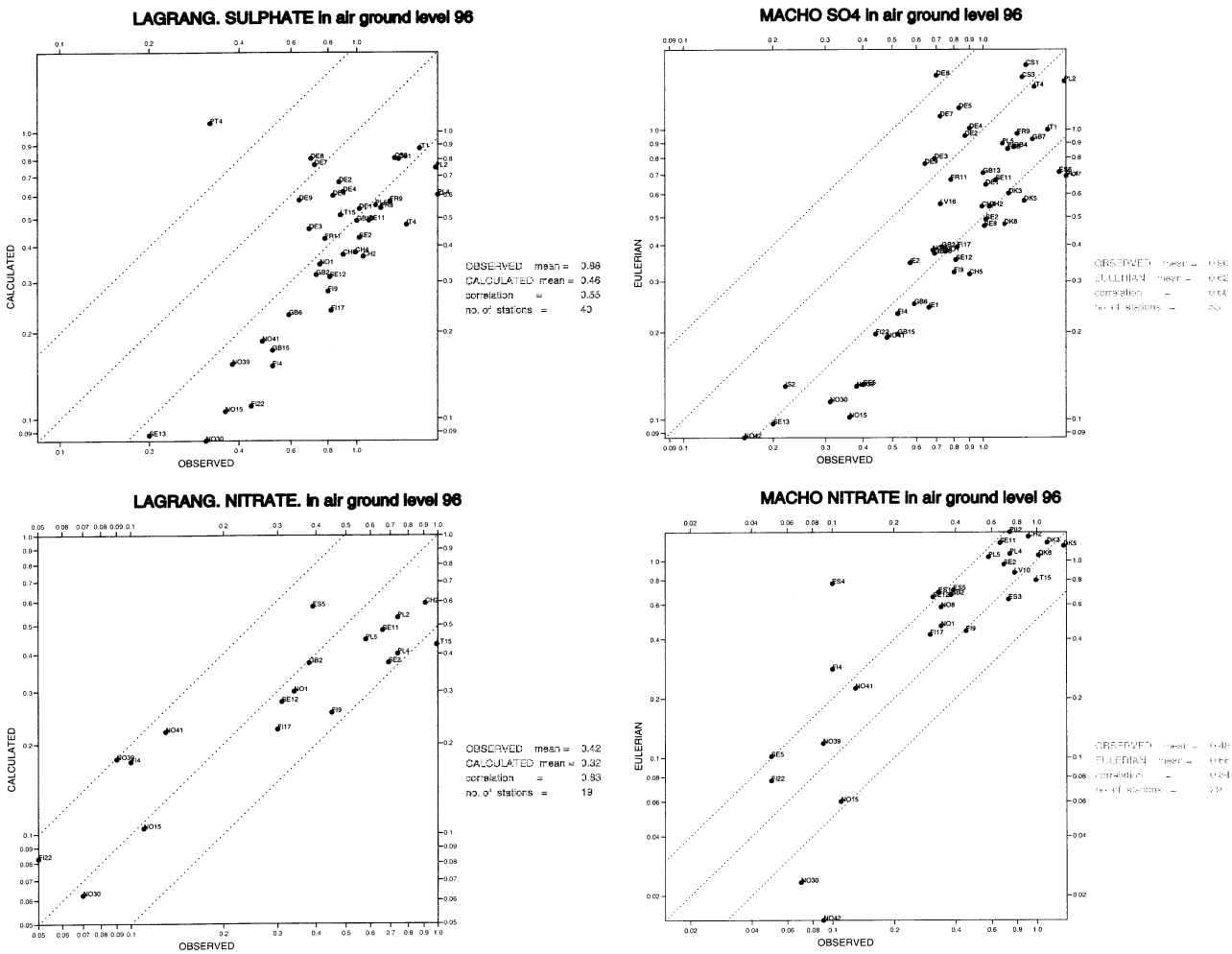

Figure 2.9: Scatter plots for calculated versus measured concentrations of suplhate in air (μg m^{-3} S) and total-nitrate in air (μg m^{-3} N), for the Lagrangian model (left) and Eulerian model (right). Stations identified by 2-letter country codes

Chapter 3

Discussion and Conclusions

This work has compared for the first time the results of the MSC-W Lagrangian photo-oxidant model and the MSC-W Eulerian oxidant model. This comparison has clearly shown that the Eulerian oxidant model is capable of operational usage for six month simulations, and it delivers performance with respect to ozone which is comparable to that of the Lagrangian model. Indeed, when comparing time-series the Eulerian model seems to show a better correlation with day-to-day measurements than the Lagrangian model. However, when comparing AOT statistics, the Lagrangian model appears to match the observed distribution somewhat better than the Eulerian model.

This comparison excercise has given a first overview of the side-by-side behaviour of the two models. However, this does not allow us to decide whether differences in model output are due to differences in the model structure (especially horizontal and vertical resolution), or due to some of the other differences noted in Table 1.1.

A number of activities are foreseen which will help in understanding the results presented here, and which will give important information for future applications of both models:

Sensitity tests The extent to which the model results depend on boundary conditions, chemistry, photolysis rates, etc., needs to be investigated, in order to understand which paramaters most affect model performance.

Harmonisation It is clear that both the Lagrangian and Eulerian models are structurally very different, but they do share a large number of features which could be harmonised to a greater extent.

Thus emission inputs should be identical, and ideally the deposition modules, boundary-condition input, and chemical schemes (including the photolysis schemes) should also be the same as far as possible. This harmonisation will enable more efficient use of resources within MSC-W, and make future model comparisons easier to interpret.

Emission control tests An important comparison will be to run a variety of emission-control simulations with both models. This should include both Europe-wide emission controls and also country-specific emissions controls. The most important question to be evaluated with these tests is how far the response to NO_x emissions controls is similar in the two models.

3.1 References

Berntsen, T.K., Isaksen, I.S.A., Myhre, G., Fuglestvedt, J.S., F.Stordal, Alsvik Larsen, T., R.S.Freckleton, and Shine, K.P., 1997, Effects of anthropogenic emissions on tropospheric ozone and its radiative forcing, *J. Geophys. Res.*, 102, 28101–28126.

DeMore, W.B., Sander, S.P. amd Golden, D.M., Hampson, R.F., Kurylo, M.J., Howard, C.J., Ravishankara, A.R., Kolb, C.E., and Molina, M.J., 1997, Chemical kinetics and photochemical data for use in stratospheric modelling, JPL Publication 97-4.

Derwent, R.G., Jenkin, M.E., and Saunders, S.M., 1996, Photochemical ozone creation potentials for a large number of reactive hydrocarbons under European conditions, *Atmos. Environ.*, 30, 189–200.

Eliassen, A., Hov, Ø., Isaksen, I.S.A., Saltbones, J., and Stordal, F., 1982, A lagrangian long-range transport model with atmospheric boundary layer chemistry, *J. Appl. Met.*, 21, No. 11, 1645–1661.

Friedrich, R., 1993, Generation of time-dependent emission data, In P. Borrel et al., editor, *Transport and Transformation of Polluntants in the Troposphere, Proceedings EUROTRAC symposium 1992*, pages 255–268. SPB Acad. Publish. bv., the Hague, Netherlands.

Hov, Ø., Hesstvedt, E., and Isaksen, I.S.A., 1978, Long-range transport of tropospheric ozone, *Nature*, 273, No. 5661, 341–344.

Hov, Ø., Eliassen, A., and Simpson, D., 1988, Calculation of the distribution of NO_x compounds in Europe., In Isaksen, I.S.A., editor, *Troposheric ozone. Regional and global scale interactions*, pages 239–262, Dordrecht. D. Reidel.

Jenkin, M.E., Saunders, S.M., and Pilling, M.J., 1997, The tropospheric degradation of volatile organic compounds: a protocol for mechanism development, *Atmos. Environ.*, 31, 81–104.

Jonson, J.E., Jakobsen, H.A., and Berge, E., 1997, Status of the development of the regional scale photo-chemical multi-layer eulerian model, Norwegian Meteorological Institute, EMEP MSC-W Note 2/97.

Kylling, A., 1995, Phodis, a programme for calculation of photo-dissociation rates in the earths atmosphere, available by anonymous ftp to pluto.itek.norut.no, cd pub/arve.

Mylona, S., 1998, Emissions data., In MSC-W (1988).

Olendrzyński, K., 1997, Emissions, In EMEP MSC-W Report 1/97, "Transboundary air pollution in Europe. Part 1: Emissions, dispersion and trends of acidifying and eutrophying agents, ed. E. Berge.

Simpson, D., Perrin, D.A., Varey, J.E., and Williams, M.L., 1990, Dispersion modelling of nitrogen oxides in the United Kingdom, *Atmos. Environ.*, 24A, No. 7, 1713–1733.

Simpson, D., Andersson-Sköld, Y., and Jenkin, M. E., 1993, Updating the chemical scheme for the EMEP MSC-W oxidant model : current status, Norwegian Meteorological Institute, EMEP MSC-W Note 2/93.

Simpson, D., Guenther, A., Hewitt, C.N., and Steinbrecher, R., 1995, Biogenic emissions in Europe 1. Estimates and uncertainties, *J. Geophys. Res.*, 100, No. D11, 22875–22890.

Simpson, D., 1992, Long period modelling of photochemical oxidants in Europe. Calculations for July 1985, *Atmos. Environ.*, 26A, No. 9, 1609–1634.

Simpson, D., 1993, Photochemical model calculations over Europe for two extended summer periods: 1985 and 1989. Model results and comparisons with observations, *Atmos. Environ.*, 27A, No. 6, 921–943.

Simpson, D., 1995, Biogenic emissions in Europe 2: Implications for ozone control strategies, *J. Geophys. Res.*, 100, No. D11, 22891–22906.

Sundet, J.K., 1997, Model studies with a 3-d global CTM using ECMWF data., Phd thesis Dep. of Geophysics, Univ. of Oslo.

Tsyro, S., 1998, Description of the lagrangian acid deposition model, In MSC-W (1988), Part 2: Numerical Addendum.

Part IV

Appendices

Appendix A

Lagrangian model: Physical and chemical formulation

A.1 Lagrangian model formulation

We briefly review some of the main parameters involved in the Lagrangian model. Further details are given in Simpson (1992,1993,1995) and Simpson et al. (1993, 1995).

A.1.1 Emissions

The emissions input required by the Lagrangian photo-oxidant model consists of national emissions of SO_2, NO_x, NMVOC and CO, disaggregated to 11 source-sectors and on the 50 x 50 km^2 EMEP grid.

The emissions used in the calculations presented here are identical to those used in Simpson et al. (1997), as documented in EMEP Report 1/97 (Olendrzyński, 1997). Although not the most-to-date, these emissions are very similar for nearly all countries to those more recently documented by Mylona (1998).

Speciation of VOC emissions are also specified separately for each source-sector, derived from the detailed United Kingdom speciation given in PORG (1993). Each of the species from this detailed inventory has been assigned to one of the EMEP model's species according to reactivity and chemical composition. Details are given in Andersson-Sköld and Simpson (1997).

Emissions of isoprene, probably the most important biogenic compound with regard to ozone formation, are calculated every hour in the EMEP model using the model's radiation, temperature, and land-use data. The emission rates used in the EMEP model are based upon the algorithms of Guenther et al. (1993), and take into account recent measurements and evaluations from both the U.S. and Europe (Simpson et al., 1995, Guenther et al., 1993).

A.1.2 Wet Deposition

Wet deposition is treated using a scavenging ratio approach, whereby the loss rate of a component X is given by $\Lambda_X.[X].P/h$, where Λ_X is the scavenging ratio, P is the precipitation amount and h is the mixing height. Scavenging ratios are given in Table A:1.

Table A:1: Scavenging ratios used in the Lagrangian model

Species	Value
HNO_3	$1.4.10^6$
SO_2	$3.10^5 + 1.10^5 \sin[2\pi(\tau - \tau_0)/\tau_a]$
	(τ = day of year;τ_0 = 80 days; τ_a = 365(366) days)
H_2O_2	$1.4.10^6$
HCHO	as SO_2
CH_3OH	$1.4.10^6$
Particulate sulphate	$1.0.10^6$
Particulate nitrate	$1.0.10^6$

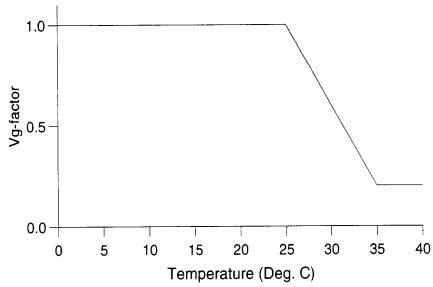

Figure A.1: Scaling factor applied to deposition velocity, to mimic stomatal closure.

A.1.3 Dry Deposition

Deposition is calculated in the model using a resistance-based approach as described in Hov et al. (1988). Briefly, maximum 1-m dry deposition velocities are first assigned for each species. These velocities are adjusted for time-of-year to reflect seasonal changes in vegetation uptake (except for HNO_3). Then the flux of ozone to the surface is calculated based upon the model's aerodynamic resistance (R_a) parameterisation. At night the deposition velocities are reduced by a factor of four to simulate the effect of stomatal closing in vegetation. Over sea areas the deposition velocities of ozone, NO_2, and PAN (& MPAN) are set to zero.

The maximum 1-m deposition velocities are given in Table A:2

Table A:2: Maximum -1m deposition velocities (cm s^{-1}) used in the Lagrangian model

Species	Value	Species	Value
Ozone	0.5	HCHO	0.3
SO_2	0.8	RCHO	0.3
NO_2	0.2	ROOH	0.5
HNO_3	4.0	ketones	0.3
H_2O_2	0.8	HCHO	0.3
Particulate sulphate	0.1	PAN/MPAN	0.2
Particulate nitrate	0.1		

At high temperatures the stomata of plants close, thus reducing the plants loss of vapour but also its uptake of ozone. Other factors (e.g. soil moisture deficit) can also play an important role (Emberson et al., 1996, Fuhrer, 1996) in this process. In order to include at least a crude representation of stomatal closure effects in the current modelling work, a very simplified representation has been adopted. When surface (2m) temperatures exceed 25°C the ozone deposition velocity is reduced by 8% for each extra degree Centigrade, up to 35 °C, as illustrated in Figure A.1.

Although simple, this formulation is roughly consistent with measured stomatal conductances (pers.comm., Emberson, 1997), and leads to lower ozone fluxes into vegetation in warmer climates. It has therefore been adopted as an interim solution which is thought to be more realistic than previous parameterisations.

A.1.4 Initial/free tropospheric concentrations

The treatment of boundary conditions in the EMEP model has been described in detail in Simpson (1992). Briefly, for a species such as ozone, we specify concentrations at a fixed latitude and month, for example 50 ppb for 45°N in June, and then modify this value for other months and latitudes.

Simpson (1992) derived boundary conditions appropriate for 1990. The CO and CH_4 have since been updated. Further, for other years we now apply a trend factor to these boundary condition values, so that for ozone for example the assumed "specified" boundary conditions vary from 20 ppb in 1900 to 50 ppb in 1990. Trends for ozone and other species are given in Table A:3

Table A:3: Trends in free-tropospheric background concentrations applied in the multi-year runs. Units: ppb.

	Trend %/yr (ref.)	1900	1950	1970	1980	1990	1995	2010
CO (land/sea)	0.85 (1,†)	70/50a	107/57	127/67	138/73	150/80,b	150/80	150/80
CH_4	0.63-0.91 (2)	1000b	1326	1504	1625	1780	1863	2135
O_3	1.0 (3,†)	20	34	41	45	50	50	
VOC	0.85 (4,†)	-	-	-	-	-	-	

Notes: 1. Trend, 1950-1990, equated with trend of 0.85%/yr for 1950-1987 of Zander et al. (1989b);
2: Trend for 1950-1975 equated with Zander at al.'s trend of 0.633 for 1951 to 1975, trend for 1975-2010 equated with Zander et al.'s trend of 0.91 for 1975 to 1985-87 (Zander et al., 1989a). Emissions are still increasing in many countries, therefore trend continued;
3. Trend of 1% per year assumed, consistent with Janach (1989), Low et al. (1990), Volz and Kley (1988), Bojkov (1986), Logan (1994);
4. Trend for ethane of 0.85%/yr from Ehhalt et al. (1991). The EMEP model also specifies n-butane and ethene as boundary conditions - for simplicity, we assign the same trends to these species as for ethane. (This completely ignores differences in sources, sinks, and lifetimes between the different VOC species, but is probably a better approximation than zero trend);
†Zero trend assumed after 1990.
a: Estimate, based upon Thompson and Cicerone (1986), and gives CO roughly consistent with measurements suggesting ca. 50 ppb in the Southern Hemisphere (Cicerone, 1988). b: CO for 1990 based upon data from Simmonds et al. (1996). c: Ehhalt et al. (), consistent with ice-core data of Stauffer and Neftel (1988).

A.2 Lagrangian model: chemical scheme

We give here a complete listing of the chemical mechanism used in the photo-oxidant model. Reaction coefficients are largely from Atkinson (1990) and Atkinson et al. (1992). Isoprene chemistry is derived from Paulson and Seinfeld (1992). Full details of the sources and methodology behind the reaction schemes are given in Simpson et al. (1993). A number of extra HO_2-RO_2-ROOH were introduced to the chemistry in Simpson (1995) in order to render the isoprene treatment consistent with that of the other VOC species in the model.

A.2.1 Photolysis rates

An updated formulation of the photolysis rates has been adopted, based upon the UK photochemical trajectory model (Derwent et al., 1996, Jenkin et al., 1997):

$$J = L.(cos\theta)^{M} exp(-Nsec(\theta))$$

Where θ is the solar zenith angle, and L, M, and N are coefficients as listed in Appendix A. The new rates give in some cases substantially different photolysis coefficients than those used previously - see Simpson et al. (1997) for more details.

Table A:4: Photolysis rate coefficients used in the Lagrangian EMEP model.

	L	M	N	Reaction
1	5.219E-04	0.322	0.079	O3 → O3P + O2
2	8.978E-05	1.436	0.936	O3 → O1D + O2
3	1.108E-02	0.397	0.183	NO2 → NO + O3P
4	1.057E-05	0.800	0.243	H2O2 → OH + OH
5	1.037E-06	1.227	0.322	HNO3 → NO2 + OH
6	4.866E-05	0.781	0.349	HCHO → HO2 + HO2 + CO
7	6.790E-05	0.565	0.275	HCHO → CO + H2
8	8.443E-06	1.177	0.437	CH3CHO → CH3 + HCO
9	6.591E-06	1.070	0.399	CH3COC2H5→ CH3COO2 + C2H5O2
10	3.887E-05	0.695	0.289	GLYOX → 2 HO2 + 2 CO
11	1.524E-04	0.270	0.156	MGLYOX → CH3COO2 + CO + HO2
12	1.030E-05	0.222	0.154	GLYOX → 0.13 HCHO + 0.87 H2 + 1.87 CO
13	2.669E-02	0.185	0.103	NO3 → NO2 + O2
14	1.853E-01	0.189	0.112	NO3 → NO2 + O3P
15	3.324E-05	0.000	0.566	N2O5 → NO2 + NO3
16	5.797E-06	0.764	0.249	CH3OOH → CH3O + OH
	"	"	"	C2H5OOH → C2H5O + OH
	"	"	"	CH3COO2H → CH3O2 + CO2 + OH
	"	"	"	CH3COCHO2HCH3 → CH3CHO+CH3COO2+OH
	"	"	"	secC4H9O2H → OH + secC4H9O
	"	"	"	CH2OOHCH2OH → HO2 + OH + 1.56 HCHO + 0.22 CH3CHO
	"	"	"	CH3CHOOHCH2OH → CH3CHO + HCHO + HO2
	"	"	"	OXYO2H → OH + MGLYOX + MAL + HO2
	"	"	"	MALO2H → OH + HO2 + MGLYOX + GLYOX

Notes: inorganic rates taken from Derwent et al. (1996), organic rates from Jenkin et al. (1997)

A.2.2 Chemical reactions

Reaction coefficients are in units of s^{-1} for unimolecular reactions, cm^3 $molecule^{-1}$ s^{-1} for bimolecular reactions, and cm^6 $molecule^{-2}$ s^{-2} for termolecular reactions. Reaction steps labelled as "Immediate" are given for clarity only.

Table A:5: Photo-oxidant Chemistry: Lagrangian Model

Rate coefficient	Reaction
Generic reaction rates	
FHO2=(1.+1.4E-21*H2O*exp(2200./t))	
KRO2NO=4.2E-12*exp(180./t)	
KHO2RO2=1.0E-11	
KRC87=1.0E-12*exp(190./t)	
KRC91=5.8E-12*exp(190./t)	
KRC92=1.9E-12*exp(190./t)	
	Inorganic chemistry
5.7E-34*(t/300.0)$^{-2.8}$	O+O2+M → O3
9.6E-32*(t/300.0)$^{-1.6}$	O+NO+M → NO2
2.0E-11*exp(100.0/t)	OD+M → O
2.2E-10	OD+H2O → OH+OH
Immediate	H+O2 → HO2
1.8E-12*exp(-1370./t)	O3+NO → NO2
1.2E-13*exp(-2450./t)	O3+NO2 → NO3
1.9E-12*exp(-1000./t)	O3+OH → HO2
1.4E-14*exp(-600./t)	O3+HO2 → OH
1.8E-11*exp(110./t)	NO+NO3 → NO2+NO2
3.7E-12*exp(240./t)	NO+HO2 → NO2+OH
7.2E-14*exp(-1414./t)	NO2+NO3 → NO+NO2
1.4E-12	NO2+NO3 → N2O5
1.4E-11	NO2+OH → HNO3
4.1E-16	NO3+H2O2 → HO2+HNO3
7.1E+14*exp(-11080./t)	N2O5 → NO2+NO3
4.8E-11*exp(250./t)	OH+HO2 → H2O
2.9E-12*exp(-160./t)	OH+H2O2 → HO2
7.7E-12*exp(-2100./t)	OH+H2 → H
1.0E-14*exp(785./t)	OH+HNO3 → NO3
FHO2*2.3E-13*exp(600./t)	HO2+HO2 → H2O2
FHO2*M*1.7E-33*exp(1000./t)	HO2+HO2 → H2O2
	Sulphur chemistry
1.35E-12	OH+SO2 → HSO3
4.0E-17	CH3O2+SO2 → SO3+CH3O
Immediate	HSO3+O2 → HO2+SO3
Immediate	SO3+H2O → SA
	Methane chemistry
$7.44 * 10^{-18} \times T^2 \times exp(-1361/T)$	OH+CH4 → CH3
Immediate	CH3+O2 → CH3O2
KRO2NO	CH3O2+NO → CH3O+NO2
5.5E-14*exp(365./t)	CH3O2+CH3O2→CH3O+CH3O
5.5E-14*exp(365./t)	CH3O2+CH3O2→CH3OH+HCHO
3.3E-12*exp(-380./t)	OH+CH3OH→HO2+HCHO
3.8E-13*exp(780./t)	HO2+CH3O2 → CH3O2H
Immediate	CH3O+O2 → HCHO+HO2
9.6E-12	OH+HCHO → HCO
Immediate	HCO+O2 → CO+HO2

continued on next page

Rate coefficient	Reaction
1.0E-12*exp(190./t)	CH3O2H + OH → HCHO + OH
1.9E-12*exp(190./t)	CH3O2H + OH → CH3O2
5.8E-16	NO3+HCHO → HNO3+HCO
2.4E-13	OH+CO → H
	Ethane chemistry
7.8E-12*exp(-1020./t)	OH+C2H6 → C2H5O2
8.9E-12	C2H5O2+NO → C2H5O+NO2
6.5E-13*exp(650./t)	C2H5O2+HO2 → C2H5OOH
5.8E-12*exp(190./t)	C2H5OOH+OH → CH3CHO+OH
1.9E-12*exp(190./t)	C2H5OOH+OH → C2H5O2
Immediate	C2H5O+O2 → HO2+CH3CHO
5.6E-12*exp(310./t)	OH+CH3CHO → CH3COO2
1.0E-11	CH3COO2+NO2 → PAN
1.34E+16*exp(-13330./t)	PAN → CH3COO2+NO2
2.0E-11	CH3COO2+NO → NO2+CH3
5.5E-12	CH3O2+CH3COO2 → CH3O+CH3
5.5E-12	CH3O2+CH3COO2 → CH3COOH+HCHO
2.8E-12*exp(530/t)	CH3COO2+CH3COO2 → CH3+CH3
1.3E-13*exp(1040./t)	CH3COO2+HO2 → CH3COO2H
1.9E-12*exp(190./t)	CH3COO2H+OH → CH3COO2
3.0E-13*exp(1040./t)	CH3COO2+HO2 → CH3COOH + O3
	Ethanol chemistry
3.2E-12	OH+C2H5OH → CH3CHO + HO2
	n-butane chemistry
1.64E-11*exp(-559./t)	OH+NC4H10 → SECC4H9O2
KRO2NO	NO+SECC4H9O2→NO2+SECC4H9O
Immediate	SECC4H9O→ 0.65 HO2 + 0.65 CH3COC2H5 + 0.35 CH3CHO +0.35 C2H5O2
1.15E-12	OH+CH3COC2H5 → CH3COCHO2CH3
KRO2NO	CH3COCHO2CH3+NO → NO2+CH3COO2+CH3CHO
KHO2RO2	CH3COCHO2CH3+HO2→CH3COCHO2HCH3
4.8E-12	CH3COCHO2HCH3+OH→CH3COCHO2CH3
KHO2RO2	SECC4H9O2+HO2→SECC4H9O2H
KRC92	SECC4H9O2H+OH→SECC4H9O2
KRC91	SECC4H9O2H+OH→OH+CH3COC2H5
	Ethene chemistry
1.66E-12*exp(474./t)	C2H4+OH → CH2O2CH2OH
KRO2NO	CH2O2CH2OH+NO→NO2+HCHO+HCHO+HO2
KHO2RO2	CH2O2CH2OH+HO2 → CH2OOHCH2OH
KRC91	CH2OOHCH2OH+OH → CH3CHO + OH
KRC92	CH2OOHCH2OH+OH → CH2O2CH2OH
1.2E-14*exp(-2630./t)	C2H4+O3→HCHO+0.44 CO+ 0.12 HO2+ 0.4 HCOOH+ 0.13 H2
	Propene chemistry
6.5E-15*exp(-1880./t)	O3+C3H6→ 0.5 HCHO+ 0.5 CH3CHO+ 0.07 CH4+ 0.4 CO+ 0.28 HO2+ 0.15 OH+ 0.31 CH3O2+ 0.07 H2
2.86E-11	OH+C3H6 → CH3CHO2CH2OH
KRO2NO	NO+CH3CHO2CH2OH→NO2+CH3CHO+HCHO+HO2
KHO2RO2	CH3CHO2CH2OH+HO2→CH3CHOOHCH2OH
KRC91	CH3CHOOHCH2OH+OH→ CH3COC2H5+OH
KRC92	CH3CHOOHCH2OH+OH→ CH3CHO2CH2OH

continued on next page

Rate coefficient	Reaction
	o-xylene chemistry
1.37E-11	OXYL+OH→OXYO2
KRO2NO	OXYO2+NO→NO2+MGLYOX+MAL+HO2
KHO2RO2	OXYO2 + HO2→OXYO2H
1.7E-11	OXYO2H + OH → OXYO2
2.0E-11	MAL+OH→MALO2
KRO2NO	MALO2+NO→NO2+HO2+MGLYOX+GLYOX
KHO2RO2	MALO2+HO2→MALO2H
2.4E-11	MALO2H+OH → MALO2
1.1E-11	OH+GLYOX→HO2+CO+CO
1.70E-11	OH+MGLYOX→CH3COO2+CO
	Aerosol chemistry
RH dependent	H2O2 → aerosol
RH dependent	CH3O2H → aerosol
RH dependent	N2O5 → 2 x nitrate
RH dependent	HNO3 → nitrate
	Isoprene chemistry
12.3E-15*exp(-2013/t)	ISOP+O3→ 0.67 MACR, 0.26 MVK+0.3 O, 0.55 OH+0.07 C3H6+0.8 HCHO+0.06 HO2+0.05 CO
2.54E-11*exp(410./t)	ISOP+OH→ISRO2
KRO2NO	ISRO2+NO→ 0.32 MACR+0.42 MVK+0.74 HCHO, 0.14 ISNI+0.12 ISRO2+0.78 HO2+0.86 NO2
4.13E-12*exp(452./t)	MVK+OH→MVKO2
KRO2NO	MVKO2+NO→ 0.684 CH3CHO+0.684 CH3COO2+ 0.266 MGLYOX+0.266 HCHO+0.05 ISNI+0.95 NO2+0.95 HO2
KHO2RO2	ISRO2+HO2→ISRO2H
2.0E-11	ISRO2H + OH→OH+ISRO2
8.0E-18	ISRO2H + O3→*0.7:HCHO
1.86E-11*exp(175./t)	MACR+OH→0.5 AOH1+ 0.5:MACRO2
1.0E-11	MACRO2+NO2→MPAN
1.34E+16*exp(-13330./t)	MPAN → MACRO2+NO2
2.0E-11	MACRO2+NO→CH2CCH3+NO2
KRO2NO	CH2CCH3+NO →NO2+CH3COC2H5+HO2
4.32E-15*exp(-2016./t)	MVK+O3→0.82 MGLYOX+0.8 HCHO+0.2 O+ 0.05 CO+0.06 HO2+0.04 CH3CHO+0.08 OH
3.35E-11	ISNI+OH→ISNIR
KRO2NO	ISNIR+NO→ 0.05 HO2+ 2.0 NO2+ 0.95 CH3CHO+ 0.95 CH3COC2H5
NO3 chemistry	
7.8E-13	ISOP +NO3→ISONO3
KRO2NO	ISONO3+NO→1.1 NO2+0.8 HO2+0.85 ISNI+0.1 MACR+0.15 HCHO+0.05 MVK
	Extra since Note 2/93 (Simpson et al. 1993)
KHO2RO2	MVKO2 + HO2 → MVKO2H
KHO2RO2	MACRO2 + HO2 → MARO2H
KHO2RO2	CH2CCH3+ HO2 → CH2CO2HCH3
KHO2RO2	ISNIR + HO2 → ISNIRH
KHO2RO2	ISONO3 + HO2 → ISONO3H
3.2E-11	CH2CO2HCH3 + OH → CH2CCH3
2.0E-11	ISONO3H + OH → ISONO3
2.2E-11	MVKO2H + OH → MVKO2

continued on next page

Rate coefficient	Reaction
3.7E-11	ISNIRH + OH → ISNIR
3.7E-11	MARO2H + OH → MACRO2

Notes:
"t" is temperature, M is third body.

Abbreviations for some species names:

OXYO2	Peroxy radical from o-xylene + OH
OXYO2H	Hydroperoxide from OXYO2 + HO2
GLYOX	Glyoxal (HCOCHO)
MGLYOX	Methyl-glyoxal (CH3COCHO)
MAL	$CH_3COCH=CHCHO$
MALO2	Peroxy radical from MAL + OH
MALO2H	Hydroperoxide from MALO2 + HO2
ISRO2	Peroxy radical from isoprene + OH
ISRO2H	Hydroperoxide from ISRO2 + HO2
MACR	Methacrolein
MACRO2	Hydroperoxide from Methacrolein
MPAN	Peroxy methacryloyl nitrate ($CH_2CH(CH_3)C(=O)O_2NO_2$)
MVK	Methyl-vinyl-ketone
MVKO2	Peroxy radical from MVK + OH
MVKO2H	Hydroperoxide from MVKO2 + HO_2
ISNI	Organic nitrate from isoprene
ISONO3	Isoprene-NO_3 adduct
ISNIR	Alkyl peroxy radical from ISNI

A.3 References

Andersson-Sköld, Y. and Simpson, D., 1997, Comparison of the chemical schemes of the EMEP MSC-W and the IVL photochemical trajectory models, Norwegian Meteorological Institute, EMEP MSC-W Note 1/97.

Atkinson, R., Baulch, D.L., Cox, R.A., Hampson, R.F., Kerr, J.A., and Troe, J., 1992, Evaluated kinetic and photochemical data for atmospheric chemistry: supplement IV, *Atmos. Environ.*, 26A, No. 7, 1187–1230.

Atkinson, R., 1990, Gas-phase troposheric chemistry of organic compounds: a review, *Atmos. Environ.*, 24A, No. 1, 1–41.

Bojkov, R.J., 1986, Surface ozone concentrations during the second half of the nineteenth century, *J. Clim. appl. Met.*, 25, 343–352.

Cicerone, R.J., 1988, How has the atmospheric concentration of CO changed?, In Rowland, R.S. and Isaksen, I.S.A., editors, *The Changing Atmosphere*, pages 49–61, New York. Wiley.

Derwent, R.G., Jenkin, M.E., and Saunders, S.M., 1996, Photochemical ozone creation potentials for a large number of reactive hydrocarbons under European conditions, *Atmos. Environ.*, 30, 189–200.

Ehhalt, D.H., Fraser, P.J., Albritton, D., Cicerone, R.J., Khalil, M.A.K., Legrand, M., Makide, Y., Rowland, F.S., Steele, L.P., and Zander, R., Trends in source gases, Chapter 8, International Ozone Trends Panel.

Ehhalt, D.H.and Schmidt, U., Zander, R., Demoulin, Ph., and Rinsland, C.P., 1991, Seasonal cycle and secular trend of the total and tropospheric column abundance of ethane above the Jungfraujoch, *J. Geophys. Res.*, 96, 4985–4994, D3.

Emberson, L.D., Kuylenstierna, J.C.I., Cambridge, H.M., Cinderby, S., and Ashmore, M.R., 1996, Mapping relative potential sensitivity of vegetation to ozone across Europe: A preliminary analysis, Presented at workshop on Critical Levels for Ozone in Europe: Testing and Finalising the Concepts, 15-17 April 1996, Kuopio, Finland.

Fuhrer, J., 1996, The critical level for effects of ozone on crops, and the transfer to mapping, Presented at workshop on Critical Levels for Ozone in Europe: Testing and Finalising the Concepts, 15-17 April 1996, Kuopio, Finland.

Guenther, A.B., Zimmerman, P.R., Harley, P.C., Monson, R.K., and Fall, R., 1993, Isoprene and monoterpene rate variability: model evaluations and sensitivity analyses, *J. Geophys. Res.*, 98, No. D7, 12609–12617.

Hov, Ø., Eliassen, A., and Simpson, D., 1988, Calculation of the distribution of NO_x compounds in Europe., In Isaksen, I.S.A., editor, *Troposheric ozone. Regional and global scale interactions*, pages 239–262, Dordrecht. D. Reidel.

Janach, W.E., 1989, Surface ozone: trend details, seasonal variations, and interpretation, *J. Geophys. Res.*, 94, 18289–18295, D15.

Jenkin, M.E., Saunders, S.M., and Pilling, M.J., 1997, The tropospheric degradation of volatile organic compounds: a protocol for mechanism development, *Atmos. Environ.*, 31, 81–104.

Logan, J.A., 1994, Trends in the vertical distribution of ozone: An analysis of ozonesonde data, *J. Geophys. Res.*, 99, No. D12, 25553–25585.

Low, P.S., Davies, T.D., Kelly, P.M., and Farmer, G., 1990, Trends in surface ozone at Hohenpeissenberg and Arkona, *J. Geophys. Res.*, 95, 22441–22453, D13.

Mylona, S., 1998, Emissions data., In MSC-W (1988).

Olendrzyński, K., 1997, Emissions, In EMEP MSC-W Report 1/97, "Transboundary air pollution in Europe. Part 1: Emissions, dispersion and trends of acidifying and eutrophying agents, ed. E. Berge.

Paulson, S. E. and Seinfeld, J.H., 1992, Development and evaluation of a photooxidation mechanism for isoprene, *J. Geophys. Res.*, 97, No. D18, 20703–20715.

PORG, 1993, *Ozone in the United Kingdom 1993*, UK Dept. of the Environment, London, UK, Third Report of the United Kingdom Photochemical Oxidants Review Group.

Simmonds, P.G., Derwent, R.G., McCulloch, A., O'Doherty, S., and Gaudry, A. ., 1996, Long-term trends in concentrations of halocarbons and radiatively active trace gases in Atlantic and European air masses monitored at Mace Head, Ireland from 1987-1994, *Atmos. Environ.*, 30, No. 23, 4041–4063.

Simpson, D., Andersson-Sköld, Y., and Jenkin, M. E., 1993, Updating the chemical scheme for the EMEP MSC-W oxidant model : current status, Norwegian Meteorological Institute, EMEP MSC-W Note 2/93.

Simpson, D., Guenther, A., Hewitt, C.N., and Steinbrecher, R., 1995, Biogenic emissions in Europe 1. Estimates and uncertainties, *J. Geophys. Res.*, 100, No. D11, 22875–22890.

Simpson, D., Olendrzyński, K., Semb, A., Støren, E., and Unger, S., 1997, Photochemical oxidant modelling in Europe: multi-annual modelling and source-receptor relationships, Norwegian Meteorological Institute, EMEP MSC-W Report 3/97.

Simpson, D., 1992, Long period modelling of photochemical oxidants in Europe. Calculations for July 1985, *Atmos. Environ.*, 26A, No. 9, 1609–1634.

Simpson, D., 1993, Photochemical model calculations over Europe for two extended summer periods: 1985 and 1989. Model results and comparisons with observations, *Atmos. Environ.*, 27A, No. 6, 921–943.

Simpson, D., 1995, Biogenic emissions in Europe 2: Implications for ozone control strategies, *J. Geophys. Res.*, 100, No. D11, 22891–22906.

Stauffer, B.R. and Neftel, A., 1988, What have we learned from the ice cores about the atmospheric changes in the concentrations of nitrous oxide, hydrogen peroxide, and other trace species, In Rowland, R.S. and Isaksen, I.S.A., editors, *The Changing Atmosphere*, pages 63–77, New York. Wiley.

Thompson, A.M. and Cicerone, R.J., 1986, Possible perturbations to atmospheric CO, CH_4, and OH, *J. Geophys. Res.*, 91, 10853–10864.

Volz, A. and Kley, D., 1988, Evaluation of the Montsouris series of ozone measurements made in the nineteenth century, *Nature*, 332, 240–242.

Zander, R., Demoulin, Ph., and Ehhalt, D.H.and Schmidt, U., 1989a, Secular increase of the total vertical column abundance of methane derived from IR solar spectra recorded at the Jungfraujoch station, *J. Geophys. Res.*, 94, 11029–11039, D8.

Zander, R., Demoulin, Ph., Ehhalt, D.H.and Schmidt, U., and Rinsland, C.P., 1989b, Secular increase of the total vertical column abundance of carbon dioxide above central Europe since 1950, *J. Geophys. Res.*, 94, 11021–11028, D8.

Appendix B

Eulerian model: Physical and chemical formulation

B.1 Eulerian Model formulation

The EMEP Eulerian photochemistry model has been designed as an extension of the EMEP Eulerian acid deposition model. The basic model description for the EMEP Eulerian acid deposition model is, with a few exceptions, also valid for the EMEP Eulerian photochemistry model. The differences between the two models is related to dry deposition and the formulation of the chemistry. Thus only those parts where the two model versions differ are reported here. For a description of the basic model formulations the reader is referred to this years report on the EMEP Eulerian acid deposition model (Bartnicki et al., 1998)

B.1.1 Emissions

Emission field estimates for SO_2, NH_3, NO_x, CO and VOC (volatile organic compounds) are based on data submitted officially to EMEP for 1996 from the participating countries. Gridded data are for many countries available in the 50 km EMEP grid. A distinction is made between surface sources (below 100 m) and high stacks sources (above 100 m). Monthly averaged lightning emissions, and seasonally averaged aircraft emissions, are included for NO_x.
Biogenic emissions of isoprene are calculated every hour in the model, based on the E-94 inventory of Simpson et al. (1995). The vegetation cover is given with 150 km resolution in the EMEP grid, and a distinction is made between 6 types of vegetation.
Emissions of NO_x from lightning is included as monthly averages on a T21 resolution from the POLINAT 2 database. The emission are originally compiled for the ECHAM database (Køhler et al. 1995).

B.1.2 chemistry

The present chemical mechanism is based on the Oslo CTM1 (Berntsen et al., 1997), and the Oslo CTM2 (Sundet, 1997) models. The mechanism applied in the EMEP Eulerian photochemistry model has been extended to also include sulphur and ammonium chemistry. As part of this extension the aqueous phase chemistry already applied in the EMEP Eulerian acid deposition model (Jakobsen et al., 1996, 1997) is also implemented in the EMEP Eulerian photochemistry model. In the EMEP Eulerian photochemistry model acetone and DMS are not included in the calculations. The chemistry scheme applied in the Lagrangian ozone model (Appendix A) and the scheme applied in the EMEP Eulerian photochemistry model (and the Oslo CTM1 and Oslo CTM2) have a common origin. The chemistry parameterization from the Oslo CTM models was chosen for the EMEP Eulerian photochemistry model in order to reduce the amount of computational resourced used by the model. As concentrations from the Oslo CTM2 are used as lateral boundary values for the EMEP Eulerian photochemistry model, it is highly beneficial to have a coherent chemistry parameterization in the two models, in particular for calculations in the upper troposphere. Below changes in the parameterization of the chemistry from the Oslo CTM2 (Sundet, 1997) are presented. A complete description of the model chemistry is included in appendix B.2.

Definition of the fractional solubility.

In the parameterization of both aqueous phase chemistry and wet scavenging we assume that Henry's law is fulfilled. For gases that undergo rapid reversible aqueous phase reactions such as acid-base

ionisation equilibria, an efficient Henry's law coefficient, H* can be defined (Schwartz, 1986). As an example, the efficient Henry's law coefficient for SO_2 is given as:

$$\begin{aligned} H^* &= ([SO_2]_{aq} + [HSO_3^-] + [SO_3^{2-}]/P_{SO_2} \\ &= H_{SO_2}(1 + \frac{K_1}{[H^+]} + \frac{K_1 K_2}{[H^+]^2}), \end{aligned} \tag{B.1}$$

where H_{SO_2} is the Henry's law coefficient for SO_2 and K_1 and K_2 are the first and second ionisation constants for sulfurous acid. P_{SO_2} is the partial pressure of SO_2 in the gas-phase.

For a soluble gas C, using the ideal gas law, the total concentration $[C_T]$ (gas + aqueous-phase) in a cloud volume can be expressed as:

$$\begin{aligned} [C_T] &= [C_g]/\alpha + [C_{aq}] \\ &= [C_{aq}](1 + \frac{1}{H_c RT\alpha}) \end{aligned} \tag{B.2}$$

where $[C_g]$ is the gas phase concentration of C, α is the volume fraction of cloud water, R is the universal gas constant ($atmM^{-1}K^{-1}$) and T is temperature in Kelvin degrees. Both $[C_T]$ and $[C_g]$ are in units M (mol/l). The fraction of the total (gas + aqueous) concentration of C desolved in cloud water, f, then becomes:

$$f = \frac{1}{1 + (H_c^* RT\alpha)^{-1}} \tag{B.3}$$

Oxidation of SO_2 to sulphate.

In the model SO_2 is oxidized to sulphate both in the gas phase and in the aqueous phase. In the calculations we always assume equilibrium between gas- and aqueous- phase. It should also be noted that in case only a fraction of the grid volume is in clouds, the total concentration (gas + aqueous) of soluble components are assumed to be uniformly distributed in the grid volume. If the cloud evaporates, the total concentration is always equal to the gas phase concentration. For both gas and aqueous phase reactions we scale the reaction rates, rather than the concentrations, by the solubility and cloud volume fractions. In the present calculations we have assumed a constant pH value of 4.5.

Oxidation of SO_2 in the gas phase.

In the gas phase SO_2 is oxidized by a chain of reactions initiated by the reaction with OH:

$$SO_2 + OH \longrightarrow .....H_2SO_4$$

We have found it convenient to define a pseudo reaction rate r'_{sg}, where r_{sg}, reaction 78 in appendix B.2, is scaled by the fractional cloud volume, W and the fractional solubility, f:

$$r'_{sg} = r_{sg}[(1 - f_{SO_2})W + 1 - W], \tag{B.4}$$

where f_{SO_2} is the fraction of SO_2 desolved in the aqueous phase in clouds. In the above equation SO_2 is oxidized both in the cloud free parts of the grid box and in interstitial cloud air.

Oxidation of SO_2 in the aqueous phase.

Although a number of oxidants may contribute in the oxidation, only O_3 and H_2O_2 are considered here. The rate of production for sulphuric acid is expressed as:

$$p_{cl} = k_{cl1}[H_2O_2][SO_2] + k_{cl2}[H^+][O_3]([SO_2] + [HSO_3^-])$$

where the reaction rate for the oxidation by O_3, $k_{cl2} = 1.810^4[H^+]^{-0.4}\text{mol}^{-1}\text{l}$ (Möller, 1980)H_2O_2, and the reaction rate for the oxidation by H_2O_2: $k_{cl1} = 8.310^5$ mol^{-1}l (Martin and Damschen, 1981). . With this parameterization all reactions, including aqueous phase reactions, are calculated as gas phase reactions. In order to get the right units, (molecules $\text{cm}^{-3})^{-1}$), the aqueous phase reaction rates are multiplied by a conversion factor Γ

$$\Gamma = 10^3/A_0\alpha$$

where A_0 is Avogadros number, and α is defined above. As for the gas phase reaction rate r'_{sg}, we define pseudo reaction rates, taking into account the the solubility of SO_2, H_2O_2 and O_3, the liquid water content and the fractional cloud cower. The pseudo reaction rates then becomes:

$$k'_{cl1} = k_{cl1}\Gamma\frac{H_{SO_2}}{H^*_{SO_2}} f_{SO_2} f_H W \tag{B.5}$$

and

$$k'_{cl2} = k_{cl2}\Gamma f_{SO_2} f_{O_3} W \tag{B.6}$$

for the for oxidation by H_2O_2 and O_3 respectively. f_H and f_{O_3} are the fractional solubilities of H_2O_2 and O_3.

Oxidation of SO_2 in gas- and aqueous- phase.

With the definitions above, the oxidation of SO_2 to sulphate in gas and aqueous phase is expressed as:

$$P = (k'_{sg}OH + k'_{cl1}H_2O_2 + k'_{cl2}O_3)SO_2T \tag{B.7}$$

Ammonium sulphate and ammonium nitrate

In the model ammonium sulphate is formed instantaneously, only limited by the availability of the least abundant of the two species. In the atmosphere ammonium sulphate is present in two forms, $(NH_4)_2SO_4$ or NH_4SO_4. We assume equal concentrations of the two forms.

Any excess NH_3 may then react with HNO_3, forming ammonium nitrate (NH_4NO_3) through an equilibrium reaction. As a first step in this calculation the equilibrium concentration of NH_3 is calculated:

$$NH_3eq = \frac{NH_3 + HNO_3}{2} + \sqrt{\frac{(NH_3 - HNO_3)^2}{4} + k_{eq}}, \tag{B.8}$$

Where k_{eq} is defined below. The equilibrium concentration of NH_4HNO_3 (ammonium nitrate) is derived from NH_3:

$$NH_4NO_3eq = NH_4NO_3 + (NH_3 - NH_3eq) \tag{B.9}$$

Provided the difference between the equilibrium concentration and the former concentration is smaller than the former concentration, the equilibrium concentration becomes the new concentration of ammonium nitrate. Nitric acid (HNO_3) is adjusted accordingly, maintaining mass balance.

The equilibrium constant k_{eq} is calculated as recommended by Mozurkewich (1993). Below the point of deliquescence the equilibrium constant, now denoted K_p is given by the equation:

$$lnK_p = 118.87 + \frac{24084}{T} - 6.025ln(T) \tag{B.10}$$

where T is the temperature in Kelvin. Above the point of deliquescence the equilibrium constant, now denoted K_{aq} is given by:

$$K_{aq} = [P_1 - P_2(1 - \frac{RH}{100}) + P_3(1 - \frac{RH}{100})^2](1 - \frac{RH}{100})^{1.75}K_p \tag{B.11}$$

where both K_p and K_{aq}, and subsequently k_{eq}, are in units of (molecules cm^{-3})^2. RH is the relative humidity in percent. and P_1, P_2 and P_3 are given as:

$$lnP_1 = -135.94 + \frac{8763}{T} + 19.12ln(T)$$

$$lnP_2 = -122.65 + \frac{9969}{T} + 16.22ln(T)$$

$$lnP_3 = -182.61 + \frac{13875}{T} + 2446ln(T)$$

and the point of deliquescence is given as:

$$lnRH_d = \frac{618.3}{T} - 2.551$$

Night time production of NO_3^-

The night time production of total nitrate (defined as the sum of HNO_3 in the gas phase and NO_3 and ammonium nitrate in particulate form) is initiated by the gas phase reaction:

$$NO_2 + O_3 \longrightarrow NO_3 + O_2$$

At least in the lower troposphere, this reaction is believed to be the rate-limiting step for the night time production of total nitrate (Dentener and Crutzen, 1993). N_2O_5 is formed in equilibrium with NO_3:

$$NO_3 + NO_2 \rightleftharpoons N_2O_5$$

N_2O_5 may further react with water on deliquescent aerosols, producing two NO_3^- molecules:

$$N_2O_5 + H_2O \longrightarrow 2NO_3^- + H^+$$

However, in daylight NO_3 is rapidly photolysed:

$$NO_3 + h\nu \longrightarrow NO + O_2$$

Thus, total nitrate is only produced through this path in the absence of sunlight. In winter, with low OH concentrations and many hours of darkness, this is believed to be the major source of total nitrate in the atmosphere. (Dentener and Crutzen, 1993). As noted above, the rate limiting step for the overall night time production of total nitrate is the initial reaction between NO_2 and O_3. However, at low humidities and/or low aerosol burden, the overall reaction can be limited by the availability of aerosols. The parameterization of this process is a simplification of the parameterization suggested by Dentener and Crutzen (1993). In the calculations we assume that the availability deliquescent aerosols is proportional to the sulphate concentration, represented as a volume fraction V of sulphate aerosols:

$$V = \frac{S \times M_s}{A_0 \rho}$$

where S is the concentration of sulphate (molecules cm^{-3}), M_s is the molecular weight of sulphate, A_0 is Avogadros number and ρ is the aerosol density (g cm^{-3}). An expression for the conversion of N_2O_5 to NO_3^- on deliquescent aerosols is expressed as:

$$K_a = V \frac{3\alpha v}{4r} RH/100. \tag{B.12}$$

where α is the sticking coefficient (10^{-2}), v is the mean molecular speed for the N_2O_5 molecules and r is the average radius of the aerosols (0.3 μ m).

B.1.3 Wet removal.

The parameterization of the scavenging of soluble chemical components is based upon the work of Berge (1993), where the scavenging is parameterized as functions of precipitation and cloud liquid water content. A distinction is made between in-cloud scavenging and sub cloud scavenging.

The in-cloud scavenging of a soluble component C is given by the expression:

$$Q = \frac{pr/\Delta Z}{CW} C f_{aq} \tag{B.13}$$

where pr (kg $m^{-2}s^{-1}$) is the locally released precipitation in a given grid box, divided by CW (kg m^{-3}), the liquid water content of the same grid box. ΔZ is the height of the grid box. f_{aq} is the fractional solubility of C as defined above.

For below cloud scavenging a distinction is made between scavenging of particulate matter and gas phase components. The scavenging of gases is calculated as

$$Q = 0.7P, \tag{B.14}$$

where P is the accumulated precipitation from the all layers above. For particles the scavenging is believed to be much less effective, as the the particles will tend to follow the air-current around the droplets (Berge, 1993). For particles, below cloud scavenging is calculated as

$$Q = \frac{A}{v} P\epsilon \tag{B.15}$$

where A is 5.2 $m^3kg^{-1}s{-}1$, v, the fall-speed of the droplets, is 5 m s^{-1} and ϵ, the scavenging efficiency, is 0.1.

B.1.4 Dry deposition.

The dry-deposition parameterization scheme applied here is the same as used in the EMEP Eulerian sulphur model (Jakobsen et al., 1995 and Berge and Jakobsen, 1998). The dry deposition velocities at 1 m (v_s) are given in Table 1. An effective dry deposition velocity for the lowest model layer, v_h, is calculated from the equation:

$$v_h = \frac{v_s}{1 + \frac{v_s}{C_H |\vec{V_H}|}} \tag{B.16}$$

where V_H is the horizontal wind vector, and C_H is the drag coefficient. The drag coefficient is calculated from Monin Obukhov similarity theory as described by Berge and Jakobsen (1998).

	O_3	HNO_3	PAN	CO	H_2O_2	NO_2
Ocean	0.1	0.1	0.	0.	0.1	0.05
Ice	0.05	0.05	0.	0.	0.01	0.02
Tundra	0.1	0.1	0.05	0.01	0.1	0.05
Agriculture	0.4	0.4	0.2	0.03	0.1	0.1
Forest	0.4	0.4	0.2	0.03	0.1	0.1
Desert	0.1	0.1	0.05	0.01	0.1	0.05
Undefined	0.4	0.4	0.2	0.03	0.1	0.1

Table B:1: *Dry deposition velocities at 1 m in* cms^{-1}.

B.1.5 Photo-dissociation rates.

The photodissosiation rates (j-values) are calculated for clear sky conditions and for two predefined clouds using the phodis routine (Kylling, 1995: Kylling et al. 1995). Ozone concentrations from a 2-D global model, extending from the surface to 50 km (Stordal et al. 1985) are scaled by observed total ozone columns Dutsch (1974). Cloud base for both the predefined clouds is at 1 km above the ground. The first predefined cloud is 3 km deep, with a water content of 0.7 g cm^{-3} and a mean droplet radius of 10 μm. The second predefined cloud is 1 km deep, with water content of only 0.3 g cm^{-3} and a mean droplet radius of 10 μm. The j-values are calculated using the new recommendations for absorption cross sections and quantum yields from DeMore et al. (1997). For most components the changes are small. However the photolysis of O_3 to O'D is now approximately 30% higher than with earlier recommendations.

B.1.6 Initial and lateral boundary concentrations.

For most of the chemical components the initial concentrations and the mass advected inn across the lateral boundaries are calculated with the Oslo CTM2 global model (Sundet, 1997) with a t21 resolution (5.625 degrees). At present monthly averaged concentrations for June 1996 are used. For SO_2, and SO_4 lateral boundary concentrations are based on the results from a Hemispheric model (Leonor Tarrason, personal communication). For a number of short-lived components initial and lateral concentrations are set to zero (O'D, $O(^3P)$, OH, HO_2).

Potential vorticity adjustment of O_3.

Across the tropopause there are large gradients in the concentrations of O_3. In an attempt to reproduce these gradients, initial and lateral boundarie concentrations of o_3 at the four uppermost layers (level four corresponds to the tropopause) are scaled according to the potential vorticity (PV). Thus, at these levels lateral boundary concentrations of O_3 (in ppb_v) are scaled to the PV as:

$$O_3 = 4.5 \times 10^{-8} \times PV \tag{B.17}$$

nr.	Reactions	Rate constants A	-E_a/R	Ref.	Note
R71	$HO_2 + C_2H_5O_2 \rightarrow CH_3O_2H$	6.5E-13	650	2	11
R72	$HO_2 + C_4H_9O_2 \rightarrow CH_3O_2H$	6.5E-13	650	2	11
R73	$HO_2 + C_6H_{13}O_2 \rightarrow CH_3O_2H$	6.5E-13	650	2	11
R74	$HO_2 + CH_3CH(O_2)CH_2OH \rightarrow CH_3O_2H$	6.5E-13	650	2	11
R75	$HO_2 + CH_3COCH(O_2)CH_3 \rightarrow CH_3O_2H$	6.5E-13	650	2	11
R76	$HO_2 + ISOR1 \rightarrow CH_3O_2H$	6.5E-13	650	2	11
R77	$HO_2 + ISOR2 \rightarrow CH_3O_2H$	6.5E-13	650	2	11
R78	$OH + SO_2 \rightarrow ....SO_4$	2.0E-12		2	11

Notes:
* Rate assumed to be 1.16 times faster than R46, as Atkinson et al. (1989) gives k_{298} 1.16 times faster for $C_2H_5O_2 + NO$ than for $CH_3O_2 + NO$.
** Rate assumed to be equal to R46 ($NO + CH_3O_2$)

Table B:3: Rate constants for three-body reactions.

Reaction	Rate constants k_0	k_{inf}	F_c
R3	6.0E-34(T/300)$^{-2.3}$[M]		
R11	2.6E-30(T/300)$^{-3.2}$[M]	2.4E-11(T/300)$^{-1.3}$	0.6
R13b	2.2E-30(T/300)$^{-3.9}$[M]	1.5E-12(T/300)$^{-0.7}$	0.6
R16	1.8E-31(T/300)$^{-3.2}$[M]	4.7E-12(T/300)$^{-1.4}$	0.6
R24	1.0E-28(T/300)$^{-0.8}$[M]	8.8E-12	0.6
R34	4.5E-31(T/300)$^{-3.0}$[M]	1.8E-12(T/300)$^{-1.7}$	0.6
R60	8.0E-29(T/300)$^{-7.0}$[M]	1.2E-11(T/300)$^{-1.0}$	0.6
R61	4.9E-3e$^{(-12100/T)}$[N_2]	4.0E+16e$^{(-13600/T)}$	0.3

B.2.1 Notes

Note 1 : $k = k_0 + k_3[M]/(1 + k_3[M]/k_2)$
where $k_0 = 7.2 \times 10^{-15} exp(785/T)$, $k_2 = 4.1 \times 10^{-16} exp(1440/T)$ and $k_3 = 1.9 \times 10^{-33} exp(725/T)$

Note 2 : $1.5 \times 10^{-13}(1.0 + 0.6P_{atm})$
where P_{atm} is air pressure in atmospheres.

Note 3 R23: $k = 1.59 * 10^{-20} * T^{2.84} * e^{-984/T}$

Note 4 : Equilibrium constant. for $NO_2 + NO_3 \rightarrow N_2O_5$ is $k_{eq} = 4.0E - 27e^{(10930./T)}$. Reaction rate for $N_2O_5 \rightarrow NO_2 + NO_3$ is then given as R13b/k_{eq} .

Note 5 : Equilibrium const. for $HO_2 + NO_2 \rightarrow HO_2NO_2$ is $k_{eq} = 2.1E - 27e^{(10900./T)}$. Reaction rate for $HO_2NO_2 \rightarrow HO_2 + NO_2$ is then given as R16/k_{eq} .

Note 6 R30 : $k = 1.51 * 10^{-17} * T^{2.0} * e^{190/T}$

Note 7 R40a + R40b= $2.93E - 12 * e^{190/T}$, R40b = $2.93E - 12 * e^{190/T}$-R40a

Table B:4: Photolytic reactions

Model ref.	Reactions
D1	$O_3 + h\nu \rightarrow O(^3P) + (O_2)$
D2	$O_3 + h\nu \rightarrow O(^1D) + (O_2)$
D3	$NO_2 + h\nu \rightarrow NO + O(^3P)$
D4	$H_2O_2 + h\nu \rightarrow 2OH$
D5	$HNO_3 + h\nu \rightarrow NO_2 + (OH)$
D6	$HCHO + h\nu \rightarrow CHO + HO_2$
D7	$HCHO + h\nu \rightarrow CO + (H_2)$
D8	$CH_3CHO + h\nu \rightarrow CHO + CH_3$
D9	$CH_3COCH_2CH_3 + h\nu \rightarrow CH_3CO + C_2H_5O_2$
D10	$CH_3COCOCH_3 + h\nu \rightarrow 2CH_3CO$
D11	$HCOCHO + h\nu \rightarrow CO + HCHO$
D12	$CH_3COCHO + h\nu \rightarrow CO + CH_3CHO$
D13	$NO_3 + h\nu \rightarrow NO_2 + O(^3P)$
D14	$NO_2NO_3 + h\nu \rightarrow NO_2 + NO_3$
D15	$CH_3O_2H + h\nu \rightarrow OH + CH_3O$
D16	$HO_2NO_2 + h\nu \rightarrow NO_2 + HO_2$

Note 8 The fraction $(1 - fa, fa = k_b/k_a + k_b)$ of organic nitrates ($RONO_2$) formed from the reaction RO_2 + NO $\longrightarrow$ (1-fa)$RONO_2$ +fa(NO_2 + TO) is calculated by the following equations (Atkinson, 1990)

$$\frac{k_a}{k_b} = \left\{ \frac{Y_0^{300}[M](T/300)^{-m_0}}{1 + \frac{Y_0^{300}[M](T/300)^{-m_0}}{Y_\infty^{300}[M](T/300)^{-m_\infty}}} \right\} F^z$$

$$z = \left[1 + \left(log_{10} \frac{Y_0^{300}[M](T/300)^{-m_0}}{Y_\infty^{300}[M](T/300)^{-m_\infty}} \right)^2 \right]^{-1}$$

where $Y_0^{300} = \alpha e^{\beta N}$, where N is the number of C atoms in the peroxy radical, and $\alpha = 1.94 * 10^{-22}$ and $\beta = 0.97$ are constants. $[M]$ is number density of the air, T is temperature and $m_0 = 0$, $m_\infty = 8.1$, $F = 0.411$ and $Y_\infty^{300} = 0.826$.

Note 9 The alkoxy radicals (RO) formed in the reaction between peroxy radical and NO will either react with O_2 or decompose. Values of fb (fb denotes the fraction reacting with O_2) are calculated on the basis of data given in Atkinson (1990).

Note 10 In the case of $C_6H_{13}O$, decomposition is assumed to be the only reaction since a C6 ketone is not included in the scheme.

Note 11 ARAD is the sum of peroxy radicals (ARAD = $CH_3COCH(O_2)CH_3 + C_6H_{13}O_2 + C_4H_9O_2 + C_2H_5O_2 + CH_3CH(O_2)CH_2OH + ISOR1 + ISOR2$). All reactions are assumed to give a $ROOH$ compound which is represented in the scheme by CH_3O_2H.

Note 12 List of abbreviations used in the chemical scheme :

ISOR1	First RO_2 radical from the reaction of isoprene with OH
ISOK	The sum of methylvinylketone (MVK) and methacrolein (MACR)
ISOR2	RO_2 radical formed from MVK + OH or MACR + OH
AR1	First RO_2 radical from the reaction of m-xylene with OH
AR2	A C-5 carbonyl compound formed from AR1 by reaction R50
AR3	A C-5 RO_2 radical formed from AR2 by R41

Note 13 The scheme for isoprene oxidation is based on Lloyd et al. 1983. Since the uncertainties in the emission estimates are so large only oxidation initialized by reaction with OH is included.

The scheme based on assumptions I-III is :

$$\begin{aligned} &\text{Isoprene} + OH \longrightarrow ISOR1 \\ &ISOR1 + NO \longrightarrow 0.1\ RONO_2 + 0.9\ (NO_2 + HO_2 + HCHO + ISOK) && \text{I} \\ &ISOK + OH \longrightarrow ISOR2 && \text{II} \\ &ISOR2 + 1.5\ NO \longrightarrow 1.5NO_2 + 0.67\ (HO_2 + CH_3COHCO) + 0.43\ HCHO \\ &\qquad +0.33(CH_3CHO + CH_3CO\ ) && \text{III} \end{aligned}$$

I : ISOK consists of equal amounts of MVK and MACR.
II : MVK and MACR have the same chemical lifetime.
III : All RO_2 radicals in ISOR2 reacts with the same rate with NO.

In Lloyd et al. (1983) 4 different RO_2 radicals are identified from the reaction of ISOK with OH depending on whether MVK or MACR is oxidized, and the mechanism for the oxidation. The fraction yields of the products in the last equation is derived by considering the fraction yields of the 4 RO_2 radicals and their reaction path to the above products. A simplification is made as the $HOCH_2CO$ radical formed from one of the RO_2 radicals formed from MVK, is treated as CH_3CO in the scheme.

Note 14 Product yields of the reaction of OH with glyoxal is given by Atkinson (1990) as

$$k_a/k = fa_{44} = \frac{3.5 * 10^{18}}{3.5 * 10^{18} + 2 * [O_2]}$$

$$k_b/k = fb_{44} = \frac{[O_2]}{3.5 * 10^{18} + 2 * [O_2]}$$

$$k_c/k = fc_{44} = fb_{44}$$

Note 15 $k = 3.2 * 10^{-18} * T^2 * e^{414/T}$, Atkinson 1990.

Note 16 Products taken from Madronich and Calvert (1990). The alkoxy radicals which are products of the reaction are treated according to note 9.

Note 17 See section B.1.

B.3 References

Atkinson R., Baulch D.L., Cox R.A., Hampson R.F., Kerr J.A. and Troe J. (1989) Evaluated kinetic and photochemical data for atmospheric chemistry: Supplement III. *J. Phys. Chem. ref. Data*, **18**, pp 881-1097.

Atkinson R. (1990) Gas phase chemistry of organic compounds: A review. Evaluated kinetic and photochemical data for atmospheric chemistry: *Atm. Environ.*, **24A**, pp 1-41.

Atkinson R., Baulch D.L., Cox R.A., Hampson R.F., Kerr J.A. and Troe J. (1992) Evaluated kinetic and photochemical data for atmospheric chemistry: *Atm. Environ.*, **26A**, pp 1187-1230.

Bartnicki, J., Olendrzynski, K. and Jonson, J.E. (1998) Description of the Eulerian acid deposition model. In Transboundary acidifying air pollution in Europe. EMEP/MSC-W Status Report 1998 - Part 1. The Norwegian Meteorological Institute, Oslo, Norway.

Berge, E. (1993) Coupling of wet scavenging of sulphur to clouds in a numerical weather prediction model. *Tellus*, **45b**, pp 1-22.

Berge, E. and Jakobsen H.A. (1998). A regional scale multi-layer model for the calculation of long term transport and deposition of air pollution in Europe. *Tellus* In press.

Berntsen T., Isaksen I.S.A. (1997) A global 3D chemical transport model for the troposphere: 1. Model description and CO and O_3 results. *J. Geophys. Res.*, **102**, pp 21,239-21,280.

DeMore W.B., Sander D.M, Golden D.M., Molina M., Hampson R.F., Kurylo M.J., Howard C.J and Ravishankara A.R. (1990) Chemical kinetics and photochemical data for use in stratospheric modeling. *NASA/jpl Publ.*, 90-1.

DeMore W.B., Sander D.M, Golden D.M., Hampson R.F., Kurylo M.J., Howard C.J, Ravishankara A.R., Kolb C.E. and Molina M.J. (1992) Chemical kinetics and photochemical data for use in stratospheric modeling. *NASA/jpl Publ.*, 92-26.

DeMore W.B., Sander D.M, Golden D.M., Hampson R.F., Kurylo M.J., Howard C.J, Ravishankara A.R., Kolb C.E. and Molina M.J. (1997) Chemical kinetics and photochemical data for use in stratospheric modeling. *NASA/jpl Publ.*, 97-4.

Dentener F.J. and Crutzen P.J. (1993) Reaction of N_2O_5 on tropospheric aerosols: Impact on the global distributions of NO_x O_3 and OH. *J. Geophys. Res.*, **98**, pp 7149-7163.

Dutsch M.U. (1994) The ozone distribution in the atmosphere. *Can.J. Chem.*, **52**, pp 1491-1504.

Jakobsen, H.A., Berge, E., Iversen, T. and Skalin, R., (1995) Status of the development of the multi-layer Eulerian model: a) Model description, b) A new method of calculating mixing heights, c) Model results for sulphur transport and deposition in Europe for 1992 in the 50 km grid. EMEP/MSC-W, Note 3/95. The Norwegian Meteorological Institute, Oslo, Norway.

Jakobsen, H.A., Jonson J.E. and Berge, E. (1996). Transport and deposition calculations of sulphur and nitrogen compounds in Europe for 1992 in the 50 km grid by use of the multi-layer Eulerian model. EMEP/MSC-W, Note 2/96. The Norwegian Meteorological Institute, Oslo, Norway.

Jakobsen, H.A., Jonson J.E. and Berge, E. (1997) The multi-layer Eulerian model: Model description and evaluation of transboundary fluxes of sulphur and nitrogen for one year. EMEP/MSC-W, Report 2/97. The Norwegian Meteorological Institute, Oslo, Norway.

Køhler I., Sausen R. and Gallardo Klenner (1995) NO_x production from lightning . In *The impact of NO_x emissions from aircraft upon the atmosphere at flight altitudes 8-15 km (AERONOX)*, edited by U.Schumann, final report to the Commission of the European Communities, Deutch Luft und Raumfart, Oberpfaffenhofen, Germany, pp 343-345.

Kylling A. (1995) Phodis, a programme for calculation of photo-dissociation rates in the Earths atmosphere, available by anonymous ftp to pluto.itek.norut.no, cd pub/arve

Kylling A., KyllingA., Stamnes K. and Tsay S.-C. (1995) Areliable and efficient two-stream algorithm for radiative transfer: Documentation of accuracy in realistic layered media. *J. Atm. Chem.*, **21**, pp 115-150.

Lloyd A.C., Atkinson R., Lurmann F.W. and Nitta B.(1983) Modeling of potential ozone impacts from natural hydrocarbons-I. Development of a chemical mechanism for the NO_x-air photo-oxidations of isoprenes and α-pinene under ambient conditions. *Atm. Environ.*, **17**, pp 1931-1950.

Madronich S. and Calvert J.G. (1990) Permutation reactions of organic peroxy radicals in the troposphere. *J. Geophys. Res.*, **95**, pp 5697-5715.

Martin L.R. and Damschen D.E. (1981) Aqueous oxidation of sulphur dioxide by hydrogen peroxide at low pH. *Atm. Environ.*, **15**, pp 1615-1621.

Möller D. (1980) Kinetic model of atmospheric SO_2 oxidation based on published data. *Atm. Environ.*, **14**, pp 1067-1076.

Mozurkewich M. (1993) The dissociation constant of ammonium nitrate and its dependence on temperature, relative humidity and particle size. *Atm. Environ.*, **27A**, pp 261-270.

Schwartz S.E. (1986) Mass-transport considerations pertinent to aqueous phase reactions of gases in liquid-water clouds. In *Chemistry of multi-phase atmospheric systems,* Edited by W. Jaeschke, Springer Verlag, Berlin, pp 415-471.

Simpson D., Guenther A., Hewitt C.N., and Steinberger R. (1995) Biogenic emissions in Europe 1. Estimates and uncertainties. *J. Geophys. Res.*, **100**, D11, pp 22,875-22,890.

Simpson D, Olendrzynski K., Semb A., Støren E., and Unger S. (1997) Photochemical oxidant modeling in Europe: multi-annual modeling and source receptor relationships. EMEP/MSC-W, Report 3/97. The Norwegian Meteorological Institute, Oslo, Norway.

Stordal F, Isaksen I.S.A. and Horntveth (1985) A diabatic circulation two-dimensional model with photo-chemistry. Simulations of ozone and long-lived tracers with surface sources. *J. Geophys. Res.*, **90**, pp 5757-5776.

Sundet J.K (1997) Model studies with a 3-d global CTM using ECMWF data. Ph.D thesis, department of Geophysics, University of Oslo.

Vaghjiani G.L. and Ravishankara A.R (1989) Kinetics and mechanism of OH reaction with CH_3OOH. *J. Phys. Chem. ref. Data*, **93**, pp 1959-1989.

Vaghjiani G.L. and Ravishankara A.R (1991) New measurements of the rate coefficient for the reaction of OH with methane *Nature* **350** pp 406-409.

Wayne R.P. (ed.) (1990) The nitrate radical : Physics, chemistry and the atmosphere. *Air pollution research report no. 31,* Commission of the European communities.

Appendix C

Lagrangian model: Time-series plots, 1989-1996

This Appendix presents time-series plots comparing daily maximum ozone values from measurements with those of the Lagrangian photooxidant model. The 6-monthly mean of daily maximum ozone are given in each plot, as are the correlation coefficents (r). Note that r is derived from the 183 daily values.

Plots are presented for essentially all sites reporting to EMEP over the years 1989-1996, as long as data-capture was at least 60% over the April-September period. For some sites, plots for 1996 have been presented in Part III of this report and so are not repeated here.

Plots are presented sorted after two-letter country codes. These codes have been given on Page 2 of this report.

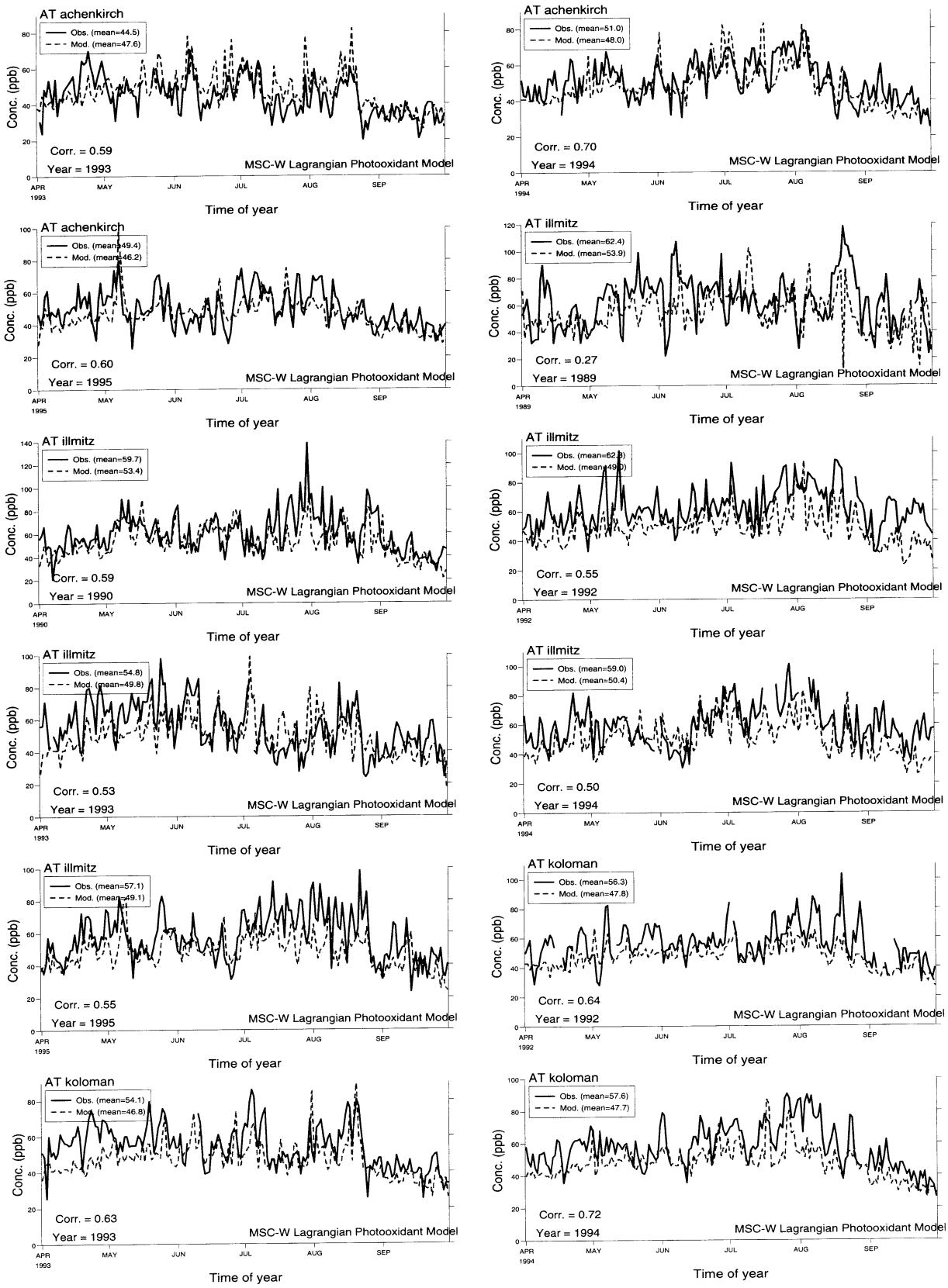

Figure C.1: Modelled versus observed daily max. ozone (ppb)

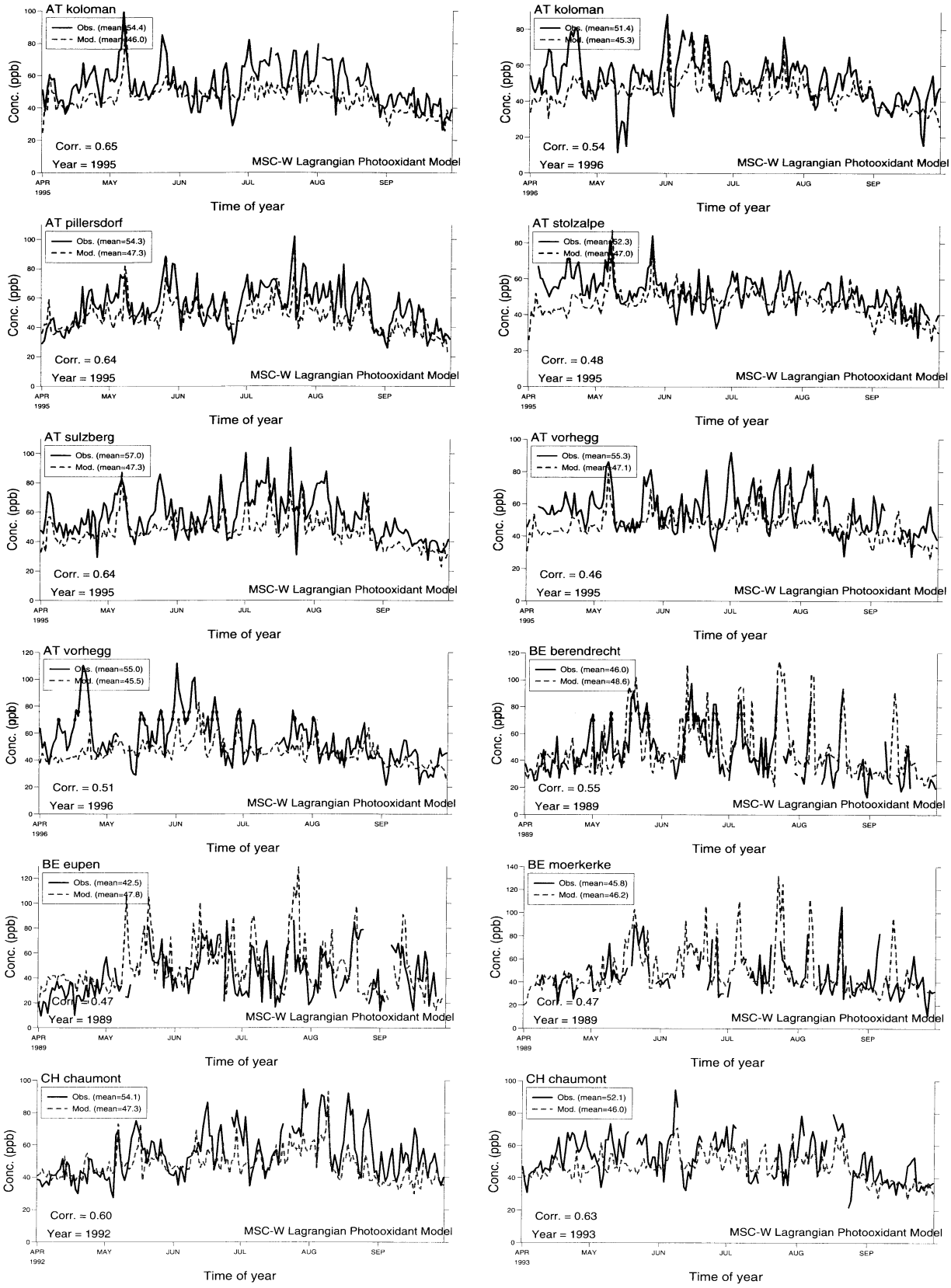

Figure C.2: Modelled versus observed daily max. ozone (ppb)

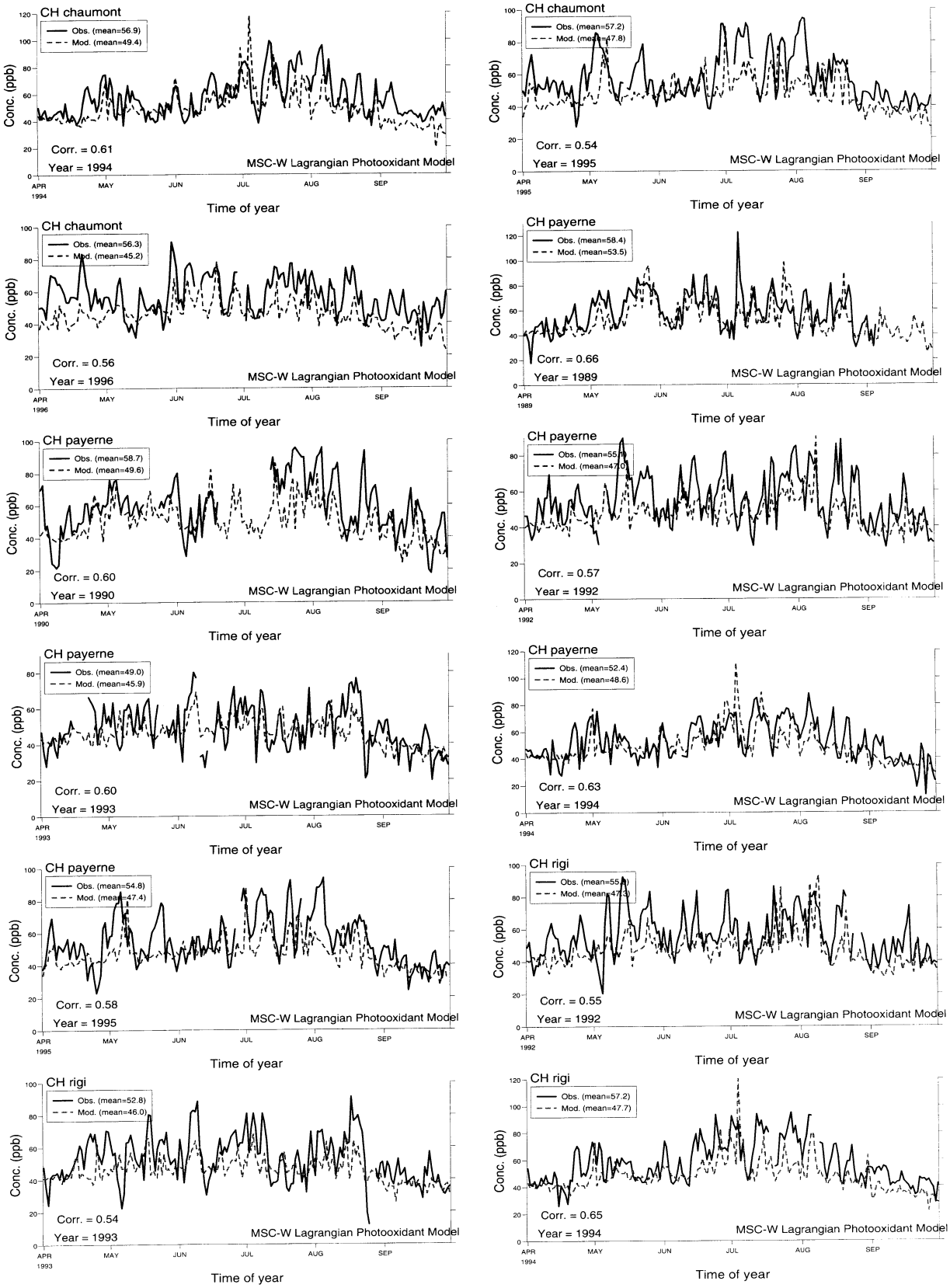

Figure C.3: Modelled versus observed daily max. ozone (ppb)

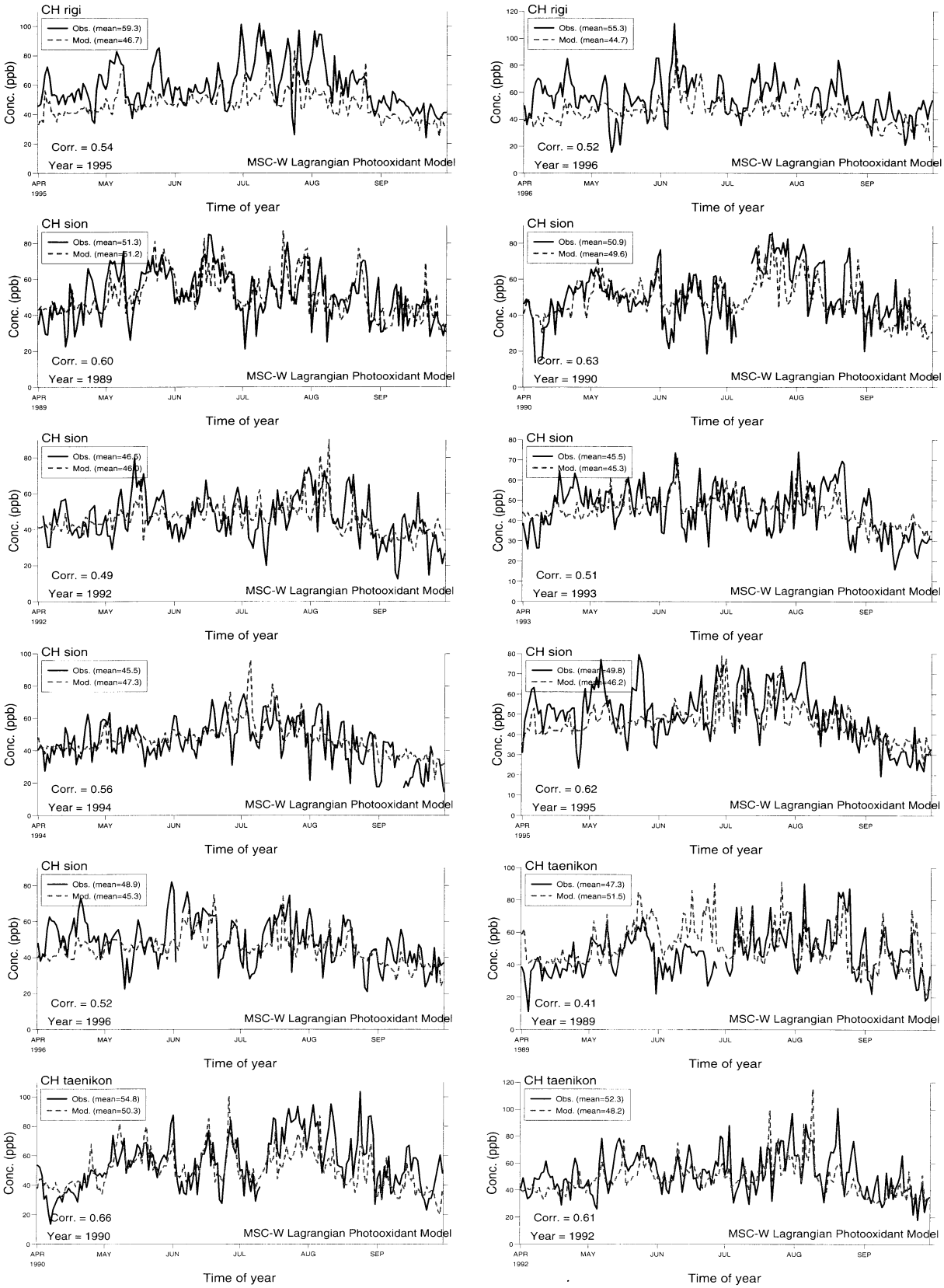

Figure C.4: Modelled versus observed daily max. ozone (ppb)

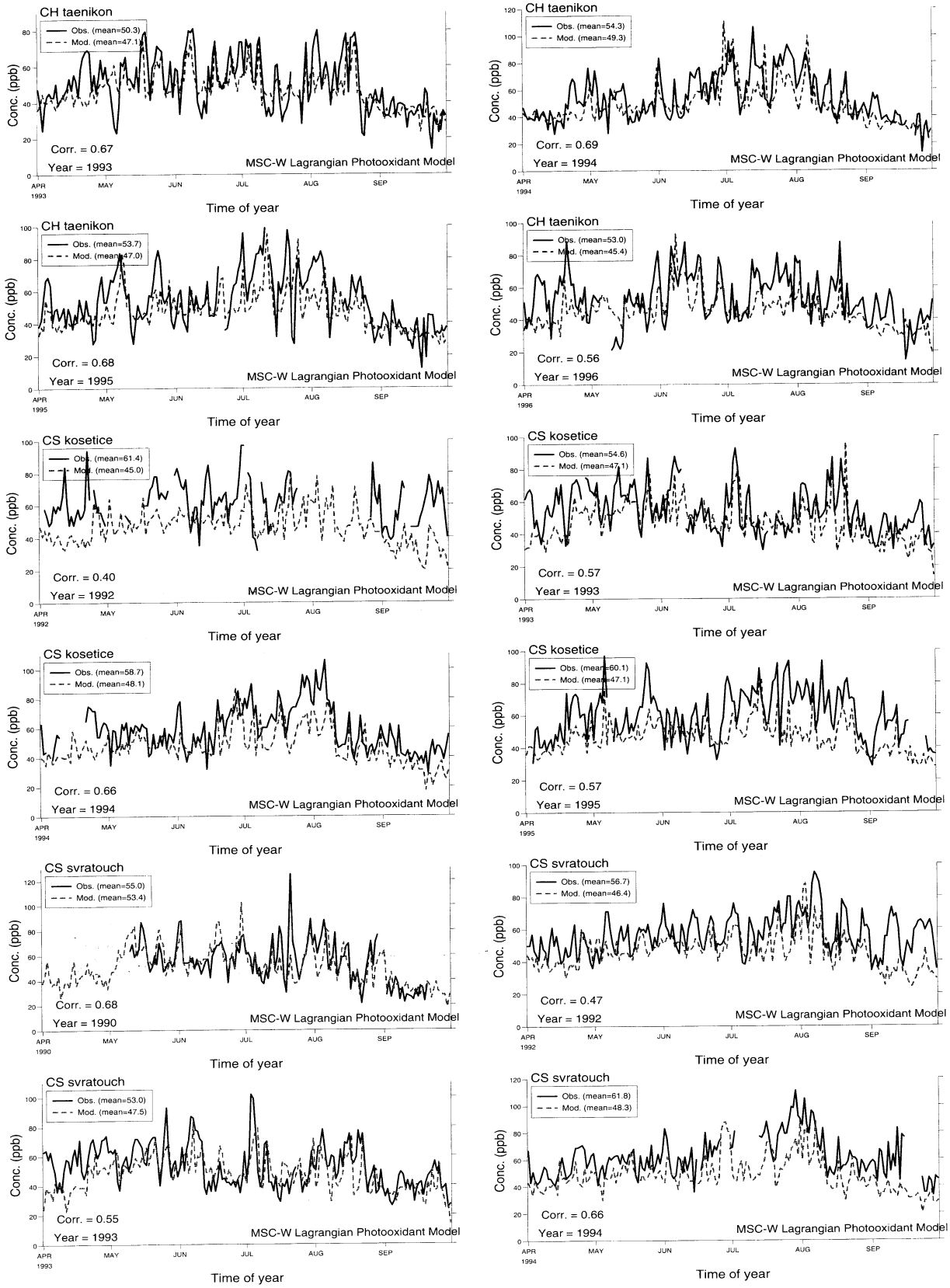

Figure C.5: Modelled versus observed daily max. ozone (ppb)

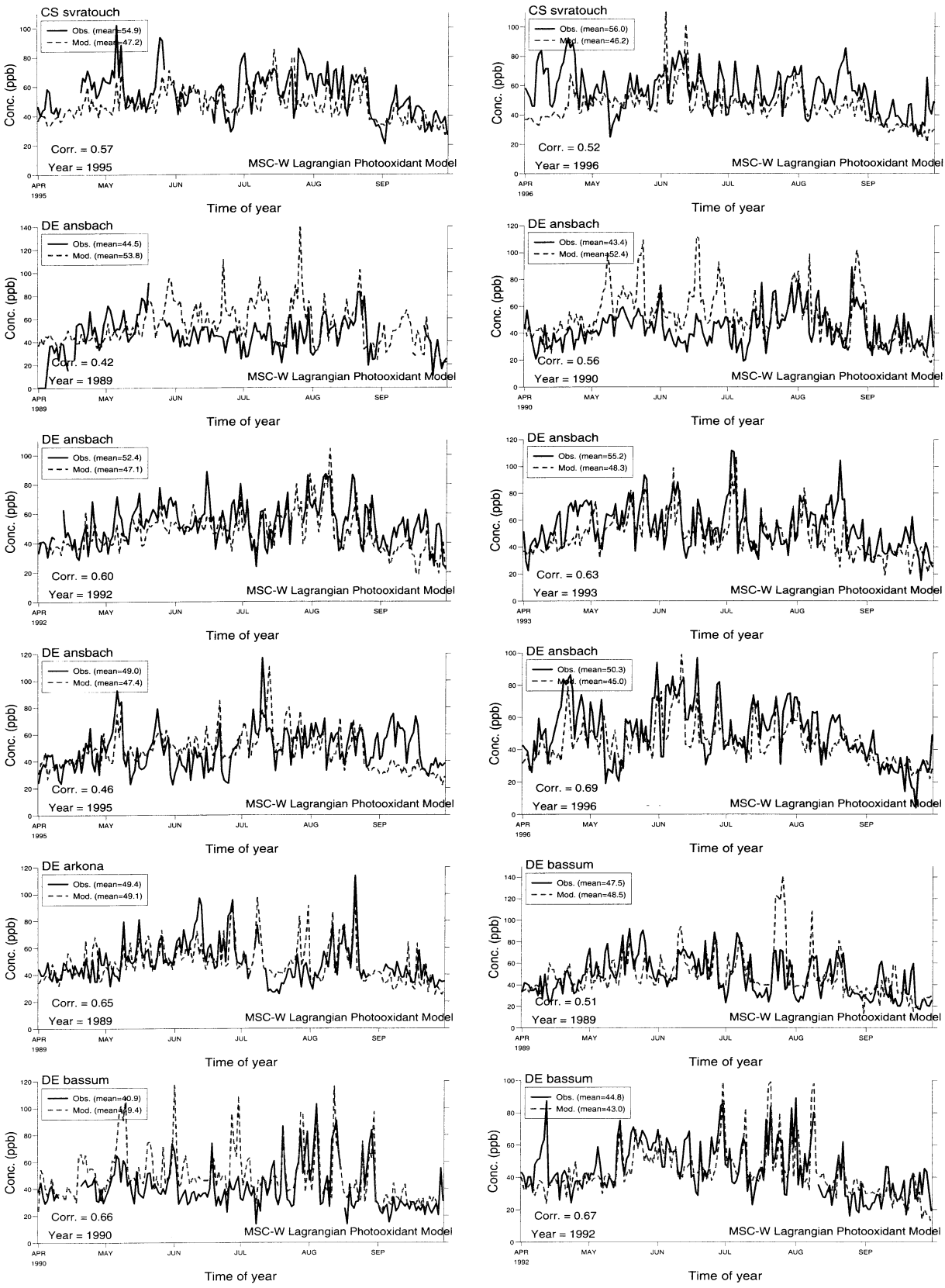

Figure C.6: Modelled versus observed daily max. ozone (ppb)

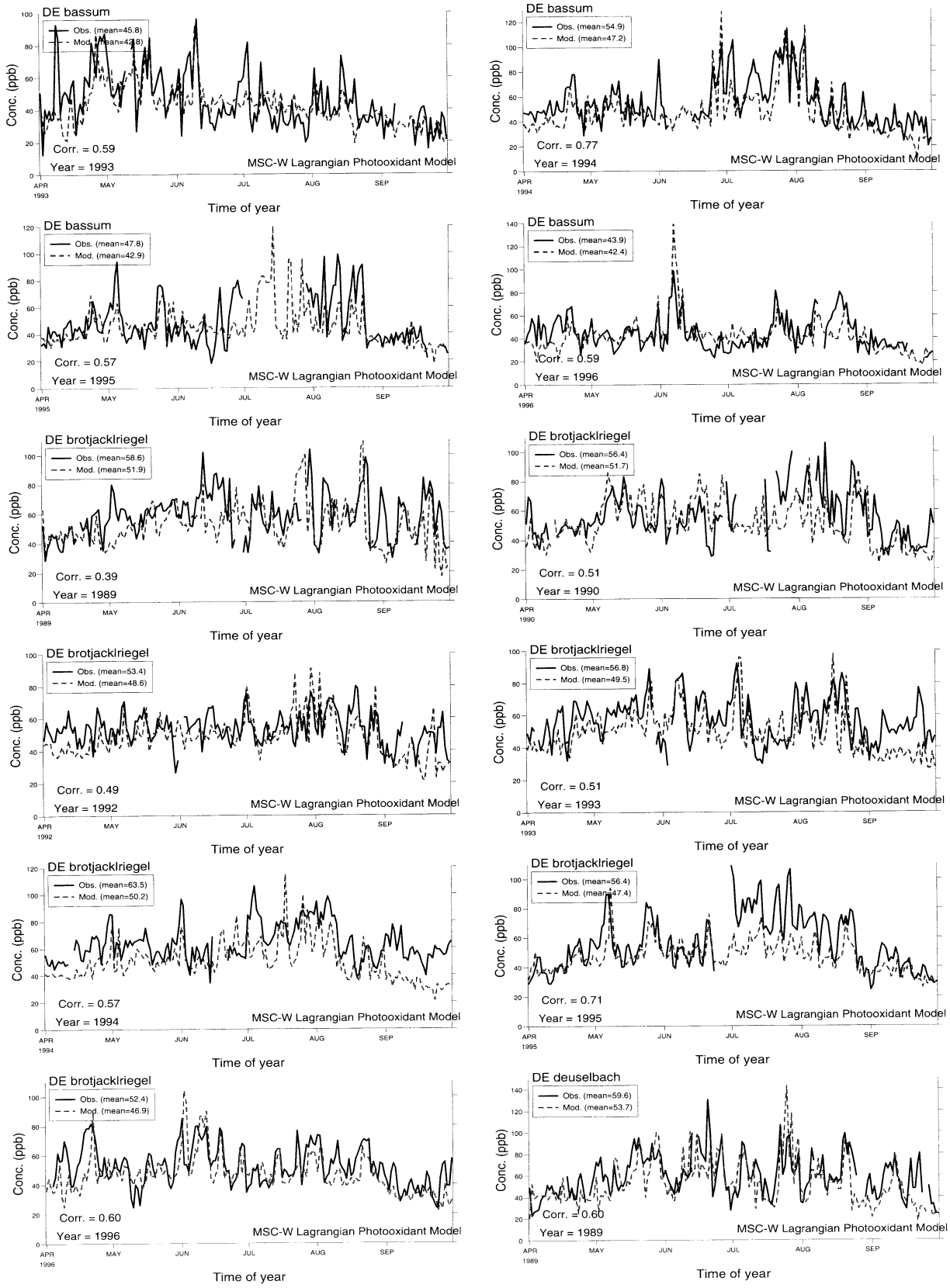

Figure C.7: Modelled versus observed daily max. ozone (ppb)

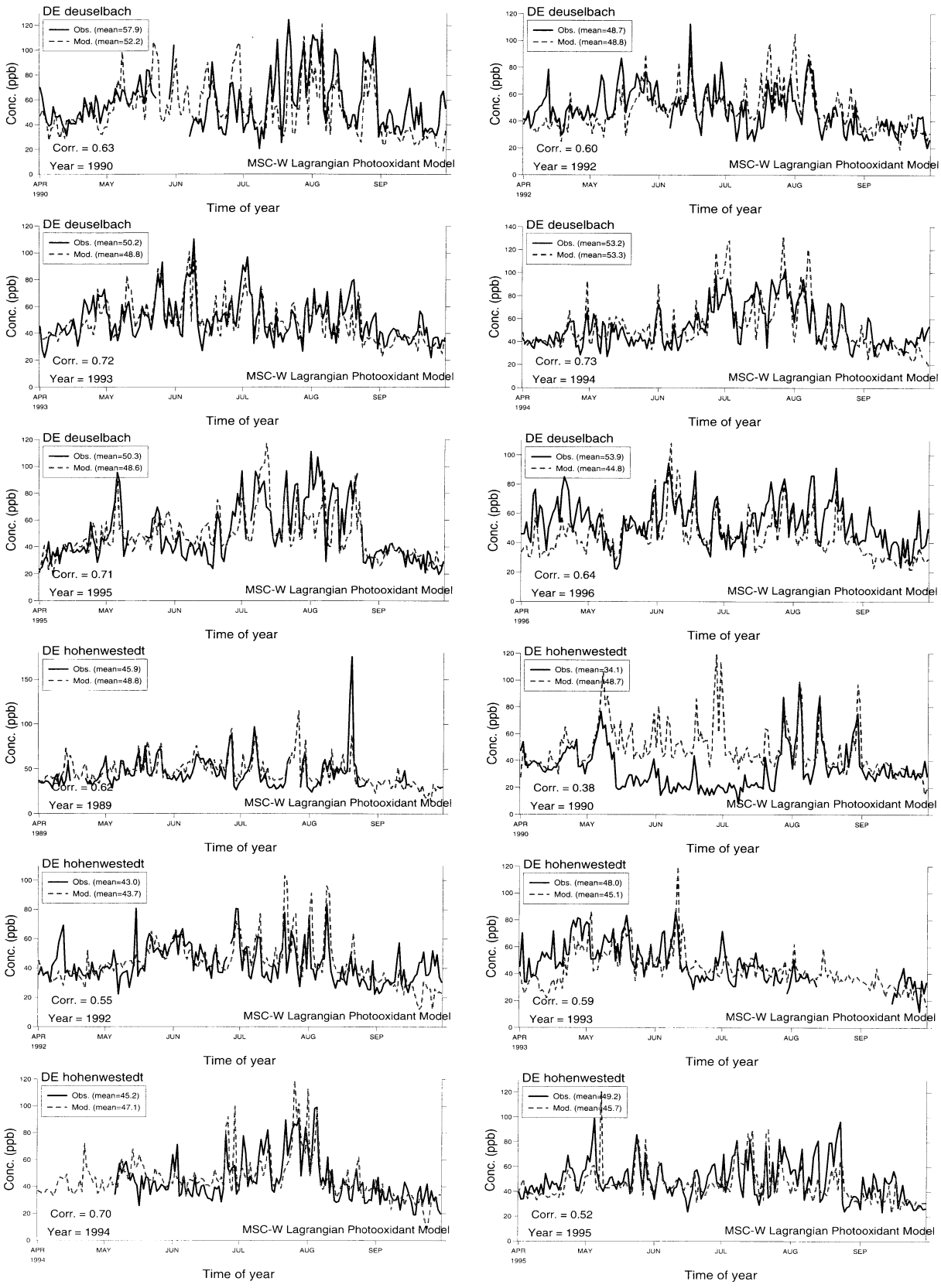

Figure C.8: Modelled versus observed daily max. ozone (ppb)

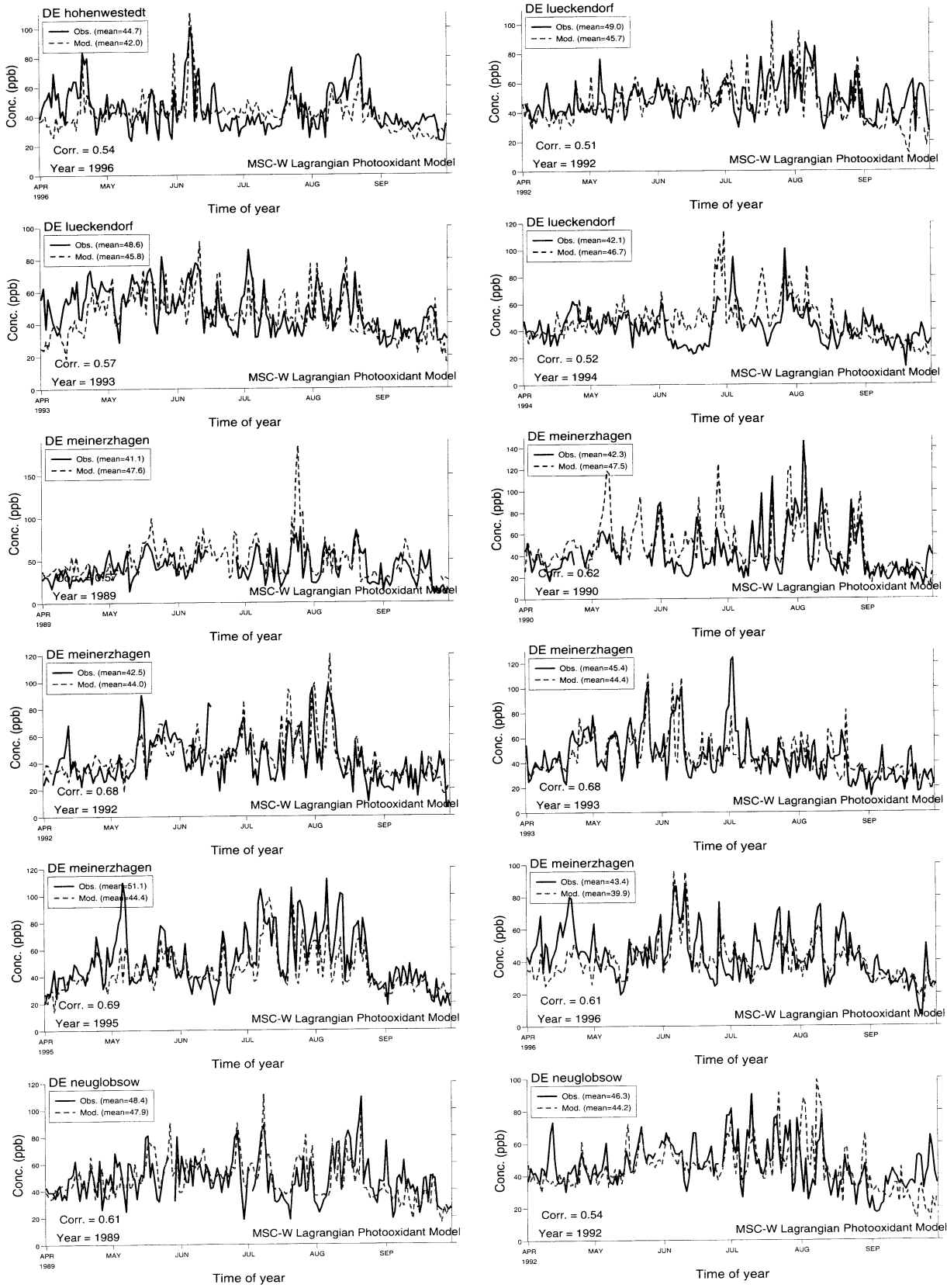

Figure C.9: Modelled versus observed daily max. ozone (ppb)

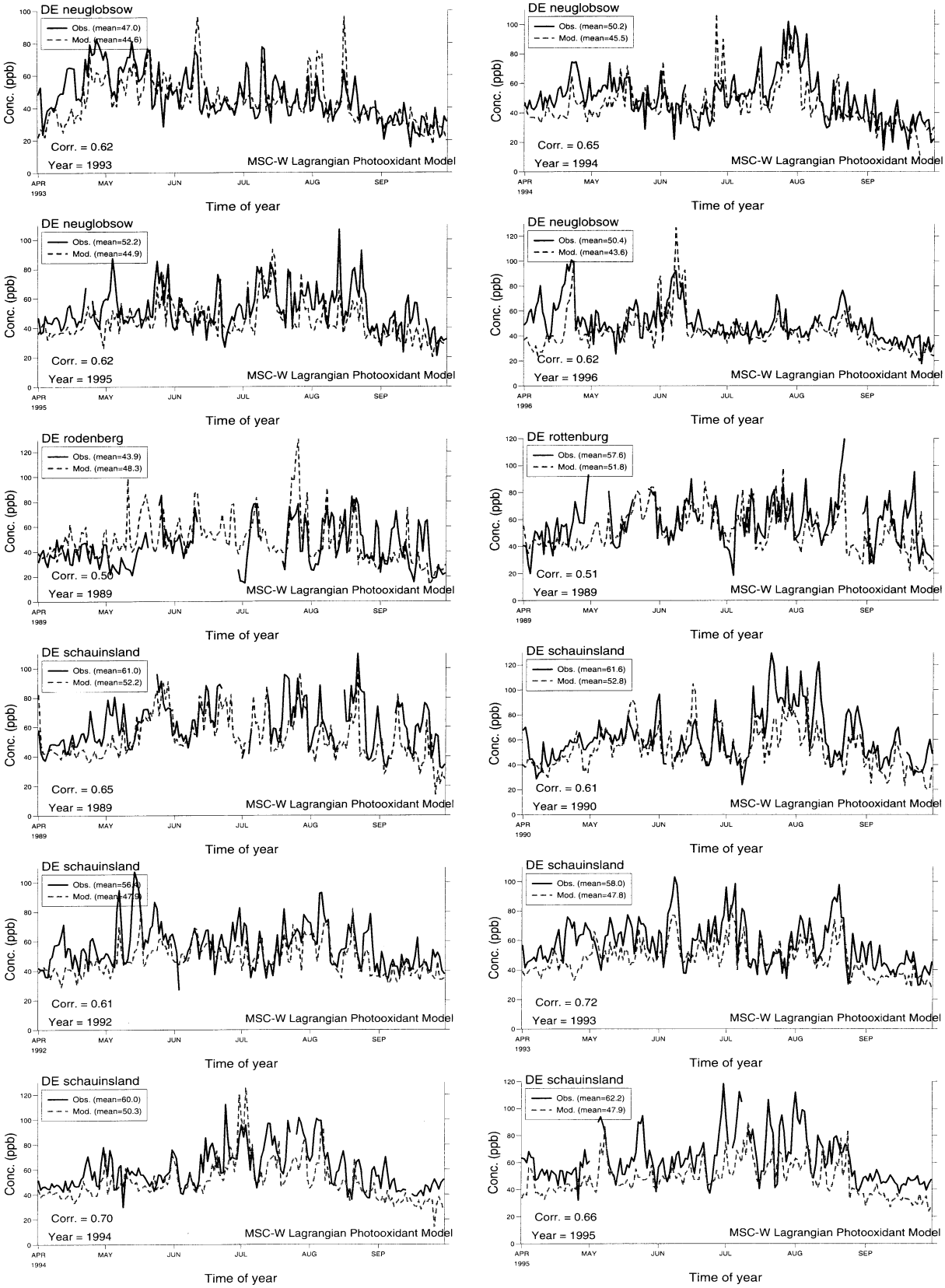

Figure C.10: Modelled versus observed daily max. ozone (ppb)

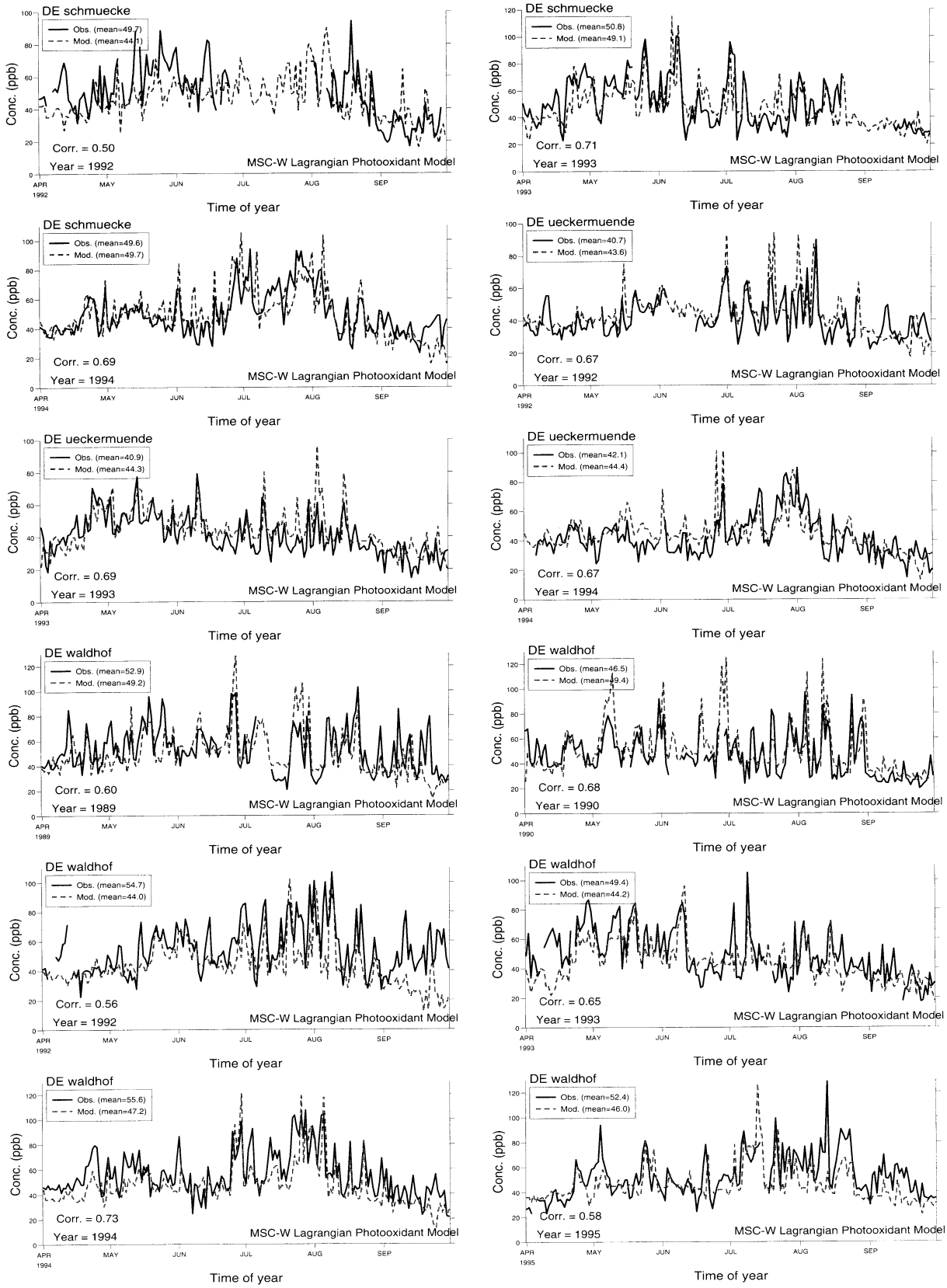

Figure C.11: Modelled versus observed daily max. ozone (ppb)

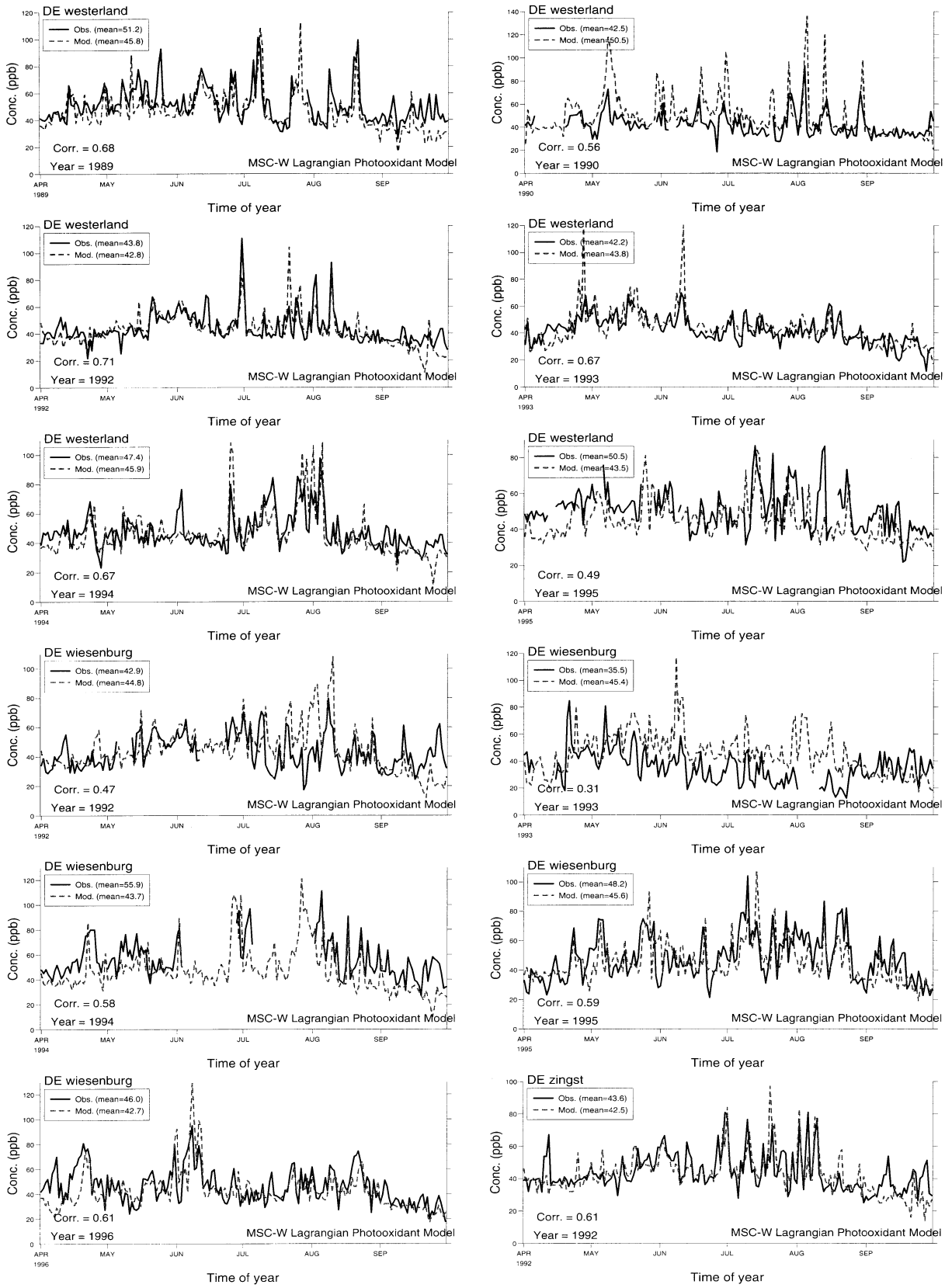

Figure C.12: Modelled versus observed daily max. ozone (ppb)

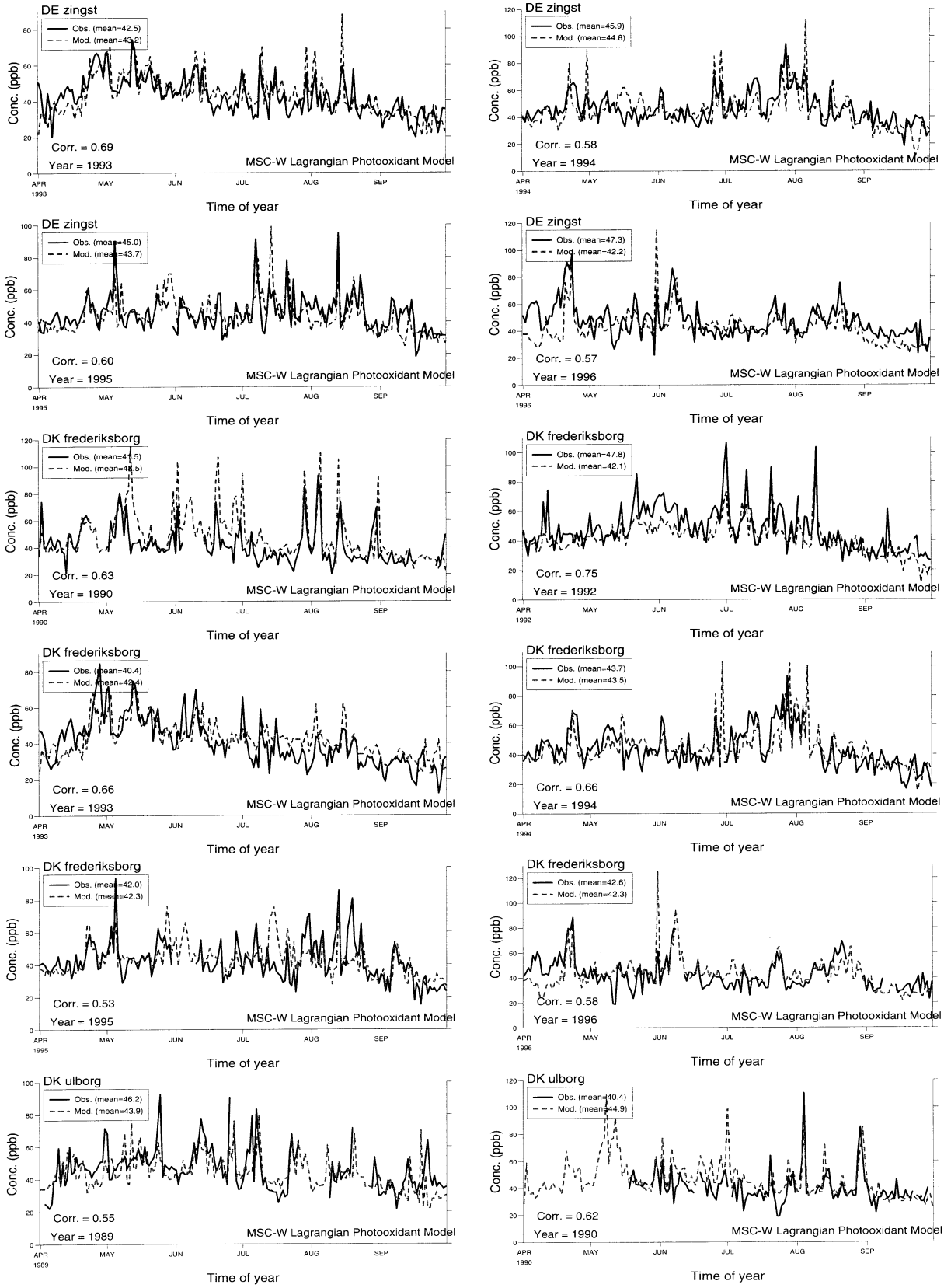

Figure C.13: Modelled versus observed daily max. ozone (ppb)

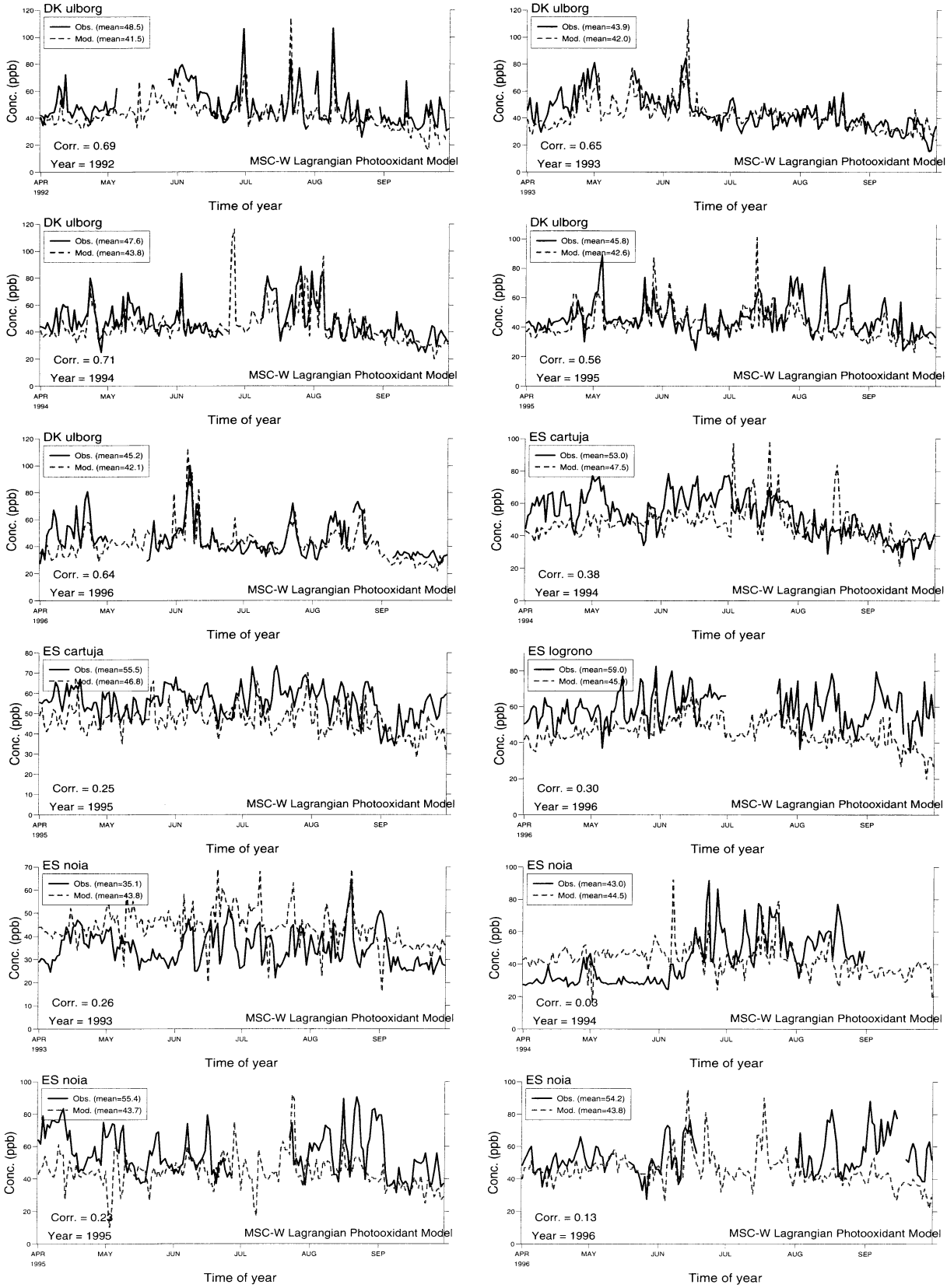

Figure C.14: Modelled versus observed daily max. ozone (ppb)

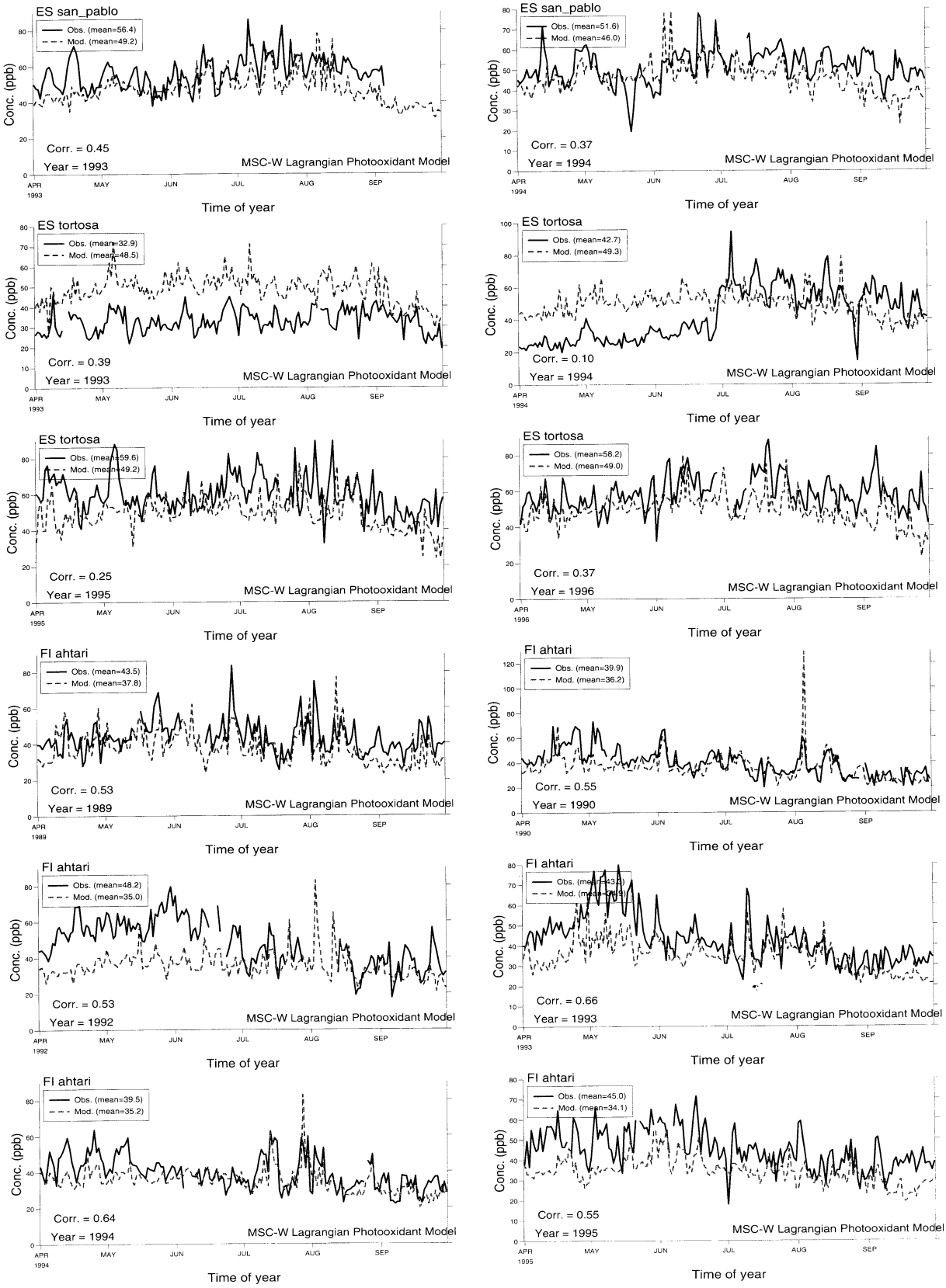

Figure C.15: Modelled versus observed daily max. ozone (ppb)

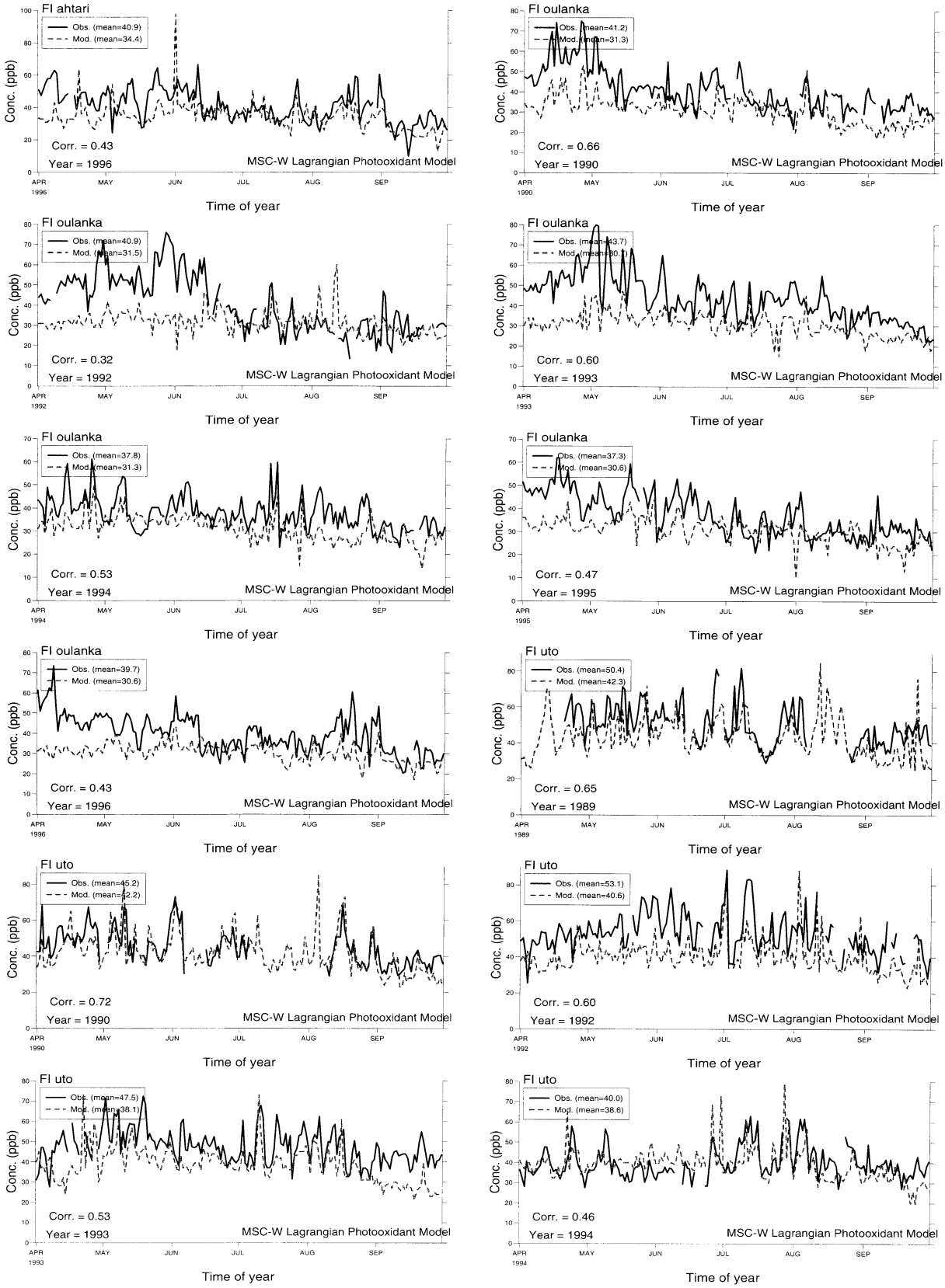

Figure C.16: Modelled versus observed daily max. ozone (ppb)

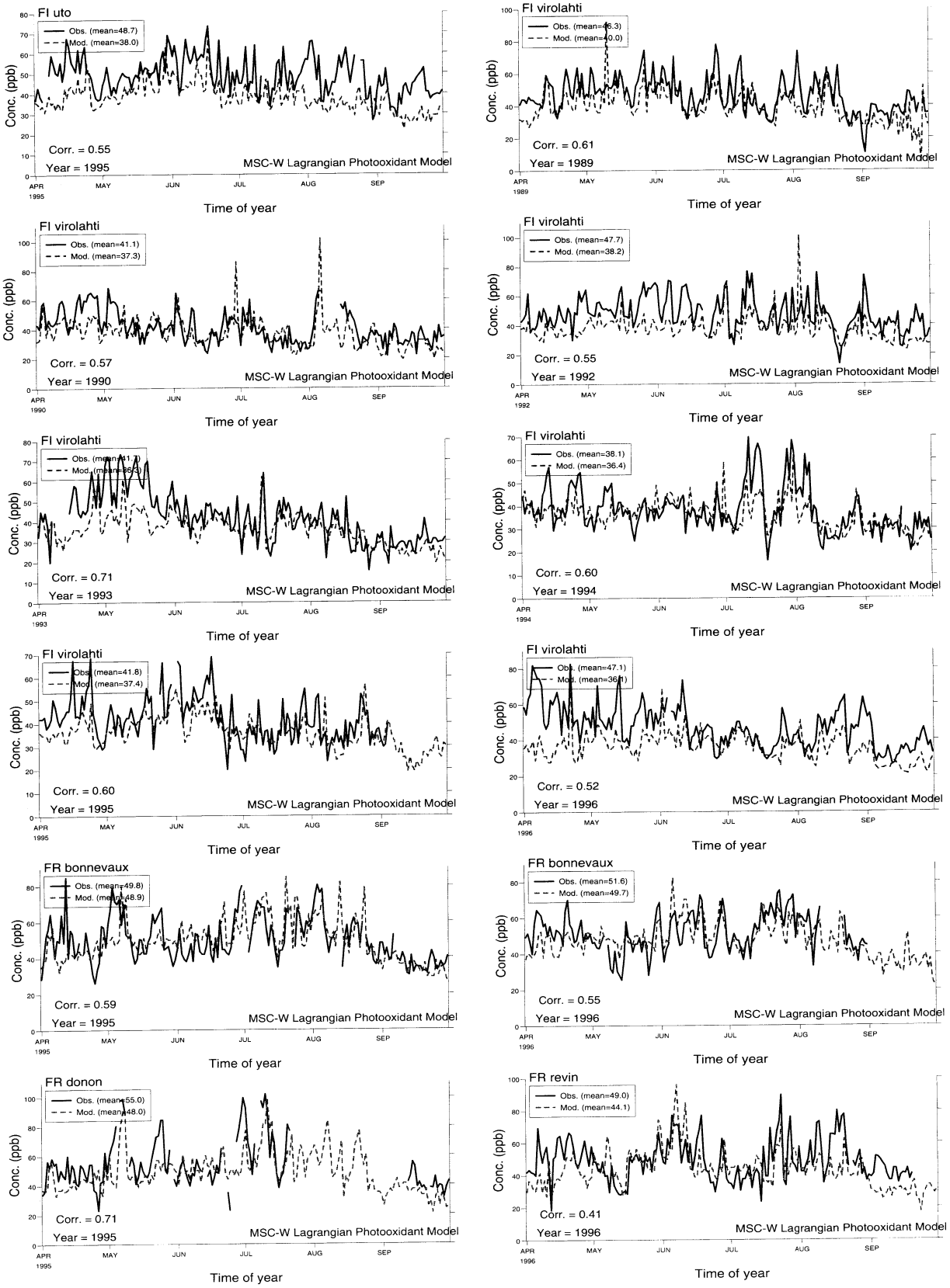

Figure C.17: Modelled versus observed daily max. ozone (ppb)

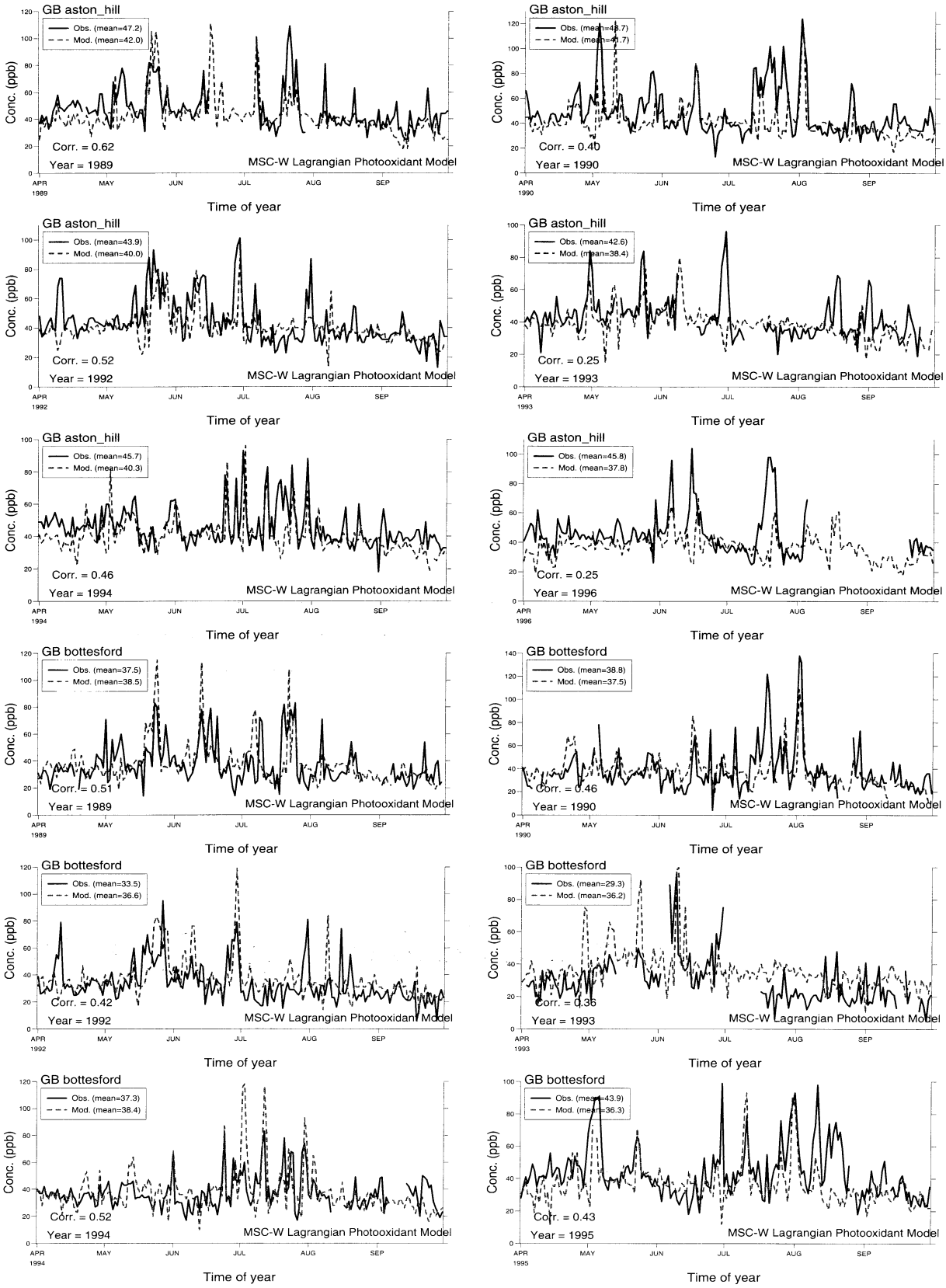

Figure C.18: Modelled versus observed daily max. ozone (ppb)

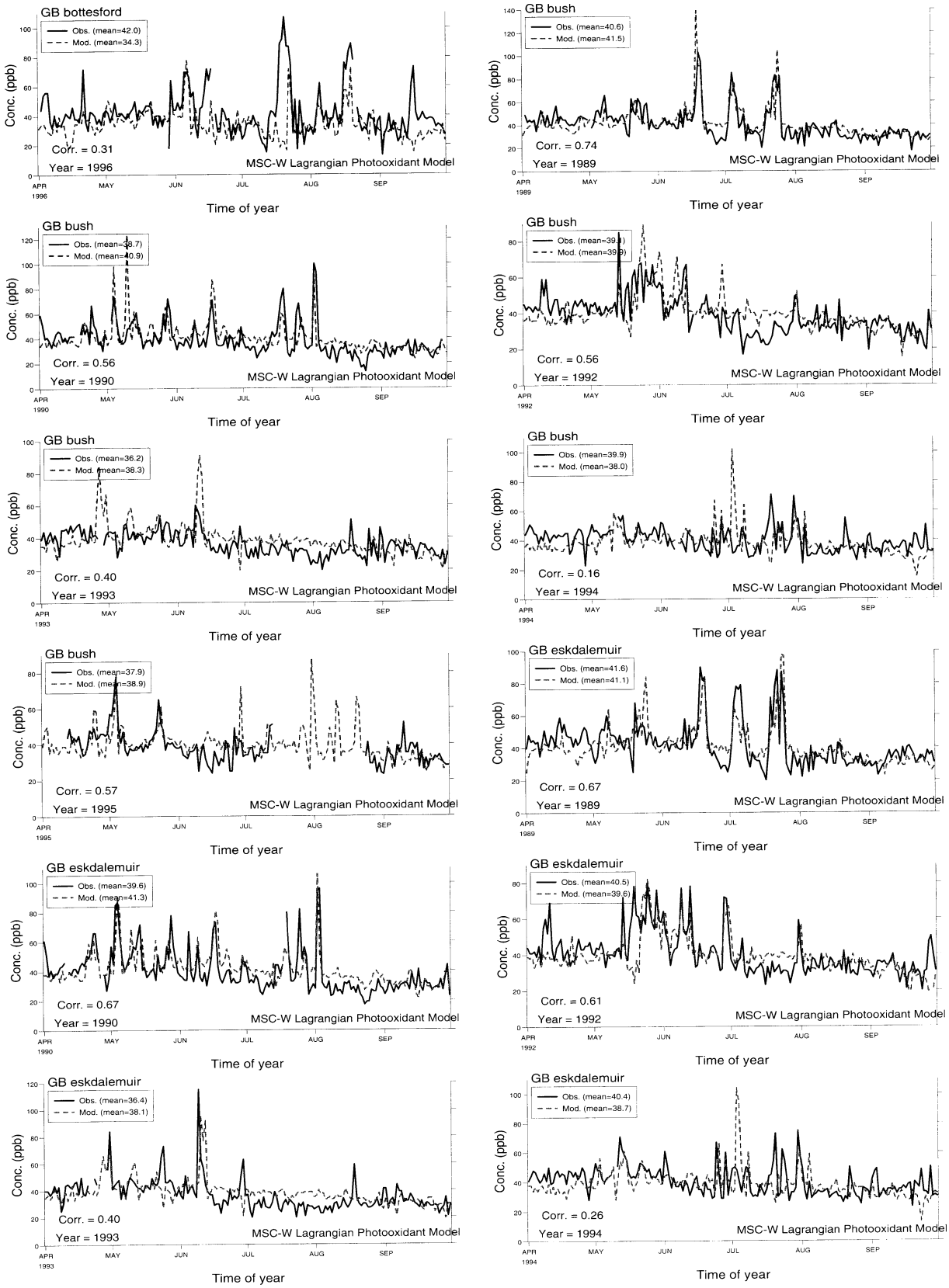

Figure C.19: Modelled versus observed daily max. ozone (ppb)

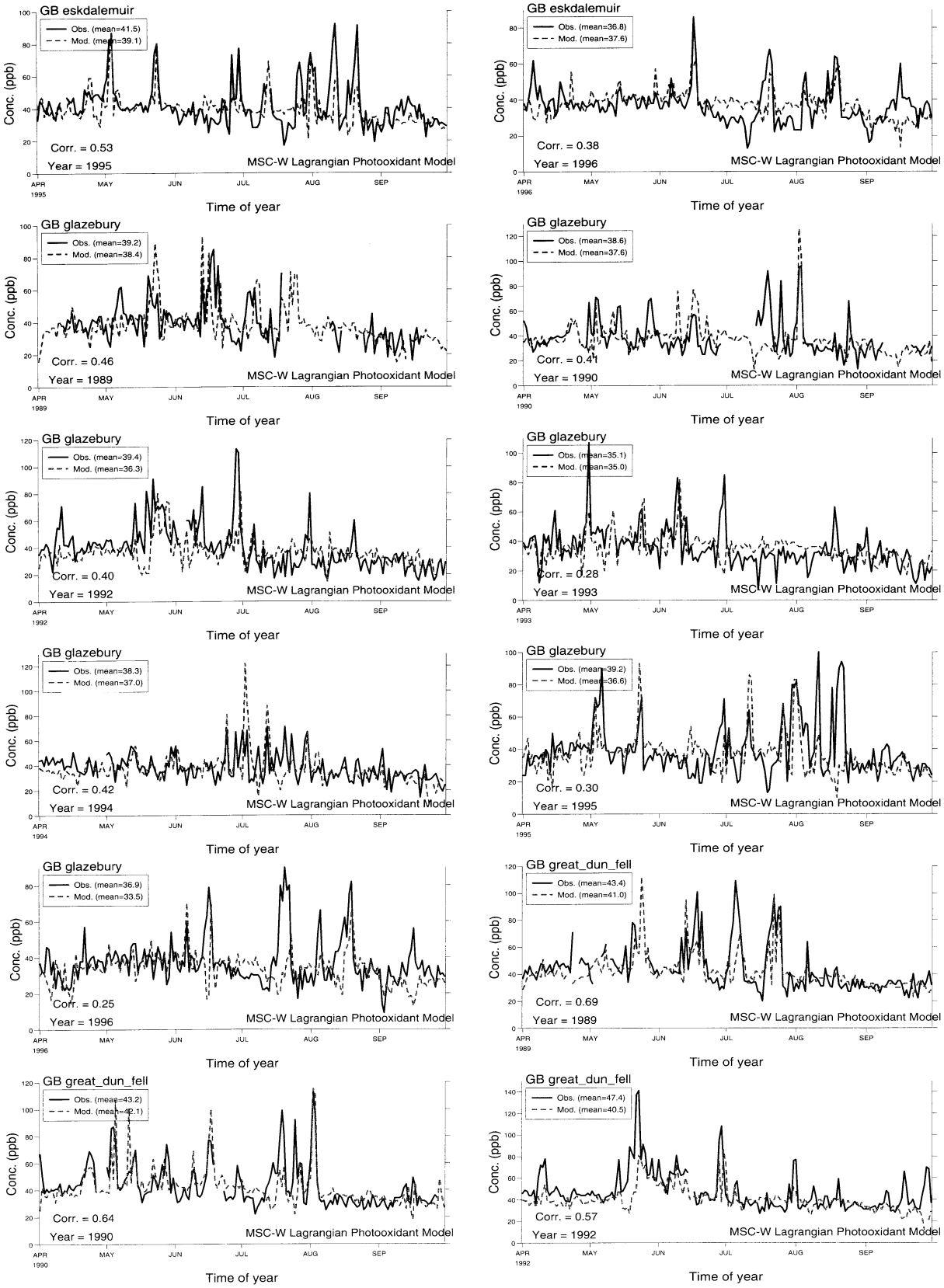

Figure C.20: Modelled versus observed daily max. ozone (ppb)

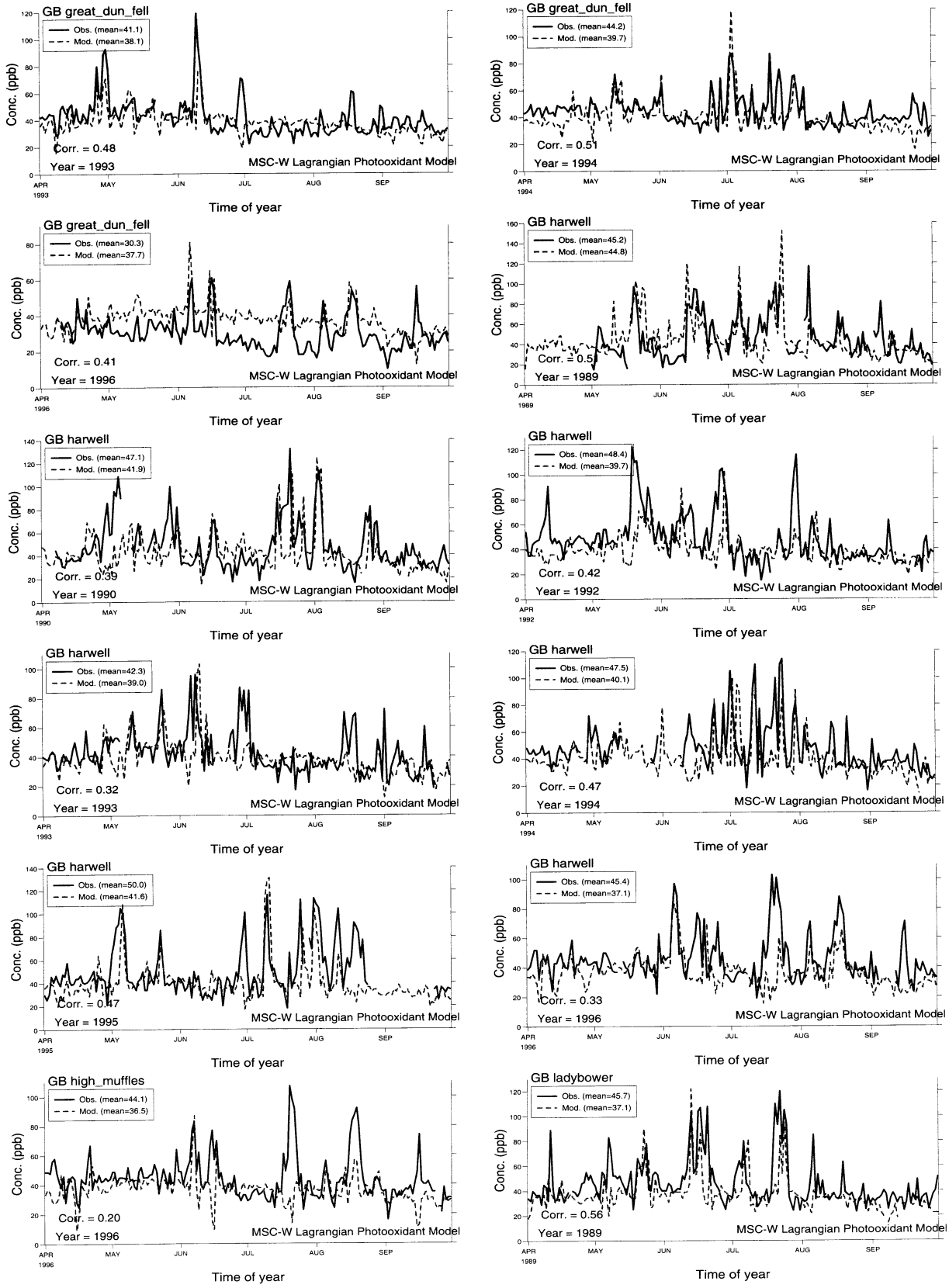

Figure C.21: Modelled versus observed daily max. ozone (ppb)

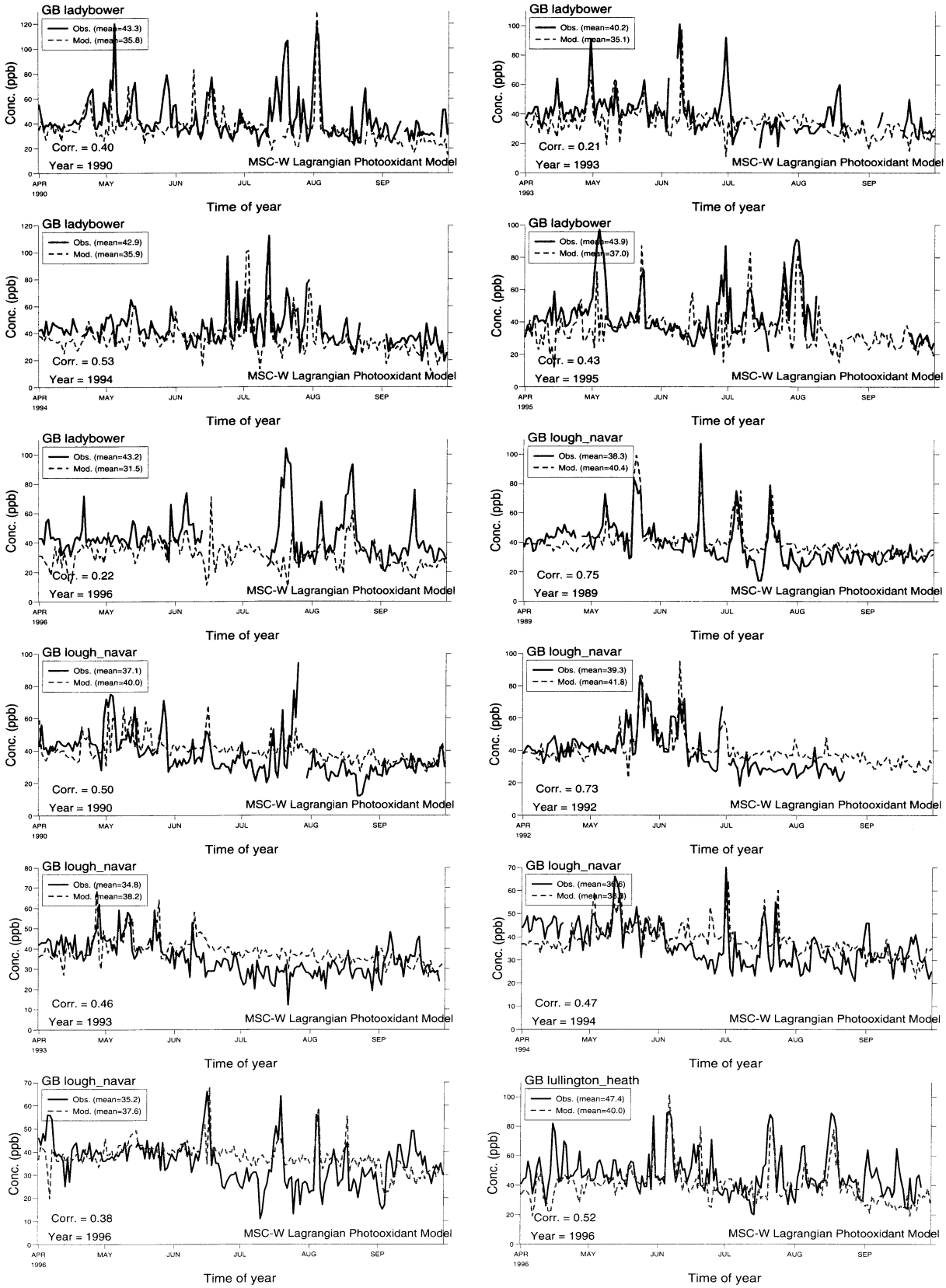

Figure C.22: Modelled versus observed daily max. ozone (ppb)

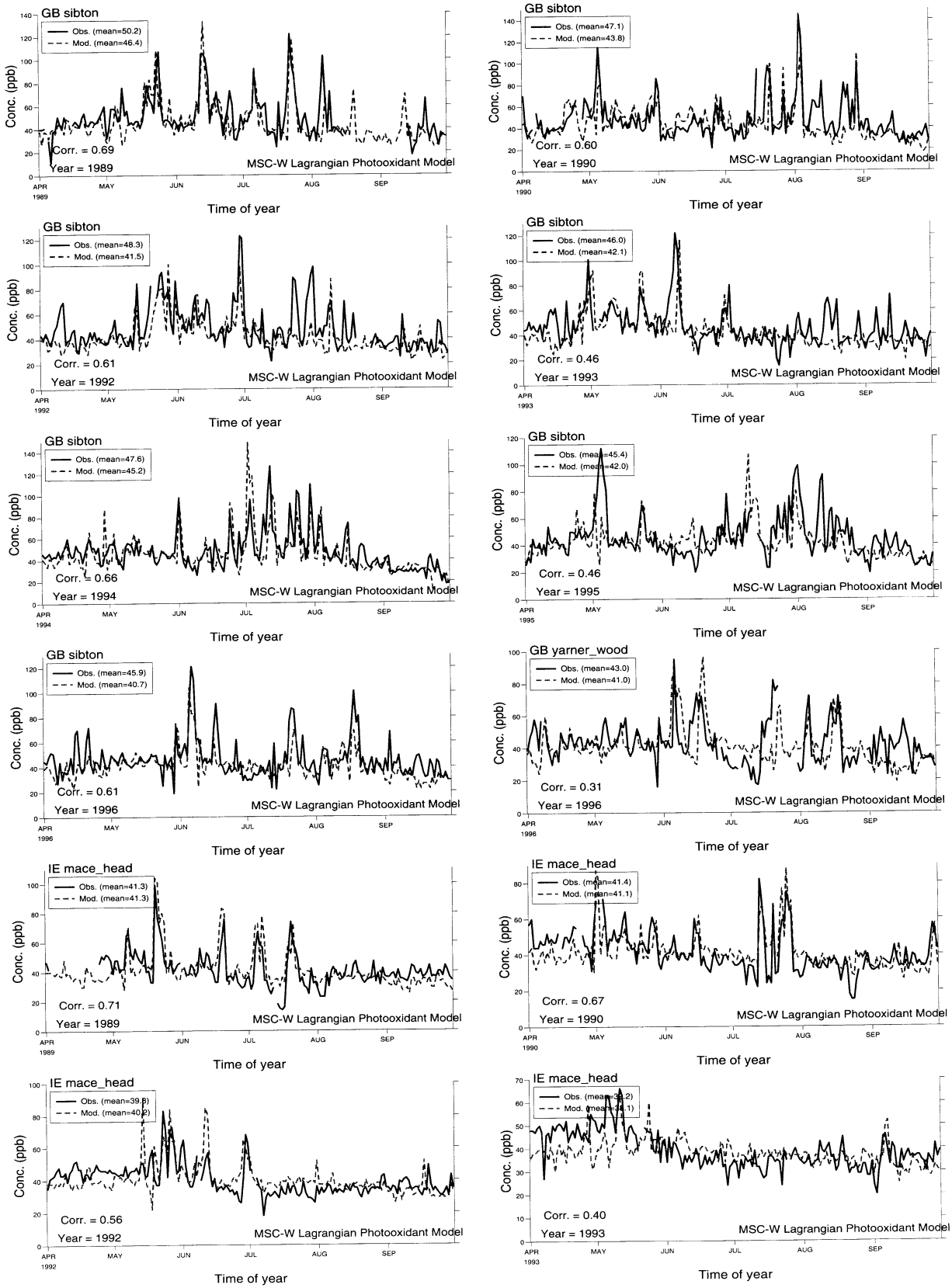

Figure C.23: Modelled versus observed daily max. ozone (ppb)

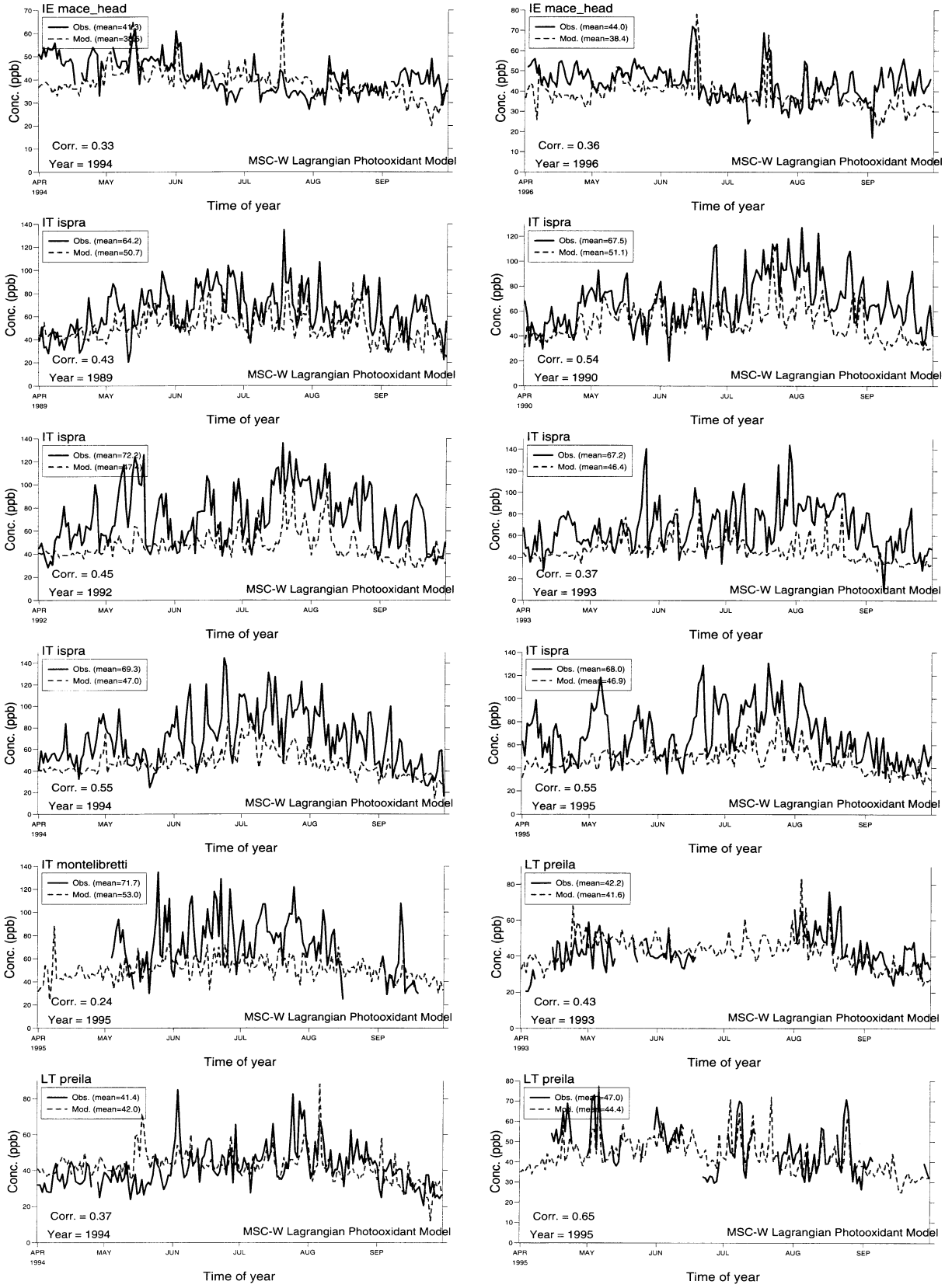

Figure C.24: Modelled versus observed daily max. ozone (ppb)

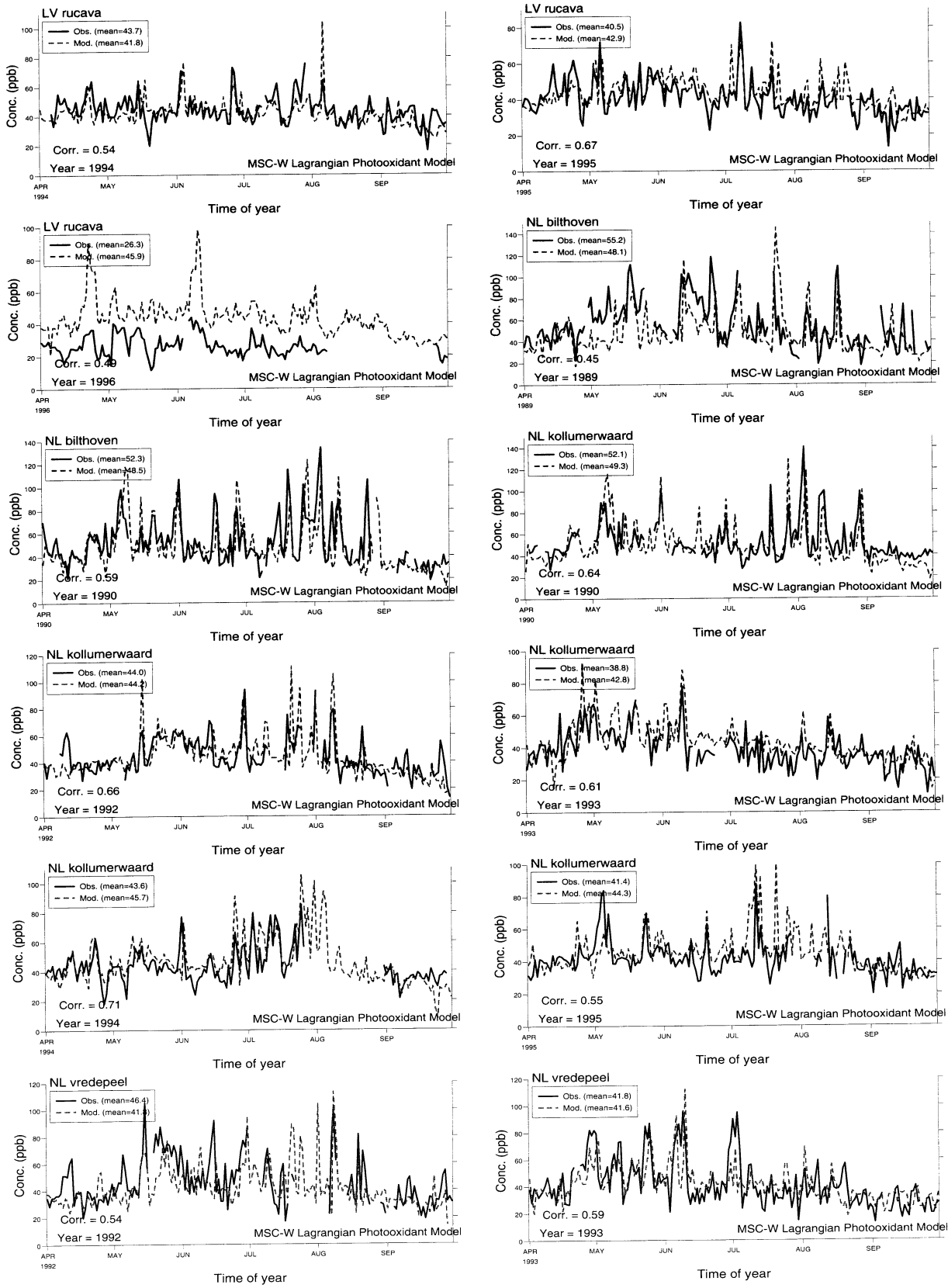

Figure C.25: Modelled versus observed daily max. ozone (ppb)

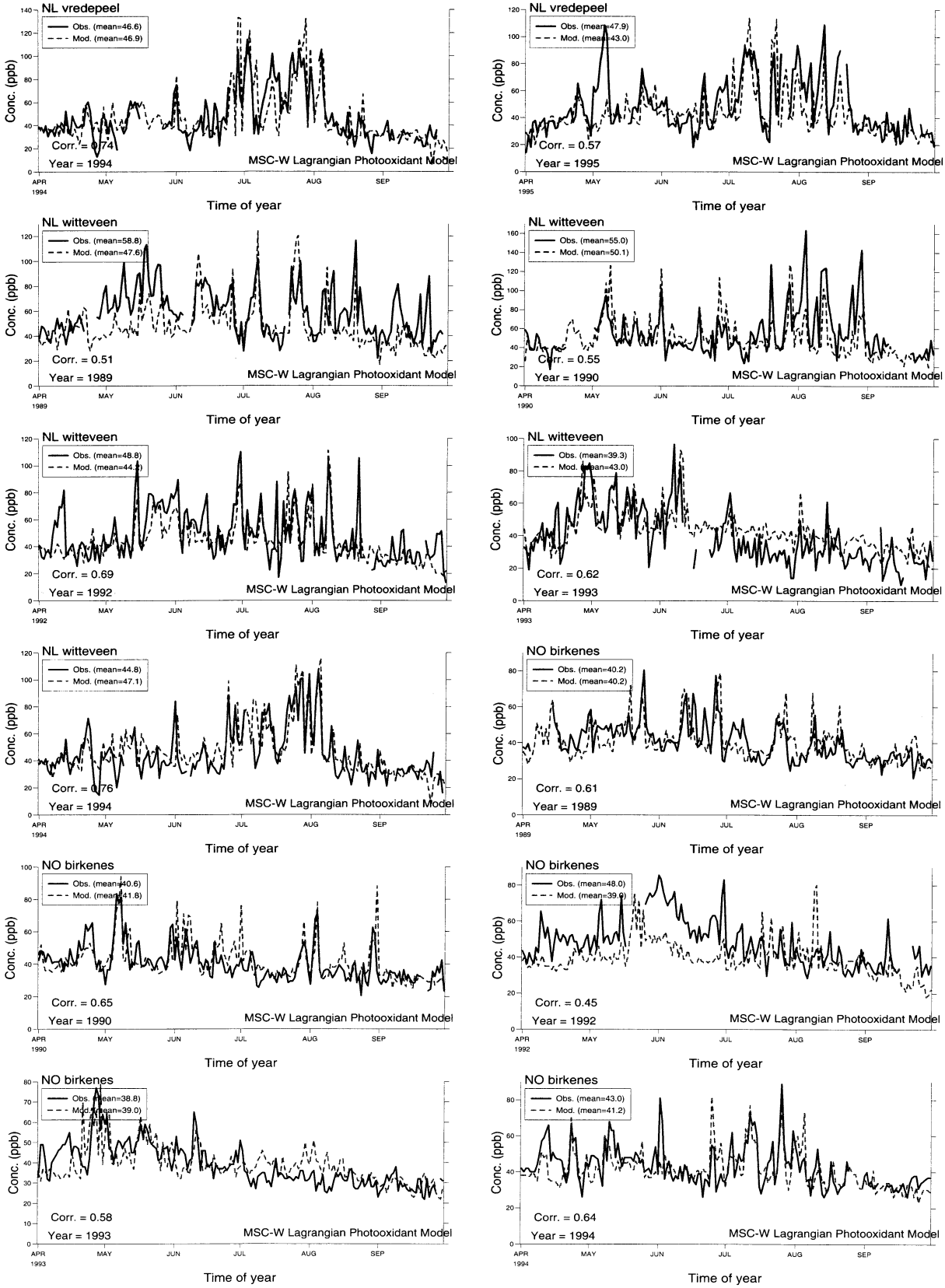

Figure C.26: Modelled versus observed daily max. ozone (ppb)

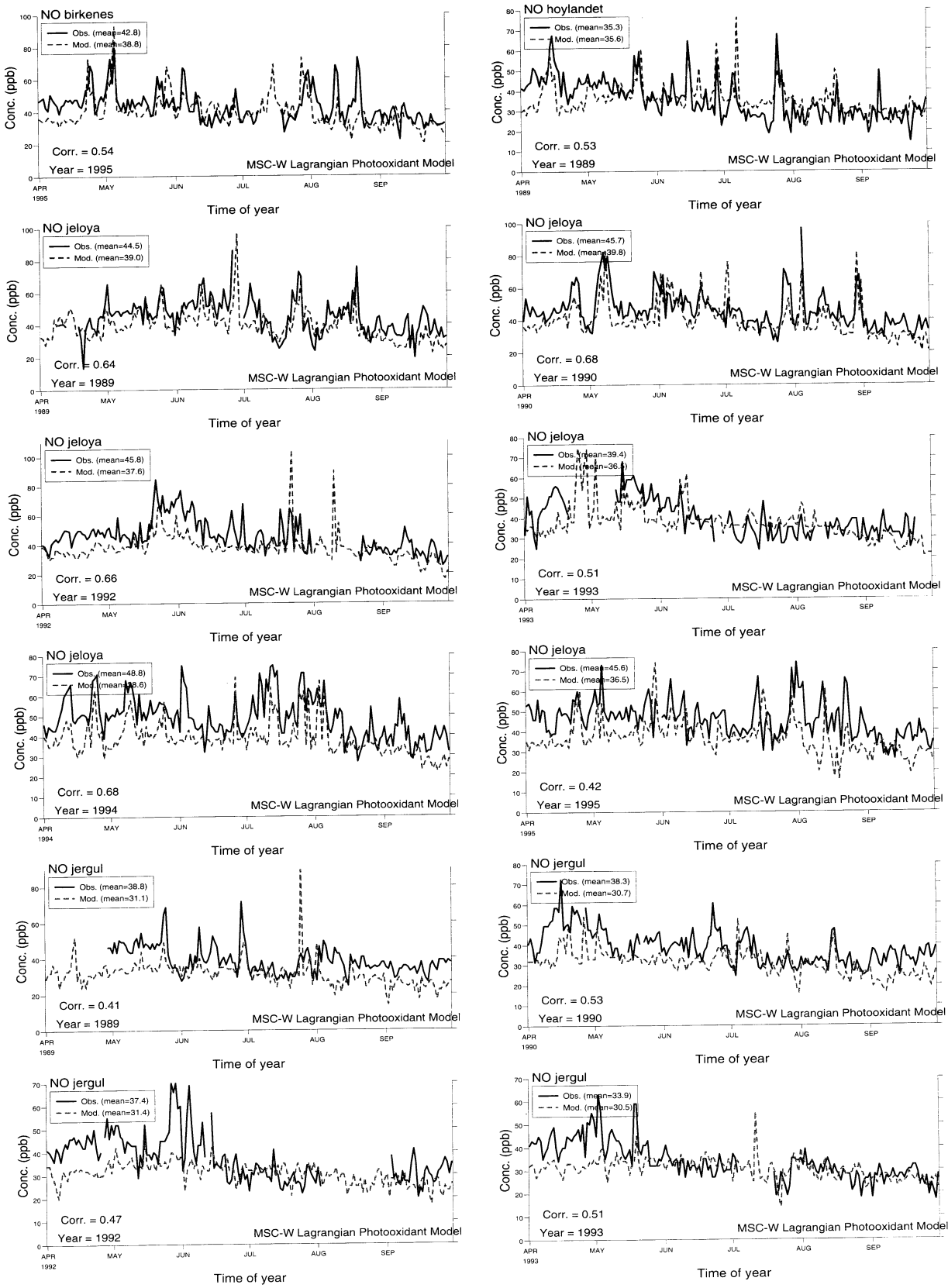

Figure C.27: Modelled versus observed daily max. ozone (ppb)

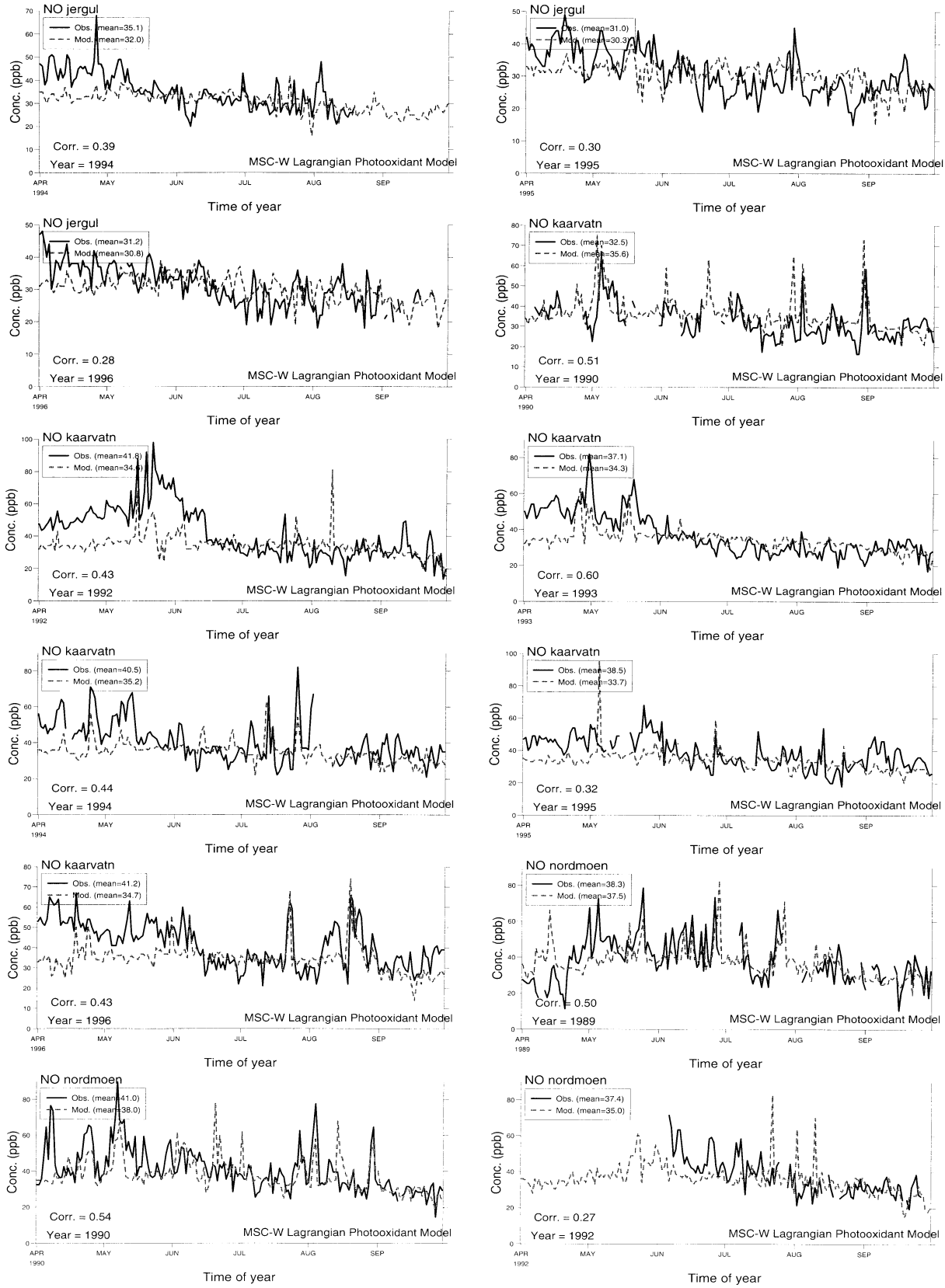

Figure C.28: Modelled versus observed daily max. ozone (ppb)

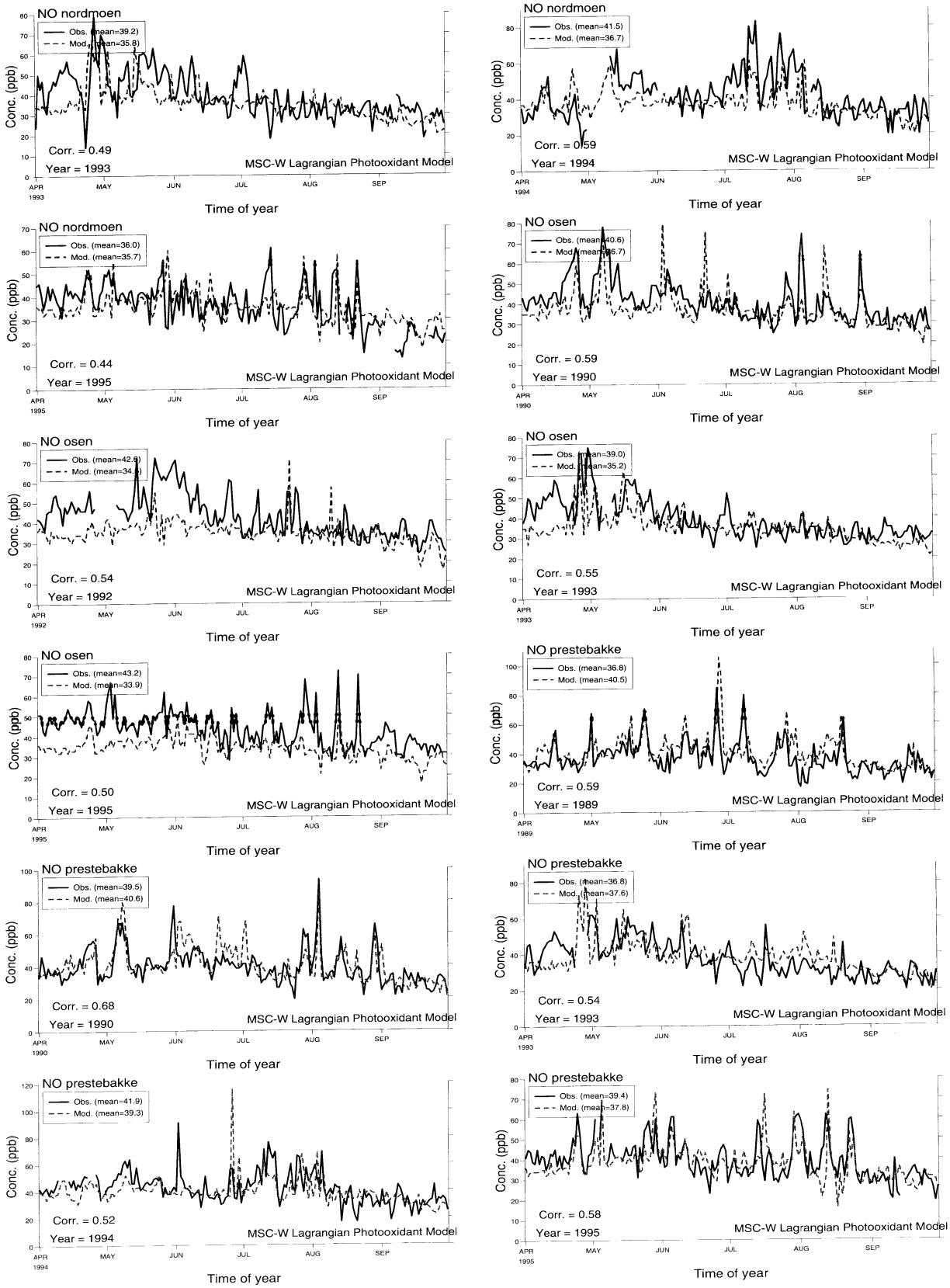

Figure C.29: Modelled versus observed daily max. ozone (ppb)

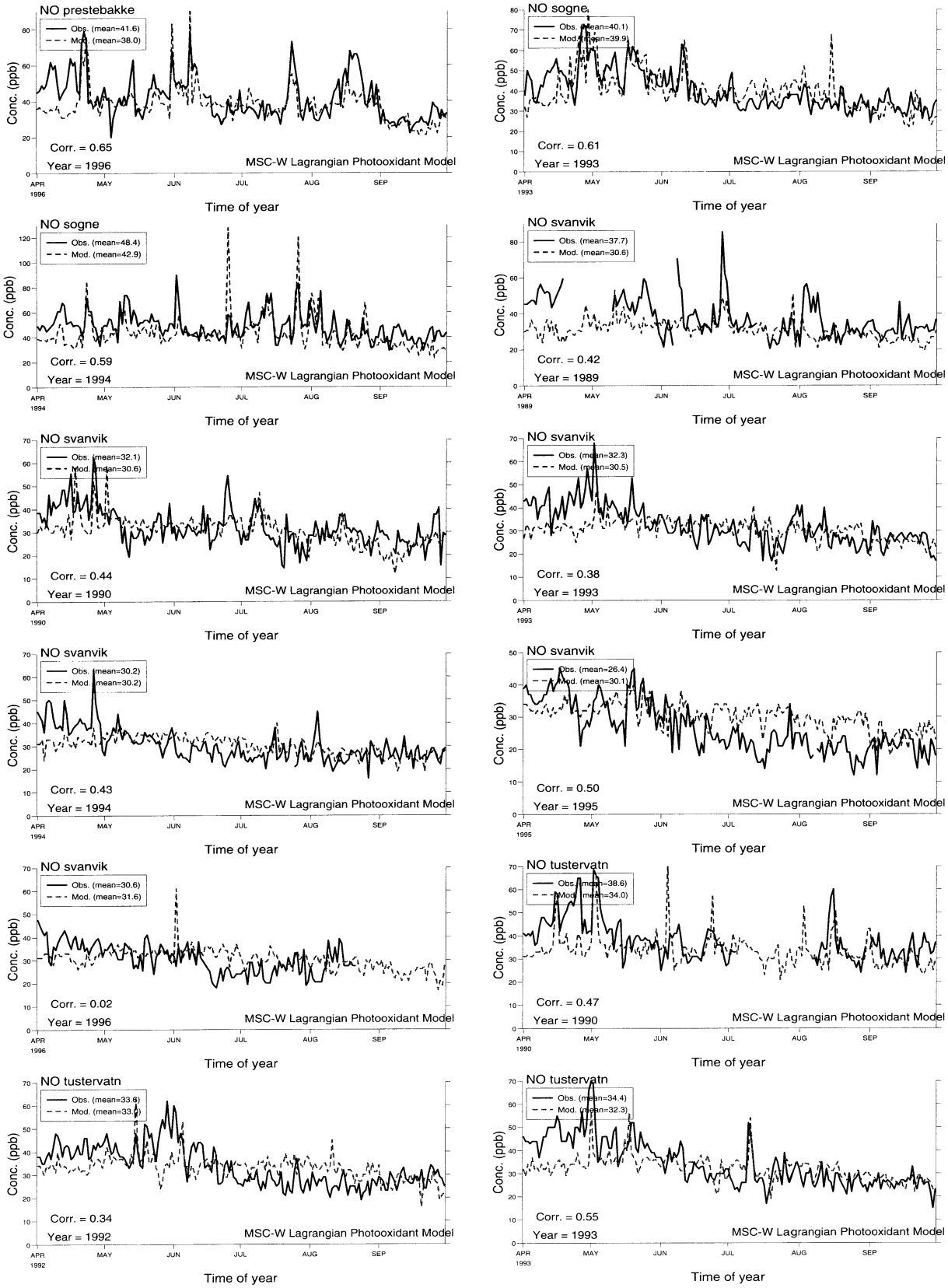

Figure C.30: Modelled versus observed daily max. ozone (ppb)

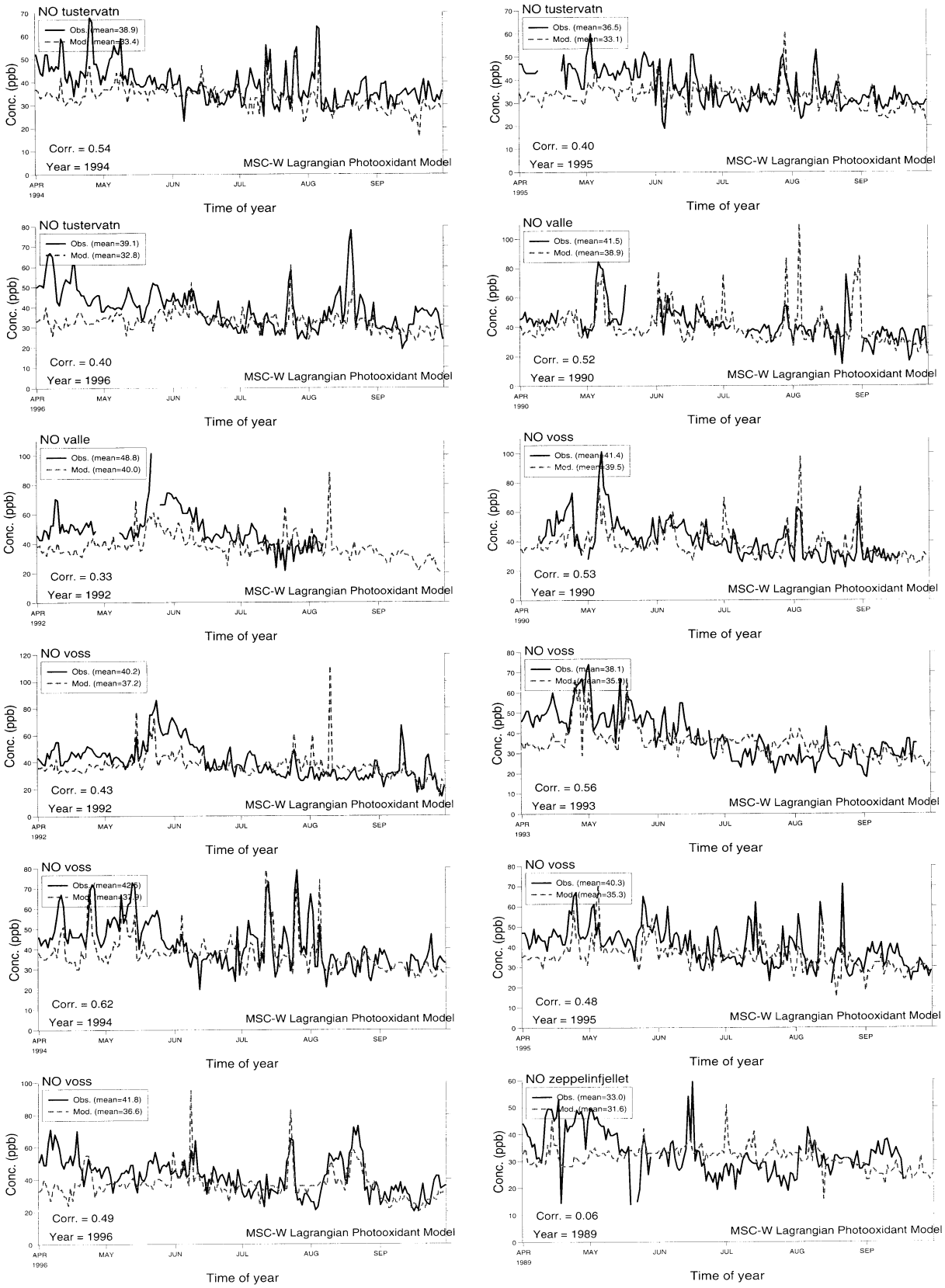

Figure C.31: Modelled versus observed daily max. ozone (ppb)

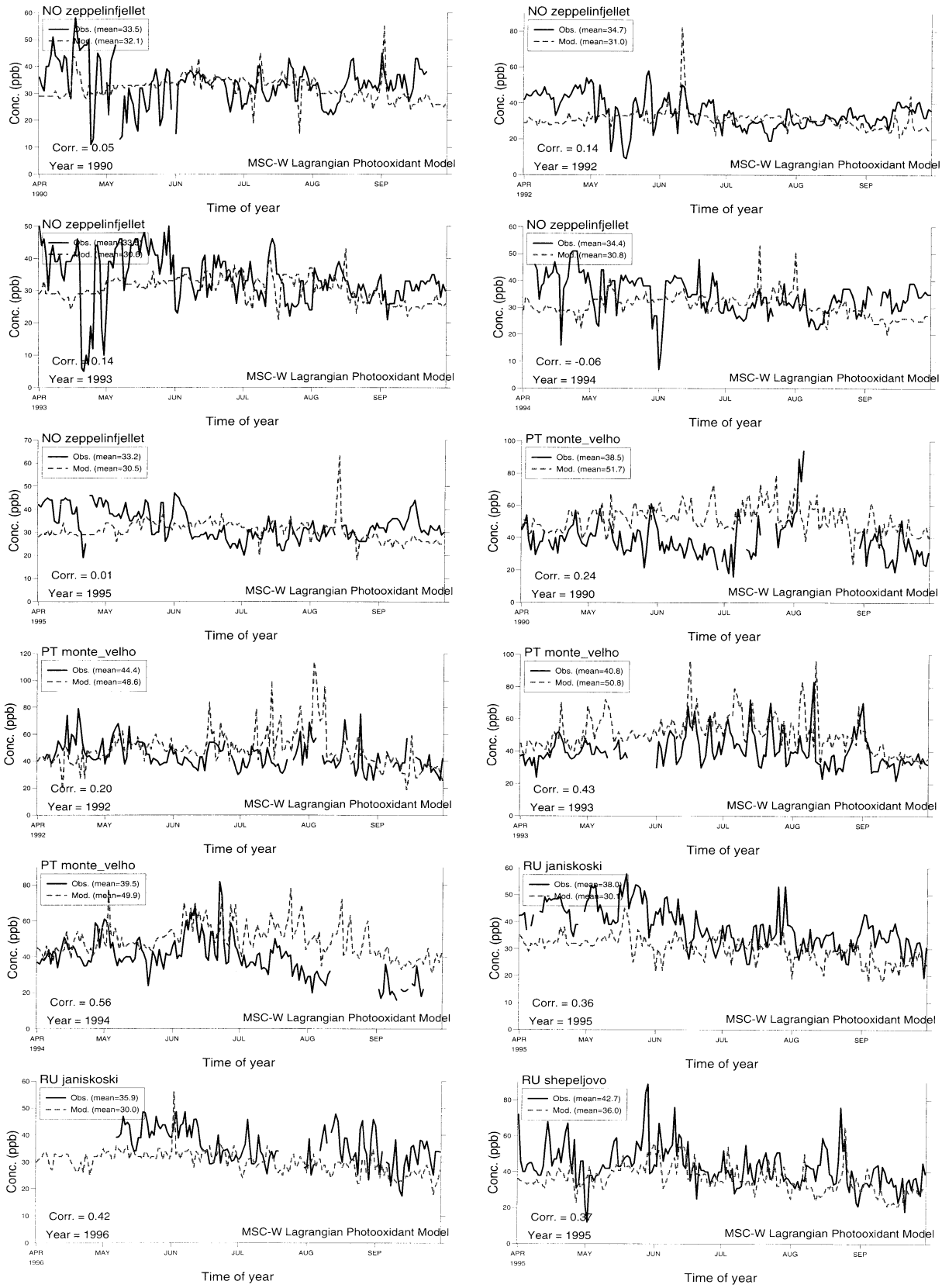

Figure C.32: Modelled versus observed daily max. ozone (ppb)

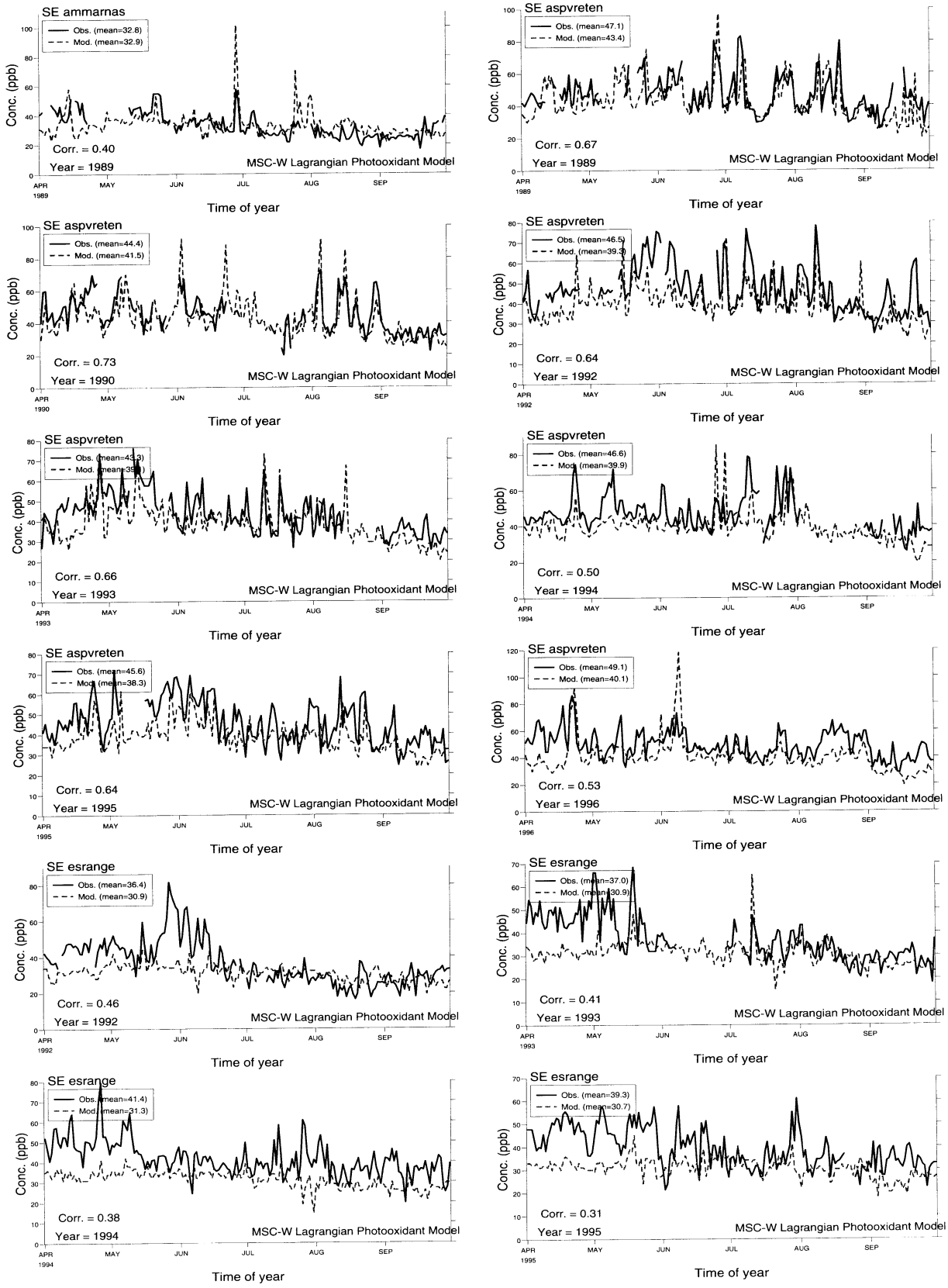

Figure C.33: Modelled versus observed daily max. ozone (ppb)

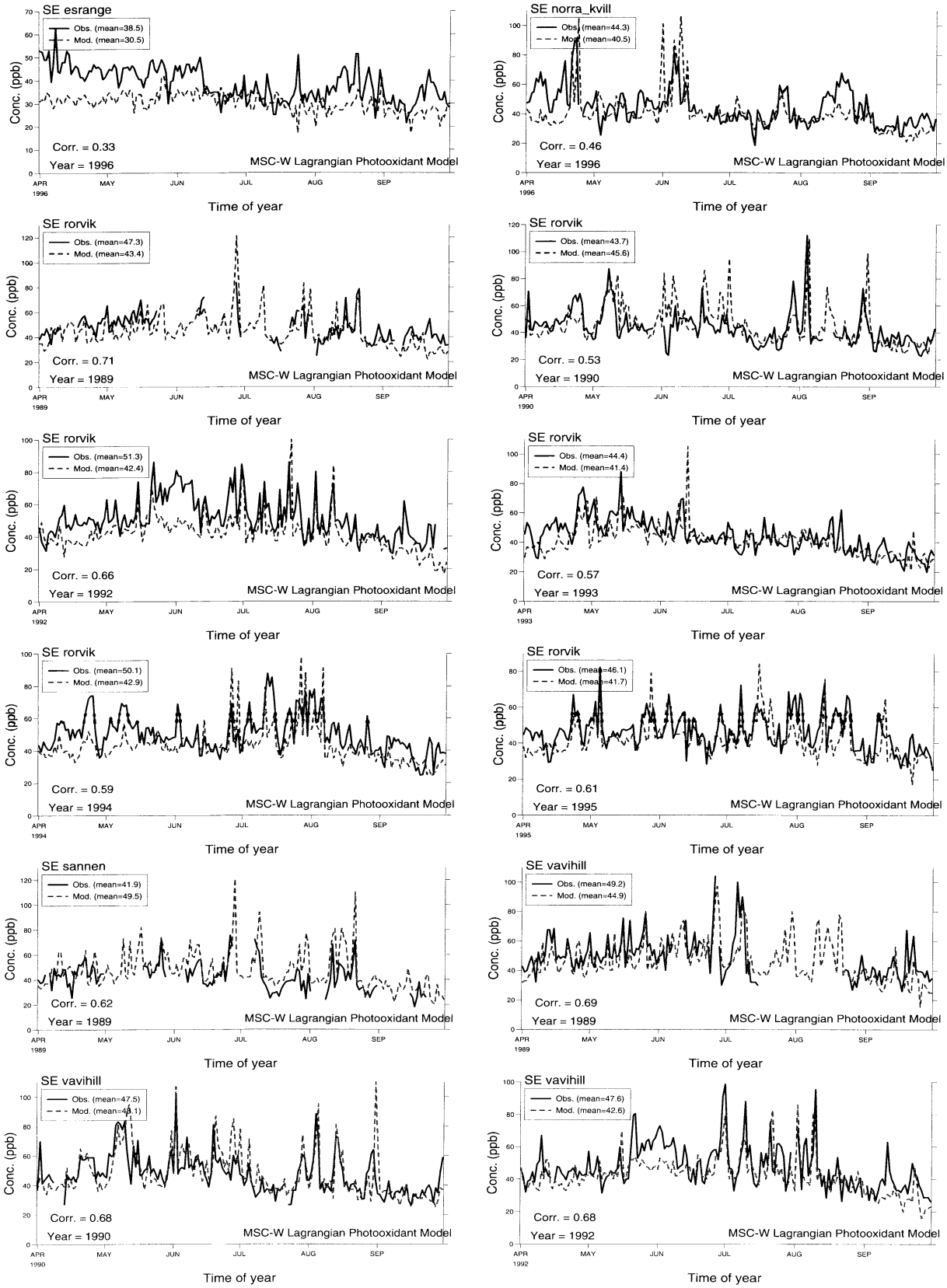

Figure C.34: Modelled versus observed daily max. ozone (ppb)

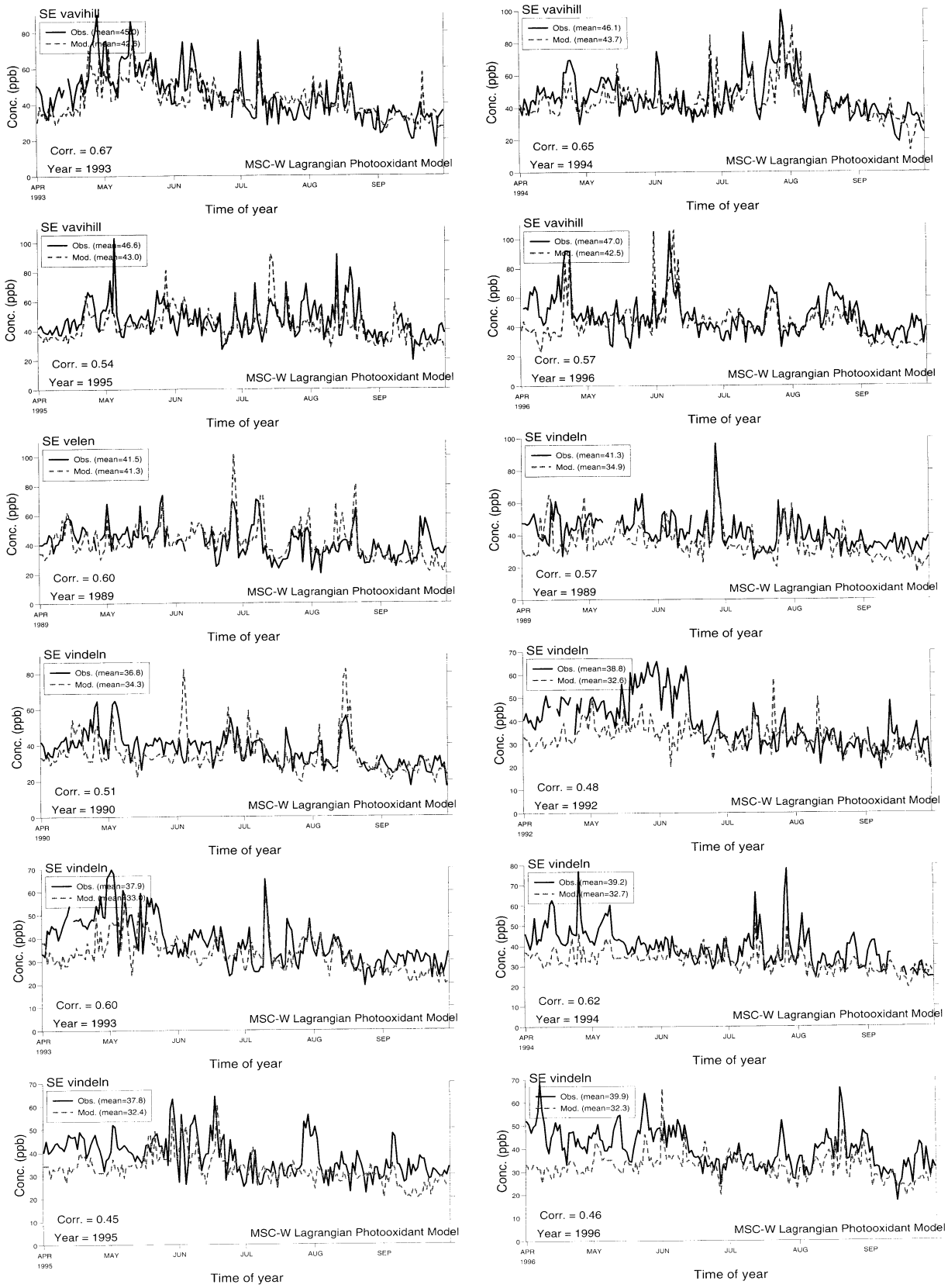

Figure C.35: Modelled versus observed daily max. ozone (ppb)

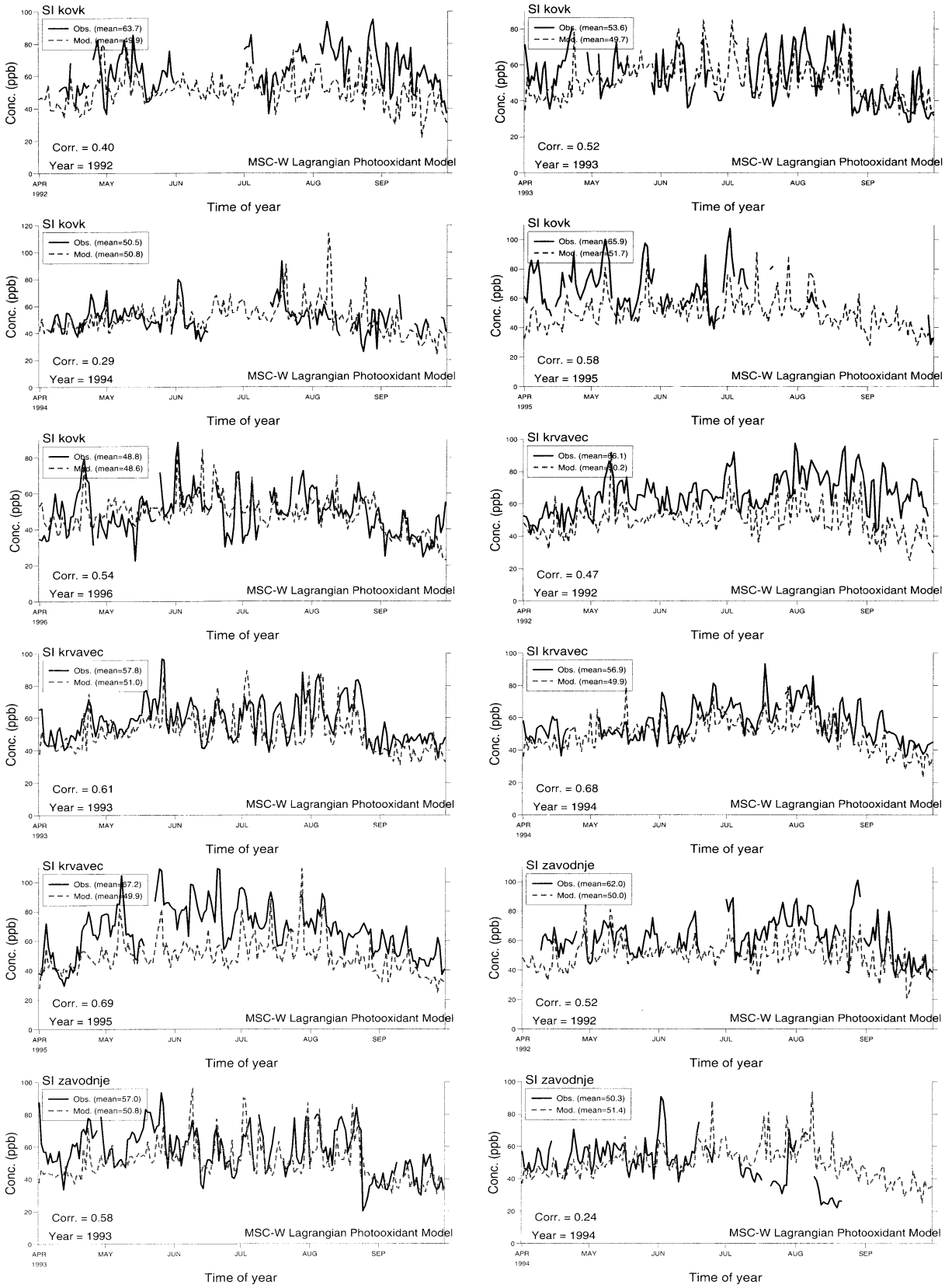

Figure C.36: Modelled versus observed daily max. ozone (ppb)

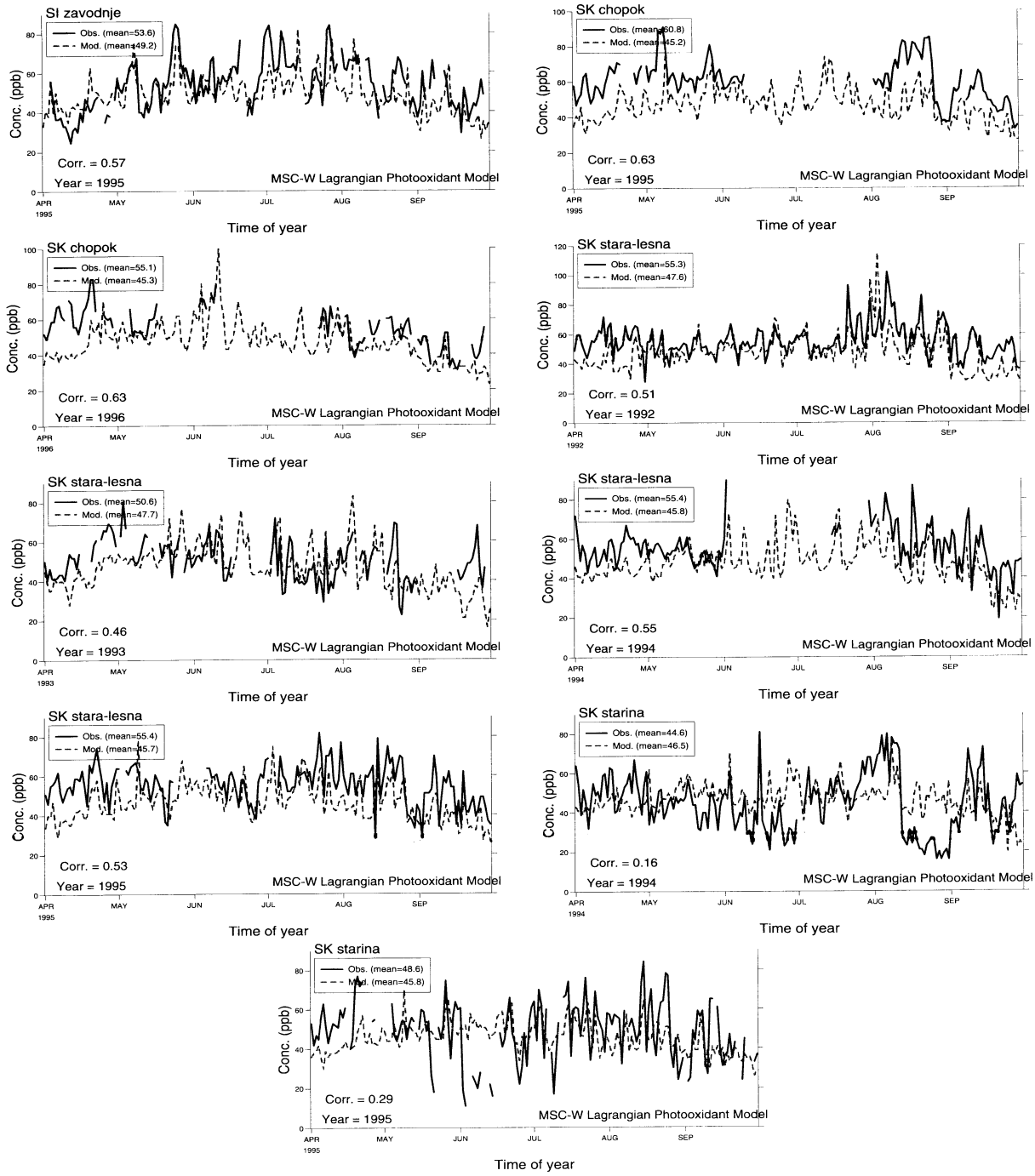

Figure C.37: Modelled versus observed daily max. ozone (ppb)